INVESTIGATION OF A SOFT TACTILE SENSING SYSTEM FOR HUMAN COLLABORATIVE ROBOTS

A Dissertation Submitted to the
College of Graduate and Postdoctoral Studies
In Partial Fulfillment of the Requirements
For the Degree of Doctor of Philosophy
In the Department of Mechanical Engineering
University of Saskatchewan
Saskatoon

By

Chenwang Yuan

PERMISSION TO USE

In presenting this dissertation in partial fulfillment of the requirements for a Postgraduate degree from the University of Saskatchewan, I agree that the Libraries of this University may make it freely available for inspection. I further agree that permission for copying of this dissertation in any manner, in whole or in part, for scholarly purposes may be granted by the professor or professors who supervised my dissertation work or, in their absence, by the Head of the Department or the Dean of the College in which my thesis work was done. It is understood that any copying or publication or use of this dissertation or parts thereof for financial gain shall not be allowed without my written permission. It is also understood that due recognition shall be given to me and to the University of Saskatchewan in any scholarly use which may be made of any material in my dissertation.

Requests for permission to copy or to make other uses of materials in this dissertation in whole or part should be addressed to:

Head of the Department of Mechanical Engineering
57 Campus Drive
University of Saskatchewan
Saskatoon, Saskatchewan S7N 5A9 Canada

OR

Dean
College of Graduate and Postdoctoral Studies
University of Saskatchewan
116 Thorvaldson Building, 110 Science Place
Saskatoon, Saskatchewan S7N 5C9 Canada

ABSTRACT

In recent years, the soft tactile sensing system for a human collaborative robot (HuBot) has received great attention. Various soft tactile sensors along with a soft sensing system (a network of soft sensors) have been developed in literature. The use of carbon nanomaterial/polymer composites (CNPCs) for the soft tactile sensors is promising. However, there is a lack of a systematic approach to designing the CNPC tactile sensing system; besides, a single CNPC tactile sensor warrants a comprehensive study.

In this dissertation, soft tactile sensors made from CNPCs are studied first. Specifically, the distribution method for fabricating the multi-wall carbon nanotube (MWCNT) filled epoxy aliphatic acrylate (EAA)/Aliphatic urethane diacrylate (AUD) composite tactile sensor is studied. The coating method for the MWCNT coated polydimethylsiloxane (PDMS) tactile senor is also studied. Axiomatic Design Theory and Adaptable Design Theory are employed to develop this systematic design approach. To demonstrate the effectiveness of the proposed design approach, a prototype of the soft sensing system for HuBot is developed and tested.

The dissertation led to the following conclusions: (1) It is possible to make MWCNT or single-wall carbon nanotube (SWCNT) filled EAA/AUD tactile sensor with the redox method. (2) The coating method is better than the distribution method in terms of constructing a CNPC tactile sensing system for HuBot. (3) A systematic design approach for the CNPC tactile sensing system for HuBots is effective. (4) A prototype of the adaptable CNPC tactile sensing system is constructed with a preliminary success.

This dissertation has made a few contributions in the field of soft tactile sensors and soft sensor networks. Contribution 1: the new knowledge has been generated regarding the feasibility for the distribution of carbon nanomaterials into the EAA/AUD polymer. Contribution 2: the coating method for CNPC tactile sensors has been found better than the coating method for HuBots. Contribution 3: the systematic design approach to soft CNPC

tactile sensor networks for HuBots has been developed. Contribution 4: a prototype of the soft CNPC tactile sensor network has been constructed.

ACKNOWLEDGMENTS

I would like to take this opportunity to express my appreciation to my co-supervisors, Prof. W. J. Zhang and Dr. R. Sammynaiken, whose encouragement, support, expertise, and guidance has led me to complete this thesis. Their enthusiasm and dedication to this research have greatly influenced and inspired me.

I would like to thank the support from the Saskatchewan Structural Sciences Centre (SSSC), particularly Dr. Jason Maley and Dr. George Belev, who gave me guidance and advice for fabricating the CNPC tactile sensors.

I also would like to give thanks to Mr. Anthony Tony and Dr. Garth Wells from the Canadian Light Source for giving my advice for the PDMS fabrication and providing me the fabrication materials.

I am grateful to the staff at Engineering Workshop at the University of Saskatchewan, who has helped me 3D print the PLA mold used in my studies.

DEDICATED TO

My wife and my parents
For their love, support, and encouragement

TABLE OF CONTENTS

LIST OF FIGURES

LIST OF TABLES

LIST OF ACRONYMS

ADDT	Adaptable Design Theory
ADT	Axiomatic Design Theory
AUD	Aliphatic Urethane Diacrylate
BPO	Dibenzoyl Peroxide
CNPC	Carbon Nanomaterials/Polymer Composite
CNT	Carbon Nanotubes
DCM	Dichloromethane
DMA	N,N-Dimethylaniline
DP	Design Parameter
EAA	Epoxy Aliphatic Acrylate
E-DP	Evolved Design Parameter
E-FR	Evolved Functional Requirement
FCBPSS	F: function, C: context, B: behavior, P: principle, S: state, S: structure
FR	Functional Requirement
HC-PP	High-crystallinity Polypropylene
HuBot	Human Collaborative Robot
LC-PP	Low-crystallinity Polypropylene
MC-PP	Medium-crystallinity Polypropylene
MWCNT	Multi-walled Carbon Nanotube
PDMS	Polydimethylsiloxane
PEDOT: PSS	Poly(3,4-ethylenedioxythiophene) Polystyrene Sulfonate
PLA	Polylactic Acid
PU	Polyurethane
SDS	Sodium Dodecyl Sulfate
SWCNT	Single-walled Carbon Nanotubes
TPE	Thermoplastic Elastomer
TPO	Trimethyl Benzoyl Diphenyl Phosphine Oxide
UV	Ultraviolet

CHAPTER 1

INTRODUCTION

1.1 Background and motivation

1.1.1 Human collaborative robot (HuBot)

The revolution of industrial automation has changed the way of manufacturing and has improved productivity greatly. With the development of control and sensing technologies, industrial robots today can do a variety of works within both manufacturing shop floors and service fields. However, industrial robots cannot complete all works independently or full automation is not a sustainable nor a resilient approach (Zhang and Lin, 2010; Zhang and Luttervelt, 2011; Wang et al., 2019; Zhang et al., 2017). This motivated the research on human collaborative robotics (HuBot for short). It is worth mentioning that HuBot is often mistakenly called Cobot (collaborative robot) (Peshkin and Colgate, 1996; Bi et al., 2008), but Cobot is a special type of HuBots within manufacturing shop-floors, which acts like a robotic fixture (Bi et al., 2008) and essentially a passive system or a system without intelligence. In this dissertation, HuBots are considered as a robotic human operator with all activities the human operator can perform.

One of the challenges with HuBots is safety to human operators in the workplace. Specifically, safety protection refers to how a HuBot avoids collision with human operators. From the safety point of view, HuBots can be classified into four categories: (1) inherently safety (or sufficient softness); (2) skin sensing of collision; (3) ground sensing of collision; (4) joint sensing of collision (Robotiq, 2020). Inherently safe HuBots are robots with weak payloads that are incapable of hurting human operators even when robots and humans collide. HuBots with joint sensing is the most widely used robot on the manufacturing shop floor today. The approach of joint sensing is to analyze the power spectrum in the motor of the robot to infer whether a crash may have taken place, as if there is a crash, the power spectrum will change. However, this approach is less sensitive and is unable to know

whether human operators hit the robot or the robot hits other objects. The approach of ground sensing with HuBots is to set up sensors on the ground in the working area of the robot and expect that these sensors may give "surprising" information when the robot hits objects including human operators. Both joint sensing and ground sensing techniques are of indirect measurement, and they are based on "inference". The approach of skin sensing is a direct sensing technique (especially the soft tactile sensing principle) that measures the force or pressure applied on the surface of a Hubot. One apparent advantage with this approach is fast response and high accuracy. The shortcoming with this approach today is the cost and lack of knowledge regarding skin sensors, i.e., accuracy, robustness, and resilience as well as of missing design methodology and fabrication techniques. This dissertation was designed to close these knowledge gaps. It is noted that the skin sensing system has two main sub-systems: a single sensor and a network of sensors.

1.1.2 Soft tactile sensors based on carbon nanomaterial/polymer composites

An important type of soft tactile sensor is built from a carbon nanomaterial/polymer composite (CNPC). CNPC is composed of carbon nanomaterials, which act as the conductive material, and polymers, which act as the substrate. The conductive material can be coated on the surface of the substrate or filled into the substrate (Figure 1.1). Thus, one architectural idea of such sensors is that polymer composite surfaces are coated with carbon nanomaterials and the other idea is that polymer composites are filled with carbon nanomaterials. This dissertation was expected to compare these two architectural ideas to examine their feasibility and suitability to the skin with the tactile sensing ability for HuBots.

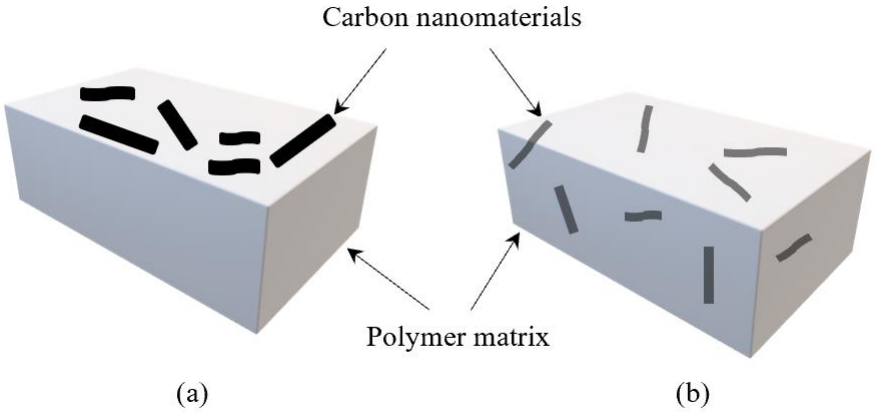

Figure 1.1 Two types of relationships between carbon nanomaterials and polymer matrix: (a) carbon nanomaterials coated on the surface of polymer matrix; (b) carbon nanomaterials filled in the body of polymer matrix.

Soft tactile sensors based on CNPCs have the following advantages. First, carbon nanomaterials, including carbon nanotube (CNT) and graphene, have extraordinary mechanical and electrical properties (Choudhary et al., 2014). Second, polymers as the substrate of the CNPC tactile sensor cover a wide range of hardness that enables different application scenarios of the tactile sensors. Third, the fabrication process of polymers is relatively easy and cost effective. Hereafter, the soft tactile sensor based on CNPCs is called **CNPC tactile sensor** for short.

1.1.3 Soft tactile sensing systems based on CNPC

One single CNPC tactile sensor is small in micro scale, which is not suitable to the intended application in this dissertation, i.e., HuBot. A soft tactile sensing system is composed of many CNPC tactile sensors, and essentially it is a network of CNPC tactile sensors. Different structures of the network are responsible for different behaviors of the sensing system, and subsequently different functions and performances in different contexts (Lin and Zhang, 2005; Zhang and Wang, 2016).

The array of sensors is the most common structure of the network of the tactile sensing system. Kong et al. (2015) developed a 5×5 array network of soft tactile sensors. The soft

tactile sensor is fabricated by filling 7 wt% multiwall carbon nanotubes (MWCNT) into PDMS composite (Figure 1.2). Besides the two-dimensional array, Cheng et al. (2011) proposed a three-dimensional array network to form a tactile sensing system. It arranges tactile sensors in an $8 \times 8 \times 2$ array. This system can detect twist force and irregular distribution pressure because of its three-dimensional structure. The main shortcoming of this structure is the lack of adaptability. Besides the array structure, the serpentine-type structure (Lu et al., 2012) and rosette-type structure (Kong, Jang, et al., 2014) are proposed as well. For these types of networks, they are not flexible to irregular shape of robotic body. One of the concerns with these types of structures is that these structures lack a padding part, which enables to adjust the sensing range, particularly increasing the sensor range. It is noted that the polymer functioned as the padding part of the tactile sensing system is named polymer substrate and the polymer functioned as the container of carbon nanomaterials (filled with or coated with carbon nanomaterials) of the CNPC tactile sensor is named polymer matrix.

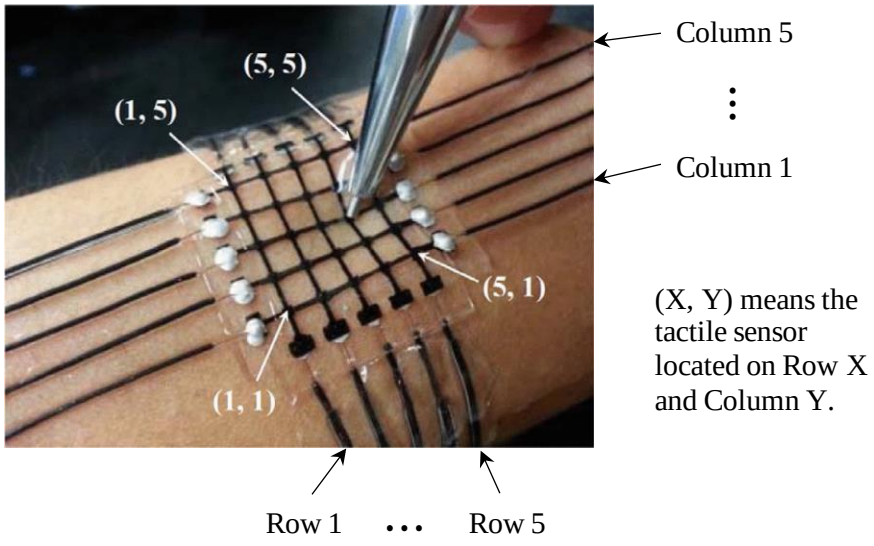

Figure 1.2 The 5×5 array network tactile sensing system mounted on a wrist (Kong et al., 2015).

1.1.4 Research motivation

Many CNPC sensors and CNPC sensing systems have been developed in literature. However, these systems were developed in the context of specific applications. There was lack of knowledge on why and how these systems work. Further, there was no systematic design methodology available in literature, which premises the achievement of both design and fabrication for the required performance of the aforementioned sensing system. In the application side, a design approach that starts with the technical specification of design requirements and proposes a design or designs which can best fulfill the design requirements and can be readily fabricated with reasonable costs. Also, considering the various kinds of HuBots and different sizes and shapes of the surfaces on HuBots, the sensing system must be expected to be adaptable to the surfaces with different sizes and shapes.

1.2 Research objectives and scopes

From the above discussion, this dissertation defined three specific objectives, and they are stated as follows:

(1) To advance the technology for constructing CNPC tactile sensors with adaptable Young's modulus for HuBots.
(2) To develop a systematic design approach for a CNPC tactile sensing system such that the design process starts with the technical specification of design requirements and ends at the specification of a skin sensor system for HuBots.
(3) To construct a prototype of the CNPC tactile sensing system, which can adapt to different sizes and shapes of the surfaces of a HuBot, and to demonstrate the effectiveness of the design approach developed in Objective (2).

The scope of this dissertation is such that the CNPC sensor along with its sensing system was considered only. In Objective (1), the potential alternative CNPC tactile sensor refers to the approach to distributing carbon nano materials into polymer matrixes, and this

approach is opposed to the existing approach to coating carbon nano materials onto the surface of polymer matrixes.

1.3 Organization of the dissertation

The remaining part of the dissertation is organized as follows. In Chapter 2, a comprehensive literature review pertinent to the proposed research objectives is presented for two purposes. The first purpose is to give a sufficient background for the rest of chapters, and the second purpose is to give a more detailed argument on the need of the proposed research (i.e., the three research objectives as defined in Chapter 1).

Chapter 3 will present a study on constructing CNPC tactile sensors by means of distributing carbon nanomaterials in the body and on the surface of polymers. This includes the discussion of material selection, fabrication, and results along with discussions. This chapter will also describe experiments that explore the features of the CNPC tactile sensors fabricated by means of the coating method.

Chapter 4 will present a systematic design approach to a CNPC tactile sensing system, i.e., a network of CNPC tactile sensors. The approach is based on general design theories and methodologies (axiomatic design theory, adaptable design methodology) in the design literature.

Chapter 5 will present the use of the approach presented in Chapter 4 to a specifical application scenario. This includes a proposal of the design of the prototype, the fabrication of the prototype of the CNPC tactile sensing system, and the testing of the prototype. This chapter serves for two purposes. The first purpose is to demonstrate the effectiveness of the proposed approach in Chapter 4, and the second purpose is to provide a prototype of the skin sensing system for HuBots.

Chapter 6 is the conclusions and recommendations for future work.

CHAPTER 2
BACKGROUND AND LITERATURE REVIEW

2.1 Background and motivation

To understand the CNPC tactile sensing system and its development method, the literature review would start from CNPC tactile sensor, followed by CNPC tactile sensing system that is a network of CNPC tactile sensors. An analysis framework called function-context-behavior-principle-state-structure (FCBPSS) is employed to elaborate the intrinsic relationship of carbon nanomaterial, CNPC tactile sensor, and CNPC tactile sensing system for comprehensiveness. The current state of technology for CNPC tactile sensing systems are reviewed as well. Section 2.2 will introduce the function-context-behavior-principle-state-structure (FCBPSS) framework and its application on CNPC tactile sensor. Section 2.3 will discuss the principle of CNPC tactile sensor. Section 2.4 will discuss the structure and state of CNPC tactile sensor. Section 2.5 will discuss the CNPC tactile sensor. Section 2.6 will discuss the design methodology for the CNPC tactile sensing system. Section 2.7 will present a conclusion which serves as a further justification of the need of the proposed research discussed in Chapter 1.

2.2 FCBPSS framework for classification and analysis of CNPC tactile sensors

The function-context-behavior-principle-state-structure (FCBPSS) is a general architecture of the conceptual model of any system (Yuan et al., 2021). It is developed by Lin & Zhang (2005), Zhang et al. (2011), and Zhang & Wang (2016). In the FCBPSS framework, there are six canonical categories of concepts: function, context, behavior, principle, state, and structure (Figure 2.1) (Zhang & Wang, 2016). According to (Lin & Zhang, 2005), “Structure is a set of entities connected in a meaningful way”. States are indicators of the presence of and properties of an entity in a system (Yuan et al., 2021). According to (Zhang & Wang, 2016), “Behavior is the causal relationship among a set of state variables.” The casual relationship is inherently guided by principle of the system.

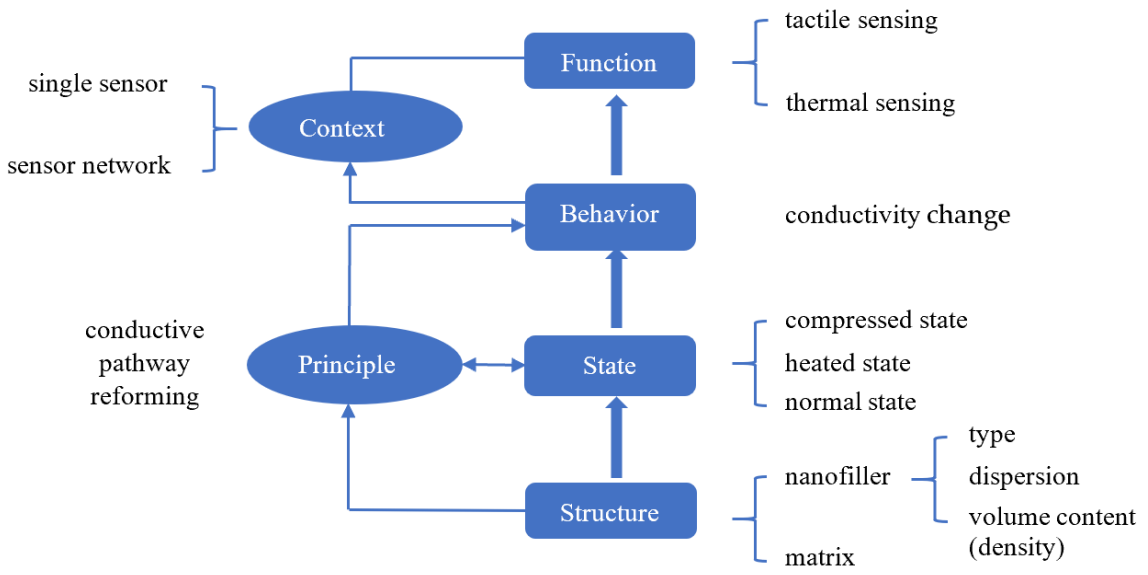

Figure 2.1 Framework of FCBPSS and the analysis based on the CNPC tactile sensor.

To apply the FCBPSS framework, the CNPC is viewed as a system. The analysis of CNPC tactile sensors based on FCBPSS can help make a comprehensive understanding on the CNPC tactile sensor (Figure 2.1). In the CNPC tactile sensor system, the structure of the system refers to the polymer matrix and nanofiller along their type, dispersion, and volume (Figure 2.2a). As a tactile sensor, there are two states: deformed state and normal state. Corresponding to the normal state, the deformed state is a state that deformation happens on CNPC when there is a force or torque applied on it. The working principle of CNPC tactile sensors is conductive pathway reforming (Miao et al., 2013; Miao et al., 2012; Miao, Chen, Lin, et al., 2011; Miao, Chen, Sammynaiken, et al., 2011). Based on different states of the network, the behavior of the CNPC tactile sensor is the relationship between the input (force) and the output (conductivity change) because of the conductive pathway reforming, resulting in the switching from the normal state to deformed state. It is worth mentioning that the transducer of the CNPC tactile sensor is a two-port system (one port being with the force and deformation rate, and the other port being with the electrical current and voltage) (Figure 2.2b), based on reforming the conductive pathway of the network. The context of the CNPC tactile sensor is of two types: (i) the CNPC tactile sensor works as a single tactile sensor for the applications such as measuring pressure in chip

testing (Yu Miao, 2013); (ii) the CNPC tactile sensor works in a sensor network as a skin sensor for HuBots. The function of the system is to sense the pressure at a particular location in the first kind of context, and to sense the pressure over a particular area in the second kind of context (Yuan et al., 2021). Hereafter, the CNPC tactile sensor is called for the first kind of context, and the CNPC tactile sensing system or network sensor is called for the second kind of context. The performance of the CNPC tactile senor is measured by gauge factor, linearity, and repeatability. Similarly, the performance of the CNPC tactile sensing system is measured by spatial resolution, force sensitivity and dynamic range, linearity (Dargahi & Najarian, 2004).

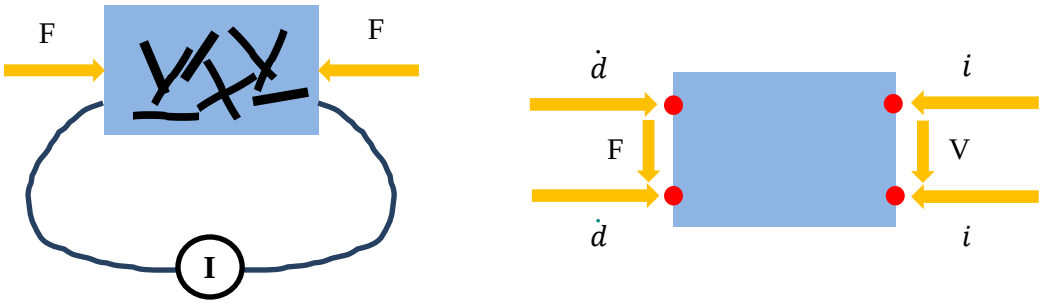

F: force; $\dot{d}$: velocity; I, i: current; V: voltage.

(a) (b)

Figure 2.2 (a) The schematic of CNPC tactile sensor; (b) The schematic of CNPC tactile sensor as a two-port system

2.3 The principle of the CNPC tactile sensor

Carbon nanomaterials contain fullerene, graphite, graphene, single-wall carbon nanotubes, and multi-wall carbon nanotubes. They have extraordinary electrical and mechanical properties (Section 2.4). Insulative polymers with different hardness are chosen as the substrate. CNPC changes from insulation to conductor are explained by percolation theory. After being changed to conductor, the conductivity change is mainly explained by conductive pathway reforming, and/or electron tunneling, and/or hopping.

2.3.1 Percolation theory and conductance

The percolation theory was proposed by Broadbent and Hammersley (1957). It was first employed to explain the behavior of connected properties in random geometries (Miao, 2013). Bunde & Dieterich (2000) extended the theory to random composites. To explain the percolation theory, a square lattice is used as an example (Figure 2.3). Percolation threshold (p_c) is an important concept in the percolation theory. The threshold is referred to the probability (p) that a particular site in the square lattice is occupied (p) or unoccupied (1-p) (Figure 2.3) (Miao, 2013). The occupied sites may stand for a property different from the unoccupied sites. For example, it is assumed that the occupied sites are electrical conductors, and the unoccupied sites are insulators. The neighboring conductor sites can form a pathway for the electrical current. When p is a small value, the conductor sites are isolated by the insulators and this situation cannot form a pathway throughout the square lattice (Figure 2.3a). The square lattice is an insulator. When p is a large value, many conductive pathways are more preferably formed between two edges (Figure 2.3c). When p is a certain value called threshold concentration p_c the current flow path is first established from one edge to the opposite edge (Figure 2.3b). The threshold concentration is called the percolation threshold (Bunde & Dieterich, 2000).

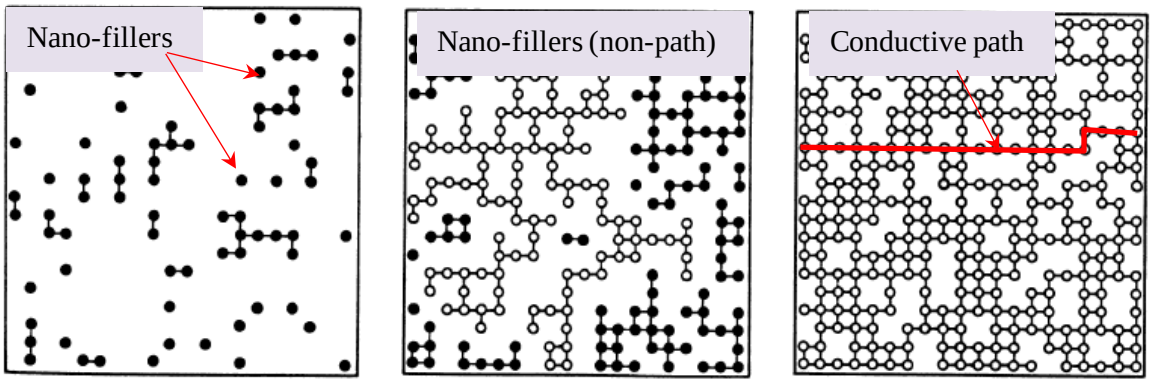

Figure 2.3 Schematic illustration of the site percolation on the square lattice. The small circles represent the occupied site for the concentrations of p=0.2, 0.59 and 0.8. Nearest-neighbor cluster sites are connected by lines representing the current paths. Filled circle

are used for broken (finite) clusters, while open circles mark the unbroken (infinite) cluster**.** When p is larger than p_c, the square lattice is a conductor; when p is smaller than p_c, the square lattice is an insulator. Adapted from (Bunde et al., 2007).

2.3.2 Electron tunneling and hopping

The electron tunneling or hopping mechanism claims that the electrons of carbon atoms can hop and move between neighboring carbon atoms that are closely spaced (Obitayo & Liu, 2012; Amjadi et al., 2014). Electrons can move through a thin layer of polymers between two neighboring carbon nanomaterials and form quantum tunneling junctions (Amjadi et al., 2016). The tunneling resistance of the quantum tunneling junction between two closely spaced carbon nanomaterials can be estimated by Simon's theory (Alamusi et al., 2011), namely

$$R_{tunnel} = \frac{V}{AJ} = \frac{h^2 d}{Ae^2\sqrt{2m\lambda}} exp(\frac{4\pi d}{h}\sqrt{2m\lambda}) \quad (2\text{-}1)$$

where V is the electrical potential difference, *A* is the cross-sectional area of the tunneling junction, *J* is the tunneling current density, *h* is Plank's constant, *d* is the distance between adjacent nanomaterials, *e* is the single electron charge, *m* is the mass of electron, and λ is the energy barrier height for polymers. It is worth mentioning that the two principles may act at the same time.

2.4 The structure and state of CNPC

A CNPC is formed by filling carbon nanomaterials into polymer matrixes. Carbon nanomaterials have different structures and are classified into carbon black, fullerene, carbon nanotube, and graphene. Among these types, carbon nanotube and graphene are widely used in CNPC to tune different performances for different applications, e.g., biosensors (Wu, Wu, et al., 2008; Wu, Zhang, et al., 2008; Wu et al., 2007; Wu et al., 2006). Although not made in this way, carbon nanotubes can be viewed by rolling graphene sheets into tubes and are further classified into single-walled carbon nanotubes (SWCNTs) and multi-walled carbon nanotubes (MWCNTs) (Figure 2.4). SWCNTs are tubes that have a

single layer of graphene sheets and MWCNTs are tubes that contain multi layers of graphene sheets.

The properties of CNPC are fundamentally determined by the nanostructure of the carbon nanomaterial and polymer. For the carbon nanomaterial, the type, dispersion state, and volume content would influence the properties of CNPC. Also, the mechanical and chemical properties of polymer substrate may affect the performance of the CNPC tactile sensors.

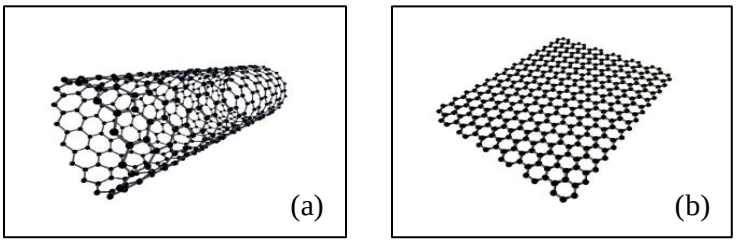

Figure 2.4 Structure of carbon nanotube (a) and graphene (b) (Wang et al., 2020).

2.4.1 Type of carbon nanomaterials

As widely used in CNPC, the carbon nanotube and graphene will be discussed and compared. Table 2.1 and 2.2 compare different properties of the carbon nanotube and graphene.

Table 2.1 The properties of different carbon nanomaterials (Ma, 2010).

Carbon Nanomaterial	Single-walled carbon nanotube	Multi-walled carbon nanotube	Fullerene	Graphite	Graphene
Specific gravity (g/cm^3)	0.8	1.8	1.7	1.9~2.3	-
Electrical conductivity (S/cm)	10^2~10^6	10^3~10^5	10^{-5}	4000 ^{P}, 3.3 ^{C}	10^3
Thermal conductivity (W/(mK))	6000	2000	0.4	298 ^{P}, 2.2 ^{C}	5000
Thermal stability in air (°C)	>600	>600	~600	450~650	600

p: in-plane; c: c-axis.

Table 2.2 Comparison between MWCNT and graphene (Ghislandi et al., 2013).

Filler	Purity of Fillers %		Aspect Ratio Average Length/Thickness (or Ø)
	Carbon Purity	CO/Metal Oxide Groups	
Graphene	~84	~16	~250
MWCNT	90	10	157.9

From Table 2.2, it can be seen that the aspect ratio of MWCNT is 157.9 and the aspect ratio of graphene is around 250, which is 58% higher than MWCNT's (Ghislandi et al., 2013). This is because the graphene is two-dimensional while the carbon nanotube is one-dimensional. The graphene sheets allow larger contact area with the polymer matrix in CNPC than carbon nanotubes which are like sticks (Marsden et al., 2018). The large contact area can help transfer stress between the nanostructures of graphene and polymer matrix (Yang et al., 2011). The carbon nanomaterial filled CNPC containing graphene shows better mechanical properties compared with CNPC made by carbon nanotubes. However, the large surface area of graphene also leads to aggregation and bundling of graphene sheets caused by van der Waals force. To avoid the aggregation of graphene sheets, several methods were developed in the fabrication process, including the use of surfactant (Grossiord et al., 2006), functionalization of carbon nanomaterials (Roy et al., 2018), and physical stirring (Pötschke et al., 2003).

Carbon nanotubes have a relatively low aspect ratio and smaller surface area compared with graphene (Yuan et al., 2021). Considering the different physical structures and properties of the CNT and graphene, researchers tried to use the mixture of CNT and graphene as the nanofiller of carbon nanomaterial filled CNPCs. Researchers claim that the mixture of the CNT and graphene would improve the conductivity of the carbon nanomaterial filled CNPC compared with the CNPC with the CNT filler or graphene filler only (Min et al., 2010). As the CNT is one-dimensional and graphene is two-dimensional, the CNT and graphene can help separate each other when the two being mixed. The mixture of the CNT and graphene can have a better dispersion in the carbon nanomaterial filled CNPC and improve the conductivity of the CNPC. It is because in a three-dimensional

space, the CNT and graphene can form a three-dimensional structure that helps disperse each other and increase the contact area with the polymer matrix (Pradhan & Srivastava, 2014). However, for carbon nanomaterial coated CNPCs, the carbon nanomaterial is two-dimensional distributed on the surface of the polymer substrate. Therefore, the mixture of the CNT and graphene does not have the similar advantage as in carbon nanomaterial filled CNPCs. Table 2.3 provides a comparison of the CNT, graphene, and mixture of CNT and graphene as the nanomaterial in the carbon nanomaterial filled CNPC.

Table 2.3 The electrical conductivity and percolation threshold of the CNT/graphene filled polymer composite (Yuan et al., 2021).

Filler	Matrix	Filler Loading	Fabrication Method	Percolation Threshold	Highest Electrical Conductivity (S/m)	Reference
MWCNT	Polyphenylene sulfide	-	Melt mixing	5 wt%	-	(Khan et al., 2013)
Graphene	Polyphenylene sulfide	-	Melt mixing	10 wt%	-	(Khan et al., 2013)
MWCNT	Epoxy	2 wt%	Milling	0.2 wt%	1.76×10^{-1}	(He et al., 2013)
Graphene	Epoxy	2 wt%	Milling	0.2 wt%	4.0×10^{-3}	(He et al., 2013)
MWCNT	Polyetherimide	5 wt%	Solution mixing	-	1.43×10^{-4}	(Kong, Mariatti, et al., 2014)
Graphene	Polyetherimide	5 wt%	Solution mixing	0.22 wt%	5.82×10^{-4}	(Kong, Mariatti, et al., 2014)
Graphene/MWCNT	Polyetherimide	5 wt%	Solution mixing	-	1.28×10^{-3}	(Kong, Mariatti, et al., 2014)
MWCNT	Polydimethylsiloxane	4 wt%	Solution mixing	-	2.53×10^{-5}	(Kumar et al., 2010)
Graphene	Polydimethylsiloxane	4 wt%	Solution mixing	-	7.89×10^{-5}	(Kumar et al., 2010)
Graphene/MWCNT	Polydimethylsiloxane	4 wt%	Solution mixing	-	1.24×10^{-3}	(Kumar et al., 2010)
MWCNT	High density polyethylene	-	Alcohol-assisted dispersion and hot pressing	0.25 vol%	-	(Du et al., 2011)

Graphene	High density polyethylene	-	Alcohol-assisted dispersion and hot pressing	1 vol%	-	(Du et al., 2011)
MWCNT	Polystyrene/ poly(2,6-dimethyl-1,4-phenylene oxide)	4 wt%	Solution blending	0.2 wt%	57	(Ghislandi et al., 2013)
Graphene	Polystyrene/ poly(2,6-dimethyl-1,4-phenylene oxide)	4 wt%	Solution blending	1 wt%	0.9	(Ghislandi et al., 2013)
CNT	Polyaniline	69.2 wt%	In situ polymerization	-	680	(Lu et al., 2011)
Graphene	Polyaniline	69.2 wt%	In situ polymerization	-	150	(Lu et al., 2011)
CNT/Graphene	Polyaniline	69.2 wt%	In situ polymerization	-	410	(Lu et al., 2011)
MWCNT	Polystyrene	5 wt%	Melt mixing	0.05 wt%	7.98×10^{-1}	(Knapp & Kohl, 2014)
Reduced GO	PolystyrenePS	4 wt%	Solution mixing	-	22.68	(Wu et al., 2012)
CTAB/wrapped GO	Poly(vinyl chloride)	6.47 vol%	Solution mixing	0.6 vol%	5.8	(Vadukumpully et al., 2011)
MWCNT	Poly(vinyl chloride)	20 wt%	Solution mixing	-	175	(Broza et al., 2007)
MWCNT	Liquid crystalline polymer	4 wt%	Melt mixing	-	1.3×310^{-1}	(Sahoo et al., 2011)
Graphene	Liquid crystalline polymerLCP	5 wt%	Solution casting and compression molding	3 wt%	4.5×10^{-1}	(Biswas et al., 2011)
MWCNT	Poly(styrene–butadiene–styrene) SBS	5 wt%	Solution mixing	0.35 wt%	-	(Qin et al., 2020)

Yang et al. (2011) studied the synergetic effects of filling the graphene and CNT in the epoxy composite and reported that the CNPC with a mixture of the CNT and graphene shows a better conductivity. They pointed out that due to the large surface area, graphene can help transfer the stress and heat between the nanofiller and polymer matrix. The CNT in the mixture can attach onto the surface of graphene and help separate graphene sheets from bundling and stacking (Pradhan & Srivastava, 2014).

For carbon nanomaterial coated polymer composites, one-dimensional carbon nanomaterials are preferred because of less aggregation during the fabrication process. The conductive networks can be easily formed by CNTs and keep the polymer substrate with high strain level (Amjadi et al., 2016). Table 2.4 lists the carbon nanomaterial coated polymer composites as a tactile sensor.

Table 2.4 List of the carbon nanomaterial coated polymer composites as a tactile sensor.

Coating material	Matrix	Stretchability (%)	Gauge Factor	Reference
CNTs	silicone rubber	500	1-2.5	(Amjadi et al., 2015)
Carbon black	PDMS	30	29.1	(Lu et al., 2012)
Carbon black	TPE	80	20	(Mattmann et al., 2008)
Graphene	Rubber	800	10-35	(Boland et al., 2014)
CNTs	PEDOT: PSS /PU	100	8.7-62.3	(Roh et al., 2015)

2.4.2 Distribution of carbon nanofillers

The distribution of carbon nanofillers has a direct impact on the conductivity and percolation threshold of the CNPC. Homogeneous distribution can increase the conductivity of CNPCs. The distribution of carbon nanomaterials is affected by the intrinsic van der Waals force, as it would be a cause to aggregate the nanomaterials. To overcome the aggregation of nanomaterials, different methods have been developed to

achieve the homogeneous distribution, including ultrasonication, high-shear mixing, surfactant, alignment, chemical modification, and polymer chain wrapping (Zhu et al., 2004). According to (Zhu et al., 2004), the homogeneous distribution cannot only improve conductivity but also mechanical properties. According to (Grossiord et al., 2006), the homogeneous distribution can lead to more conductive pathways and therefore increase the conductivity.

Another view was proposed by researchers that aggregation of carbon nanomaterials has positive effects on increasing the conductivity of the CNPC. Delozier et al. (2006) claimed that the homogeneous distribution would lower the possibility that carbon nanofiller bundles can connect each other to form the conductive pathways. This claim is not convincing because the aggregation of carbon nanofillers may not be able to connect to neighboring bundles when filling the same volume of carbon nanomaterials. Du et al. (2006) further concluded that electrical conductivity can be increased by the heterogeneous distribution of SWCNT instead of the uniform distribution.

Li et al. (2007) proposed a mathematical model for the relationship between the conductivity of the CNPC and the distribution of carbon nanomaterials. They calculated that the percolation threshold of the CNPC can be represented by

$$P_c = \frac{\delta \varepsilon \pi}{6} + \frac{(1-\delta)27\pi d^2}{4l^2} \quad (2\text{-}2)$$

where P_c means the percolation threshold of the CNPC, δ means the volume fraction of the aggregated CNTs, ε means the volume content of CNTs in an aggregation, d means the diameter of the CNTs, and l means the length of the CNTs. However, this equation needs further experiments for justification. In summary, the distribution of carbon nanomaterials is important to the performance of the CNPC. A more quantitative analysis needs to be developed to further understand the relationship between the conductivity and the distribution of the carbon nanomaterials.

2.4.3 Volume content (areal density) of carbon nanofillers

Besides the distribution of carbon nanofillers, the volume content (areal density) of carbon nanomaterials is also an important factor that determines the performance of the CNPC. For the carbon nanomaterial filled polymer composite, it is the volume content of carbon nanomaterials. For the carbon nanomaterial coated polymer composite, it is the density of the carbon nanomaterial on the coating area of the substrate. The CNPC would become conductive after the volume content (areal density) of nanomaterial achieves the percolation threshold. Stauffer et al. (1994) proposed an equation to predict the electrical conductivity of the carbon nanomaterial filled polymer composite based on the percolation threshold, i.e.:

$$\rho = \rho_0 (\nu - \nu_c)^t \tag{2-3}$$

where ρ is the composite resistivity, ρ_0 is the resistivity of the conductive filler, ν is the volume content of the filler, ν_c is the percolation threshold of the filler, and t is the critical exponent. To prove this equation, many experiments were conducted. According to (Hu et al., 2006; Martin et al., 2004; Regev et al., 2004; Sandler et al., 2003), the critical exponent value ranges from 0.7 to 3.1. However, this equation is only suitable for the volume content of carbon nanofillers, which is close to the percolation threshold. When the volume content of nanofiller is much higher than the percolation threshold, this equation is not suitable as the aggregation appears and affects the conductivity (Liao et al., 2008). Liao et al. (2008) designed an experiment to fill different volume contents of MWCNT into high-crystallinity polypropylene (HC-PP), medium-crystallinity polypropylene (MC-PP), and low-crystallinity polypropylene (LC-PP) and then tested their conductivities, as shown in Figure 2.5. From this figure it can be found that all three composites share the same trend of a conductivity decrease when the MWCNT volume content is higher than a specific value.

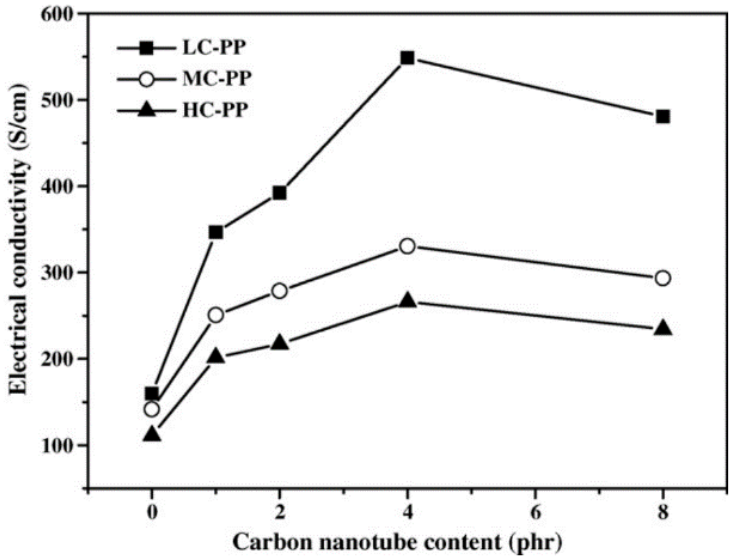

Figure 2.5 The bulk electrical conductivity of the nanocomposite bipolar plates with various MWCNT contents (Liao et al., 2008).

Engel et al. (2006) conducted an experiment that revealed the relationship between the volume content of MWCNT and the resistance change of the CNPC. They found that when the volume content of MWCNT is close to the percolation threshold, the resistance change of the CNPC has a sensitive response to deformation, though it is nonlinear. When the volume content of MWCNT is much higher than the percolation threshold, the CNPC's resistance change to deformation goes down but with a better linearity.

For the carbon nanomaterial coated polymer composite, according to the percolation model, their conductance is dependent on the density of carbon nanomaterial networks, which is described by

$$\sigma \infty (N - N_c)^{\alpha} \tag{2-4}$$

where σ refers to the conductance of CNT networks, N to the density of CNT networks, Nc to the critical density and α to the critical exponent, which is equal to 1.33 in a two-dimensional region and 1.94 in a three-dimensional region, respectively (Pike & Seager, 1974). Miao (2013) did experiments and approved that the relationship between the resistance and density of the CNT network follows Equation (2-4).

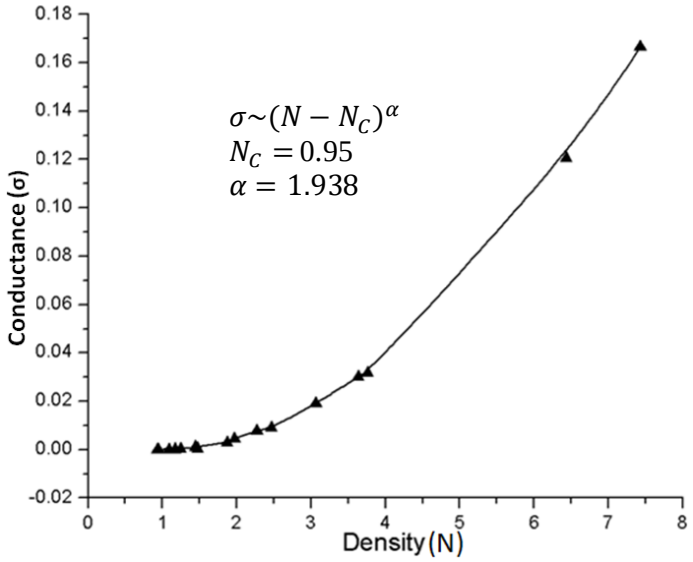

Figure 2.6 The relation between the density and conductance of CNT networks in the CNT film; the onset conduction is indicated by the amplitude value 0.95 on the inset figure when the first percolative path formed in CNT networks. Adapted from (Miao, 2013).

In summary, the volume content (areal density) has an important effect on the performance of the CNPC, especially the sensitivity and linearity of CNPC.

2.4.4 Type of the polymer matrix

Polymers are classified into elastomers, thermoplastics, and thermosets in terms of their molecular force. Elastomer has good stretchability, as the molecular force in elastomer is the weakest among the four types of polymers. Thermoplastics and thermosets are two commonly used in plastic products. Thermoplastics become soft when being heated and can be molded to a desired shape. Thermosets become solid and infusible when heated. The difference between thermoplastics and thermosets is that thermoplastics will not form any cross-link, but thermosets will form cross-links between polymer chains and form a 3D structure when heated. Various kinds of polymers have been used as the polymer matrix of CNPCs. The property of the polymer matrix that would affect the performance of CNPC

is Young's modulus. The polymer matrix performs as an agent to transfer the deformation to the resistance change of the CNPC.

Choosing the polymer matrix of the CNPC tactile sensor needs to trade-off between the sensitivity and the measurement range. If a polymer with low Young's modulus is used as the matrix, the CNPC tactile sensor would have a relatively higher sensitivity but smaller measurement range. If a polymer with high Young's modulus is used as the matrix, the CNPC tactile sensor would have a relatively lower sensitivity but a larger measurement range. This is because the polymer with lower Young's modulus would have a larger deformation under the same pressure and lead to a larger resistance change.

It is worth mentioning that there is a type of polymer with its Young's modulus varying with the change of the composition ratio of the raw materials. Patel et al. (2017) reported a family of highly stretchable and ultraviolet (UV) curable elastomers that are made from the curing epoxy aliphatic acrylate (EAA) and aliphatic urethane diacrylate (AUD) in different mixing ratios. This type of elastomer has tunable Young's modulus and high stretchability, which is suitable as the substrate of the CNPC tactile sensor. Patel et al. (2017) coated silver nanoparticles on the surface of the elastomer to make a soft conductive switch (Figure 2.7). In Chapter 3, the feasibility of developing the CNPC tactile sensor by taking this elastomer as a polymer matrix, into which carbon nanomaterials were distributed, was studied.

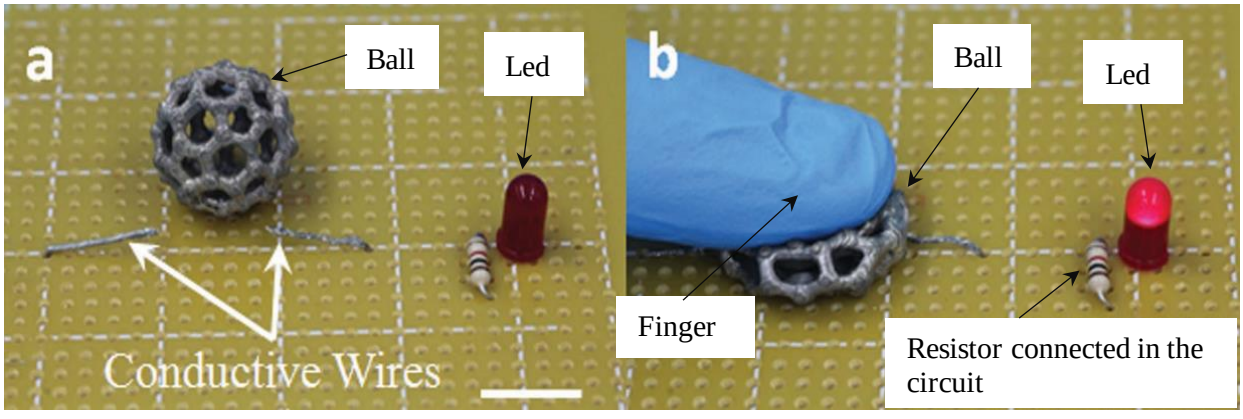

Figure 2.7 Use an EAA/AUD elastomer ball coated with silver nanoparticles as a soft conductive switch (Patel et al., 2017). (a) An EAA/AUD elastomer ball completely coated with silver nanoparticles. (b) A LED turns on after the ball is compressed and the two conductive wires are connected (Patel et al., 2017).

There are several methods to pretreat the polymer matrix to achieve a better performance of the CNPC tactile sensor. Li et al. (2019) proposed a micro-porous structure of the polymer matrix that increases the sensitivity (gauge factor over 300) and gets a wide range of applied pressure (1 Pa to 25 kPa) at the same time. The enhanced sensitivity is attributed to the nanoscale porous structure of the polymer matrix for the increased interaction surface. Another method of the treatment of the polymer matrix is stretching. Fan et al. (2021) fabricated a tactile sensor made from the SWCNT/$Ti_3C_2T_x$MXene composite film. They used a thermal shrinkage method to create a crumpled structure of the composite surface and got a wide measurement range. The increased measurement range is because the cramped structure increases the deformation limitation of the matrix.

In conclusion, the polymer matrix has the direct impact on the performance of the CNPC tactile sensor. Choosing the polymer matrix with lower Young's modulus can lead to higher sensitivity of the CNPC tactile sensor, but its drawback is that the sensing range of the CNPC tactile sensor will be smaller. Methods including creating porous structure and pre-stretching can be taken to overcome the drawback.

2.5 Context and performance of the CNPC tactile sensor

Different CNPC tactile sensors have been fabricated and applied in various application contexts. Most of the CNPC tactile sensors are applied as a single sensor. However, to extend the sensing coverage, CNPC sensors are lined in sensor networks to function as a sensing system. The performance of a single CNPC tactile sensor or a sensor network is measured by several indexes, including gauge factor, linearity, repeatability, resolution, response and recovery time, and durability (Yuan et al., 2021). Among these indexes, gauge factor is the most important one. This dissertation concerned the gauge factor as the

performance of the single tactile sensors. For tactile sensing systems, there is no clear definition of the sensitivity of a CNPC tactile sensing system. Therefore, in this dissertation, the gauge factor of the single tactile sensor is used as the sensitivity of the tactile sensing system. It is because the tactile sensing system is composed of a tactile sensor network and the sensitivity of the tactile sensing system is determined by the tactile sensors. Various CNPC tactile sensors and sensor networks were reported. Table 2.5 lists several tactile sensing systems based on CNCP along with their structures and performances.

Table 2.5 Tactile sensing systems based on CNPC.

Structure	Nanomaterial	Matrix	Loading	Performance	Reference
Single sensor	Graphene	Polysilicon	6.8 vol%	Gauge factor = 535	(Boland et al., 2016)
Single sensor	Carbon black	SEBS–Block copolymer	50 wt%	Gauge factor = 20	(Mattmann et al., 2008)
Single sensor	MWCNT	Polysulfone	0.5 wt%	Gauge factor = 2.78	(Oliva-Avilés et al., 2011)
Band	Graphene	Rubber	0.2 vol%	Gauge factor = 35	(Boland et al., 2014)
Band	Reduced graphene oxide	VHB elastomer	-	$S = \frac{\Delta R/R}{\Delta P} = 1.37 kpa^{-1}$	(Chang et al., 2019)
5 × 5 array	MWCNT	Polydimethylsiloxane	7 wt%	ΔR/R0 = 0.6	(Kong et al., 2015)
16 × 17 array	Carbon black	Polymer foam	-	-	(Göger & Wörn, 2007)
6 × 8 array	MWCNT	Polydimethylsiloxane	6 wt%	$S = \frac{\Delta R/R}{\Delta P} = 16.9 kpa^{-1}$	(Sun et al., 2018)
Serpentine structures	Carbon black	Polydimethylsiloxane	25 wt%	Gauge factor = 29.1	(Lu et al., 2012)
11 × 11 array	MWCNT	Thermoplastic Polyurethane	11.1 wt%	Gauge factor = 2800	(He et al., 2019)
Rosette-type	Carbon black	Polydimethylsiloxane	15 wt%	-	(Kong, Jang, et al., 2014)
8 × 8 × 2	-	Conductive polymer	-	-	(Cheng et al., 2011)
5 paddings	Graphite	Rubber	-	-	(Chen, et al., 2016)

14 lines	MWCNT	Acrylate monomer	1 wt%	-	(Vatani et al., 2013)

From Table 2.5, it can be seen that different loadings, polymer matrixes, carbon nanomaterials, structures lead to different performances. The better performance, as discussed above, is due to the appropriate volume content, polymer matrix with lower Young's modulus, and better homogeneous distribution. There are two tactile sensing systems that have relatively high gauge factors. One was proposed by Boland et al. (2016). The tactile sensor was produced by filling graphene in a highly viscoelastic silicone polymer and achieved the gauge factor higher than 500 (Boland et al., 2016). From Figure 2.8, it can be seen that the highest value of gauge factor of the tactile sensor is 535 when the volume content of graphene is 6.8%. The ultrahigh sensitivity of the tactile sensor is due to the soft polymer matrix they used, which is a lightly crossed-linked silicone polymer, commonly known as Silly Putty. However, its working strain range is limited at 0-2%. The other highly sensitive tactile sensor was reported by He et al. (2019). The gauge factor of He's tactile sensor achieved 2800 in the working strain range of 5-100% (He et al., 2019). However, the sensor has the hysteresis of resistance change when the strain is higher than 20%. Hysteresis would affect the repeatability and accuracy of the tactile sensing. The limited working strain range and hysteresis happened frequently on highly sensitivity tactile sensors. The hysteresis property is intrinsically caused by the principle of the CNPC tactile sensor.

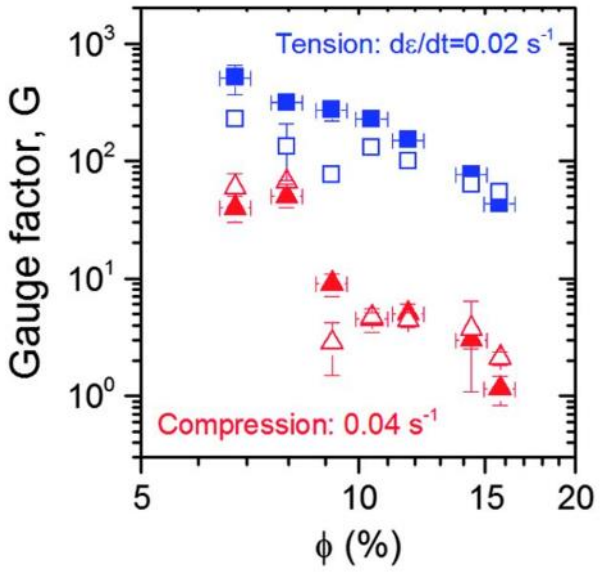

Figure 2.8 Gauge factor of the graphene filled silicon composite tactile sensor (Boland et al., 2016).

As the single sensor has a limited coverage, researchers developed different structures of sensor networks to cover a larger area. Sun et al. (2018) fabricated a 6 × 8 tactile sensor network that can work stably from -20 to 50 °C. The tactile sensor of the network was fabricated by filling the MWCNT into the polydimethylsiloxane (PDMS) composite (Sun et al., 2018). However, this sensor network has a poor linearity of resistance change versus pressure. Despite its high sensitivity, there is a notable hysteresis of resistance change in the 100-300 pa pressure range.

Chang et al. (2019) developed a stretchable pressure sensor for surgical robots. This stretchable pressure sensor is fabricated by the coating reduced graphene oxide on the surface of a VHB elastomer. The attractive part of this sensor is its wrinkle architecture, which is made by pre-stretching the elastomer before coating. The winkle architecture allows the sensing space for stretching. They applied this tactile sensor on surgical robots. However, the problem with this tactile sensor is that the whole band is the sensing element that cannot locate the accurate position of the applied strain.

Another tactile sensing system was fabricated by coating the carbon nanomaterials on the surface of a CNPC by Chen et al. (2016). They coated the graphene-filled latex on the rubber and observed the piezo resistive response from the sensor. Cheng et al. (2011) developed an 8 × 8 × 2 sensor network that can sense the twist force and irregular distribution force (Figure 2.9). The tactile sensor was fabricated by filling carbon nanomaterials into a conductive polymer. The two-layer structure enables it with extra sensing abilities. This sensing system has a poor linearity of the resistance change versus the pressure and resistance change versus the twisting angle. Another problem is that wires are needed to collect resistance change from each electrical circuit of the tactile sensor. The signal collection system restrains its application.

Based on the analysis above, there are different types of tactile sensing systems made from CNPCs. To a single tactile sensor, it has a relatively simple system for data collection. A sensor network can enlarge the sensing coverage. Different structures of sensor networks are developed, including the band, serpentine, rosette-type, and array. The more complicated structure, the more complicated data collection for the sensing system. The array structure is a commonly used one for the tactile sensor network. In literature, the sensitivity of the tactile sensing system is determined as the sensitivity of the tactile sensor. Few researchers discussed the other technical specifications of a CNPC tactile sensing system, including the sensing coverage area, minimum detectable force, and number of sensors per unit area.

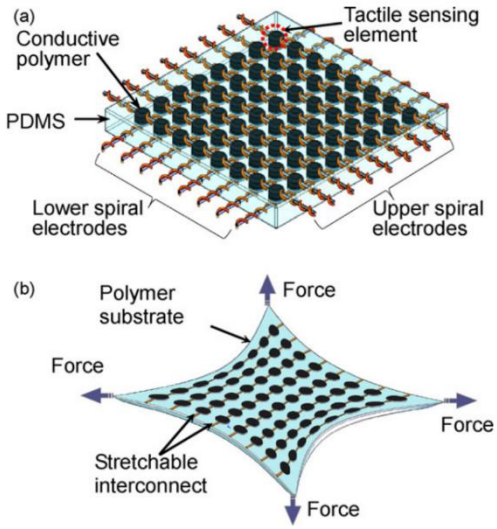

Figure 2.9 (a) The schematic of a tactile sensing system. (b) The sensing system under stretching (Cheng et al., 2011).

2.6 Design methodology for the CNPC tactile sensing system

Some prototypes of CNPC or other nano-filler material tactile sensors as well as their networks were developed in literature. Design methods for these prototypes have been implied. For instance, Ji et al. (2016) developed a flexible tactile sensing array for the robotic skin. The sensing principle for a single sensor is based on the capacitive principle, and the network is an array. The design does not start with the specification of requirements derived from the robot on which the sensor network is supposed to wrap. As such, their design cannot be fully explored for other robotic applications. Fan et al. (2021) proposed a wearable tactile sensor that has broad measurement range. The sensor was developed based on the $Ti_3C_2T_x$MXene /SWCNT composite. The prototype was tested to have a measurement range from 33 Pa to 130 kPa with a high sensitivity (116.15 kPa^{-1} bellow 40 kPa and 12.7 kPa^{-1} at $40 - 130$ kPa). A 4×4 sensor array was built based on the tactile sensor and was applied to monitor finger movements, voice detection and wrist pulse. Again, the generality of their design is as similar as that of the design of Ji et al. (2016).

It appears that there is no systematic design approach available in literature, which starts with the technical specification of the requirements for skin sensors for specific HuBots and ends at the design that can be manufacturable. Certainly, there is no study on how to make a robotic skin that can be adaptable, so the skin can be resilient (Zhang and Luttervelt, 2011; Zhang and Lin, 2010).

2.7 Conclusions

In this chapter, various single CNPC tactile sensors and sensing systems (or networks of sensors) were comprehensively reviewed in terms of their structures, states, principles, contexts, and design processes. Conclusions can be drawn as follows:

(1) The principle of CNPC tactile sensor has two types, i.e., conductive pathway reforming and electron hopping. It remains unknown which one is governing the conductivity of the CNPC piezo resistance response.

(2) The distribution of carbon nanomaterials has a direct impact on the performance of the CNPC tactile sensor. The homogeneous distribution of nano-fillers in polymer matrixes is important factor to the performance of the CNPC tactile sensor.

(3) The volume content of carbon nanomaterials influences the sensitivity of the CNPC tactile sensor. When the volume content of carbon nanomaterials reaches the percolation threshold, the CNPC becomes conductive. The highest sensitivity of a CNPC tactile sensor is achieved when the volume content of carbon nanomaterials is near the percolation threshold.

(4) The polymer substrate would also influence the sensitivity of the CNPC tactile sensor. The lower Young's modulus the polymer substrate has, the higher sensitivity the CNPC tactile sensor.

(5) There is a high degree of uncertainty in the fabrication of such sensors.

(6) For the single CNPC tactile sensor, the limited sensing coverage restrains its application. A tactile sensor network is preferred to expand its sensing coverage.

(7) The increasing number of tactile sensors in a network makes the wiring of the tactile sensing system complicated. A better wiring is needed to simplify the procedure.

(8) The development of a tactile sensing system lacks a systematic design methodology, and the sensing system is not adaptable.

(9) The technical specifications of a tactile sensing system need to be considered in the design approach, including the sensitivity, sensing coverage area, number of sensors per unit area, and minimum detectable force.

Further, the discussion in this chapter shows the need of the proposed objectives in Chapter 1 for this dissertation. Specifically, Conclusions (2) and (4) above will support the need of the first objective, i.e., to conduct a comprehensive study on how a single CNPC sensor can be fabricated. Conclusion (8) and (9) will support the need of the second objective, i.e., a systematic design methodology is warranted. Finally, a prototype that can demonstrate a soft substrate sensor network with some new features such as adaptability is significant to the field of robotic skin for sensing the environment including human operators and other objects.

CHAPTER 3
SINGLE TACTILE SENSOR AND ITS FABRICATION

3.1 Introduction

This chapter presents the work related to Objective 1, i.e., design and fabrication of a single CNPC tactile sensor, specifically study of the modulation of the structure of the sensor for different Young's modulus. The polymer substrate of the CNPC is composed of the curing epoxy aliphatic acrylate (EAA) and aliphatic urethane diacrylate (AUD), inspired from the work of Patel et al. (2017). Modulation in this case means to change the ratio of the materials (EAA and AUD). Two fabrication techniques for making such CNPC tactile sensors were attempted: distributing carbon nanomaterials into the solution of the polymer (Section 3.2) and coating carbon nanomaterials onto the surface of the polymer (Section 3.3). It is noted that the research methodology is experimental, and the testing of Young's modulus was by means of the Instron 3363, which can be found in Appendix A. There is a discussion and conclusion in Section 3.4.

3.2 Carbon nanomaterial filled EAA/AUD tactile sensors

EAA and AUD were selected as the polymer materials, as according to Patel et al. (2017), a different mixing ratio of EAA and AUD can lead to different Young's modulus[1]. There are two steps to make such a sensor, namely (1) fabricating the polymer with varying Young's modulus and (2) dispensing carbon nanomaterials, CNTs in this case, into the polymer solution. Three methods were attempted: the photo initiator method, thermal initiator method, and redox initiator method. The photo initiator method was chosen due to the successful construction of the EAA/AUD polymer by Patel et al. (2017), and in this dissertation, it was considered as a reference control system. However, dispensing carbon nanomaterials into the polymer solution was not attempted by Patel et al. (2017). The

[1] Young's modulus here may be better called stiffness associated with the pressure force and displacement along the force direction. However, without confusion, this dissertation still uses this term.

thermal initiator method was chosen because the high reaction temperature may increase the fluidity of the resin and therefore help the distribution of the carbon nanomaterials in the EAA/AUD polymer solution. The redox initiator method was chosen because there are no air bubbles generated in the reaction in the fabrication process.

3.2.1 The CNT filled EAA/AUD composites with the photo initiator method

There are two steps to construct such composites. The first step is to construct the EAA/AUD polymer (Section 3.2.1.1) and the second step is to disperse CNTs into the polymer solution (Section 3.2.1.2)

3.2.1.1 Fabrication of the EAA/AUD polymer with the photo initiator method

Six elastomers or composite samples made by mixing EAA and AUD were fabricated, see Table 3.1. Specifications for the fabrication are as follows:

- **Method**: Light curing with photo initiator.
- **Raw material**: Epoxy aliphatic acrylate (EAA), aliphatic urethane diacrylate (AUD).
- **Photo initiator**: Trimethyl benzoyl diphenyl phosphine oxide (TPO).
- **Solvent**: Dichloromethane (DCM).

Table 3.1 Elastomers with different mixing ratios of EAA and AUD.

Number	Content of EAA (g)	Content of AUD (g)	Total (g)	Weight ratio (EAA/AUD)
1	1.333	2.665	3.998	0.5
2	2.002	2.001	4.003	1
3	2.669	1.335	4.004	2
4	3.003	1.005	4.008	3
5	3.197	0.802	3.999	4
6	3.339	0.669	4.008	5

The fabrication process has the following steps:

(1) Add EAA and AUD with specific weight ratios listed in Table 3.1 into a beaker.

(2) Add 10 ml DCM into the beaker and stir for 5 minutes.

(3) Place the beaker on a hotplate at 70℃ and stir for 20 hours with a magnetic stir bar.
(4) Add 80 mg TPO into the solution as the photo initiator and stir for another 5 minutes.
(5) Use an ultraviolet light to cure the resin from the top for 30 minutes (Figure 3.1a).

The features of UV light used are listed in Table 3.2. To get the compressive modulus, a set of EAA/AUD elastomer samples with 31 mm diameter and 4 mm thickness are fabricated (Figure 3.2) with the mixing ratio listed in Table 3.1. For each mixing ratio, 5 samples are tested by the Instron 3363 and the average value was calculated as the compressive modulus. The details of the testing are attached in Appendix A. The compressive modulus of the EAA/AUD elastomers with different mixing ratios are shown in Figure 3.3. The result shows the change of Young's modulus with the change of the EAA/AUD mixing ratio. The higher the ratio of EAA/AUD, the smaller Young's modulus the polymer composite.

Table 3.2 Features of the UV light.

Wavelength	Class	Irradiation Distance	UV Light Spot Size	UV Light Intensity
365±5 nm	UVA	25 mm	ϕ10 mm	1000 mw/ cm²

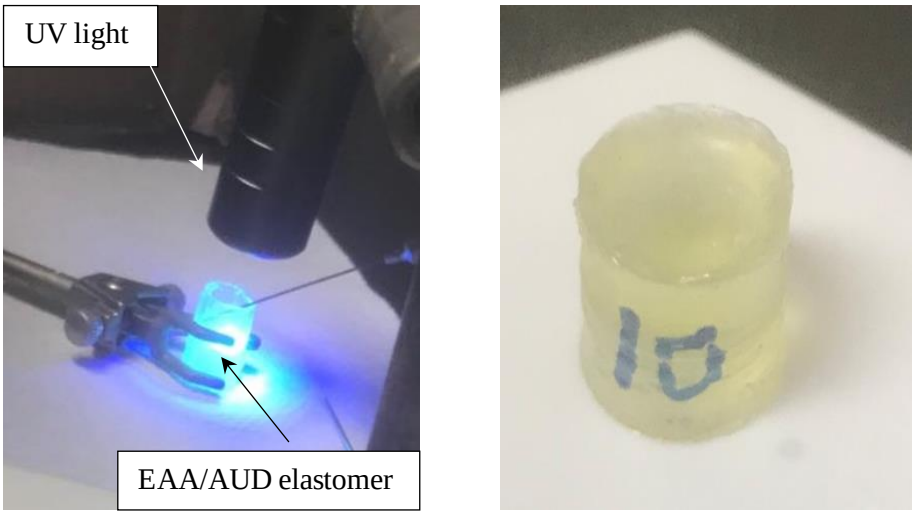

(a) (b)

Figure 3.1 (a) UV light curing the EAA/AUD polymer; (b) The cured EAA/AUD polymer sample.

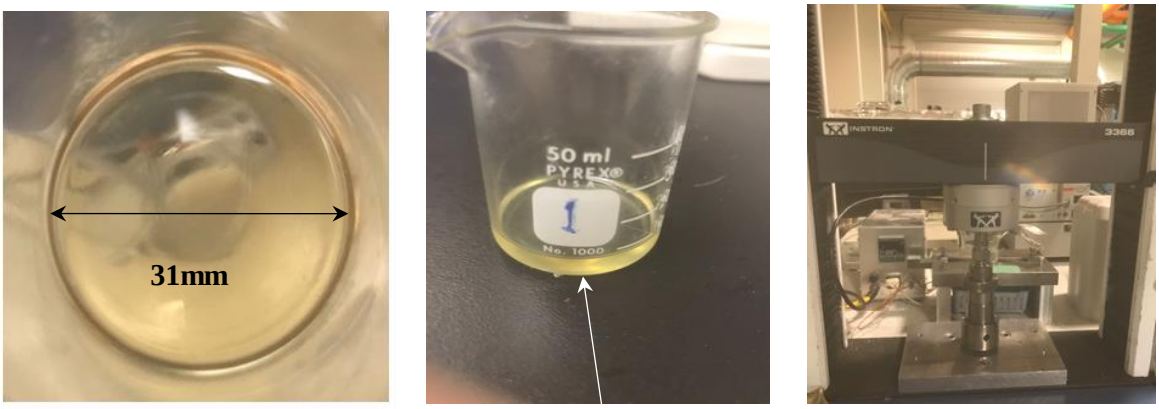

Diameter of the EAA/AUD elastomer sample for testing

EAA/AUD elastomer

Instron 3363

(a) (b) (c)

Figure 3.2 (a) and (b) show the sample for compressive modulus testing; (c) Compressive modulus testing by Instron 3363.

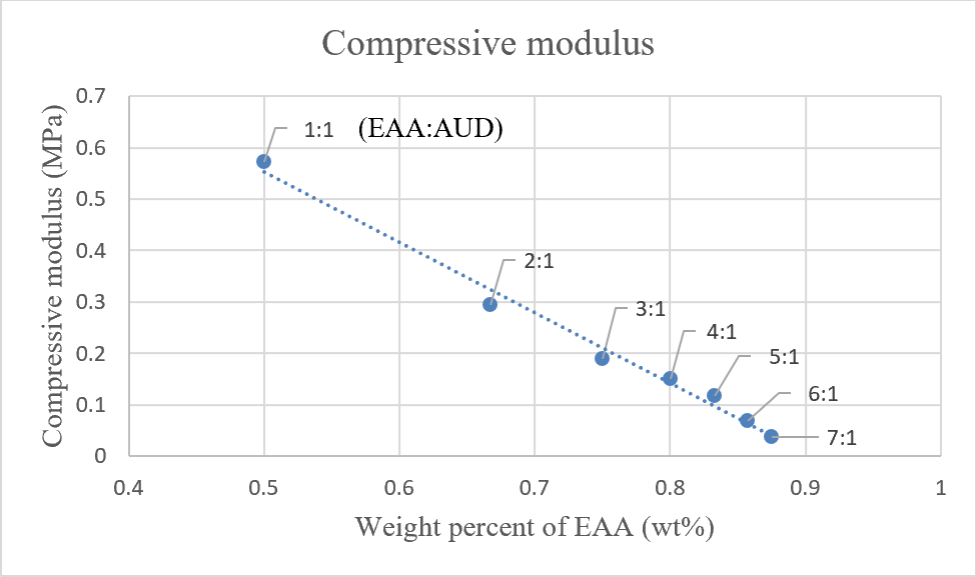

Figure 3.3 The compressive modulus of EAA/AUD polymer with the mixing ratio from 1:1 to 7:1.

3.2.1.2 Dispersion of CNTs into the EAA/AUD polymer solution

MWCNTs were chosen to be distributed into the EAA/AUD resin, because MWCNTs have lower surface areas and higher aspect ratios, which enable good dispersibility and high electrical conductance of polymer matrixes (Nurazzi et al., 2021). Sodium Dodecyl Sulfate (SDS) was chosen as the surfactant to facilitate the dispersion of MWCNTs into the resin as SDS was shown feasible in the previous work of (Miao, 2013). The specification of the fabrication is as follows:

- **Method:** Photo initiator method.
- **Material:** 375 mg epoxy aliphatic acrylate (EAA), 125 mg aliphatic urethane diacrylate (AUD), 5 mg MWCNT.
- **Photo initiator:** 10 mg trimethyl benzoyl diphenyl phosphine oxide (TPO).
- **Surfactant:** 5 mg SDS.
- **Solvent:** 5 ml dichloromethane (DCM).

The fabrication process is as follows:

(1) Add 375 mg EAA and 125 mg AUD into a beaker.

(2) Add 5 ml DCM into the beaker and stir for 5 minutes.

(3) Add 5 mg MWCNT and 5 mg SDS into the beaker and stir for 5 minutes.
(4) Use an ultra-sonification probe (Branson sonifier 150) to sonicate the solution for 1 hour.
(5) Place the beaker on a hotplate at 70℃ and stir for 20 hours with a magnetic stir bar.
(6) Add 10mg TPO into the solution as photo initiator and stir for 5 minutes.
(7) Move the solution to a transparent tube.
(8) Use an ultraviolet light to cure the solution for 30 minutes.

The result is shown in Figure 3.4. Only the surface of the solution was cured. Ultraviolet light was used as it has higher energy than visible light and infra light. The problem was that the ultraviolet light cannot penetrate the material to a sufficient depth when the carbon nanomaterial was added (diffraction between the carbon nanomaterial in the polymer). From the experimental result it was found that the 5 wt% MWCNT added in the polymer failed to reach the percolation threshold of the piezo resistance, because none of the fabricated samples are conductive. Ultraviolet light can only penetrate the polymer filled with 5 wt% MWCNT to around 0.5 mm depth at maximum.

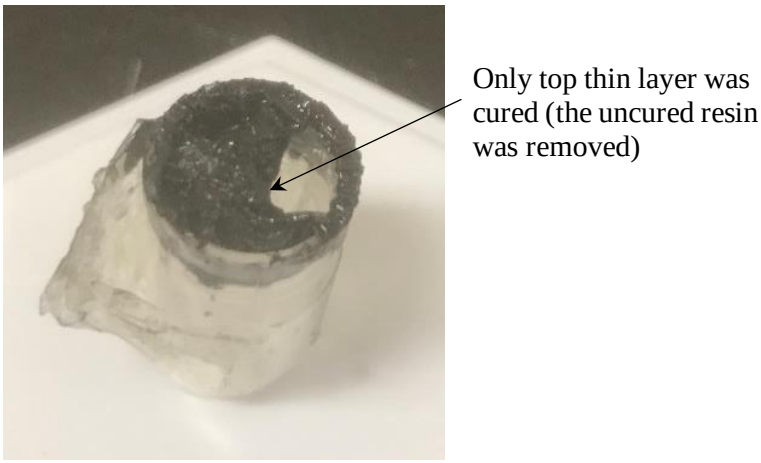

Figure 3.4 The cured part of the resin.

In conclusion, the light curing for EAA/AUD polymer filled with carbon nanomaterials has a dilemma. On the one hand, it requires a high energy light, such as the ultraviolet light,

to trigger the release of free radicals from the photo initiator for curing. On the other hand, a high energy light has a short wavelength that can only penetrate (or diffract) into a thin layer throughout the polymer. This dilemma limits the application of the light curing method. This is an interesting finding for the usage of the light curing method in resin filled with carbon nanomaterials. The curing depth is related with the weight percentage of the carbon nanomaterials, the wavelength, and the intensity of the UV light. It can also be a future work for 3D printing of the carbon nanomaterials filled EAA/AUD polymer composite.

3.2.2 The EAA/AUD polymer with the thermal initiator method

Dibenzoyl peroxide (BPO) was used as the thermal initiator. It can help cure the resin after heated. The specification of the fabrication is as follows:

- **Method**: Thermal initiator method.
- **Material**: 1.5 g epoxy aliphatic acrylate (EAA), 0.5 g aliphatic urethane diacrylate (AUD).
- **Thermal initiator**: 20 mg BPO.
- **Solvent**: 10 ml dichloromethane (DCM).

The fabrication process is as follows:

(1) Add 1.5 g EAA and 0.5 g AUD into a beaker.
(2) Add 10 ml DCM into the beaker and stir for 5 minutes.
(3) Place the beaker on a hotplate at 60 ℃ and stir for 20 hours with a magnetic stir bar.
(4) Add 20 mg BPO into the solution as the thermal initiator and stir for 5 minutes.
(5) Increase the temperature of the hotplate to 110 ℃ for 5 minutes.

The EAA/AUD polymer was cured but several air bubbles occurred in the body of the polymer (Figure 3.5). The air bubbles were distributed randomly in the body of the cured resin. The sizes and shapes of the air bubbles were different from each other. This phenomenon is because the thermal initiator BPO may decompose and generate carbon dioxide when heated. To keep BPO releasing free radicals for curing, the release of carbon

dioxide cannot be avoided. One solution is to control the speed of the decomposition of BPO and to eliminate the carbon dioxide once generated. Several studies in literature discussed the decomposition of BPO in different solvents, e.g., Bartlett & Nozaki (1947), Swain et al. (1958), and Barnett & Vaughan (1947). According to (Barnett & Vaughan, 1947), the speed of decomposition of BPO is different in different solutions. However, there is no study in literature that discusses the decomposition of BPO in the solution of the mixed EAA and AUD. Different methods were tried to eliminate the carbon dioxide, including lowering the curing temperature and putting the solution in a vacuumed environment when heated. This dissertation attempted to address the issue of bubbles removal, which is presented in the following.

The decomposition of BPO is affected by several factors, which are the temperature, solvent, and volume content of BPO. The vacuumed environment was achieved by using an air pump, a glass tube, and a cylindrical-shaped oven (Figure 3.6). Comparative experiments were conducted, and the result is shown in Table 3.3. For each experiment, 5 samples were fabricated. The result was compared by the measurement of CO_2 bubbles volume content. Figure 3.7 shows the samples of Experiment 1 and Experiment 2.

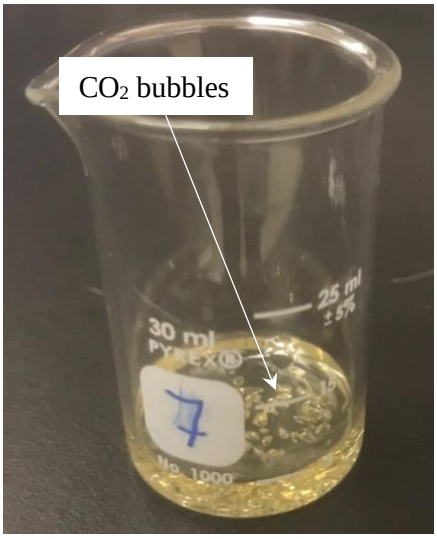

Figure 3.5 Air bubbles occur in the EAA/AUD polymer.

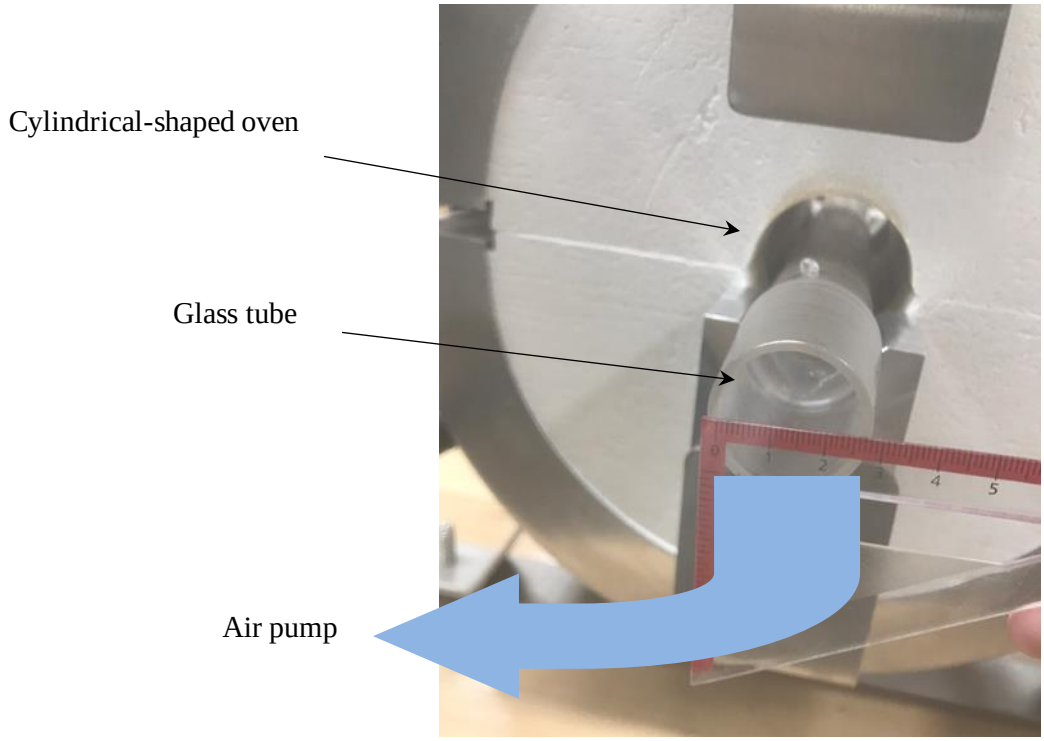

Figure 3.6 Vacuumed glass tube in the oven.

Table 3.3 Comparative experiments of the thermal method.

Experiment	Curing temperature	Curing time	Vacuum environment	Result (approximate volume content)
1	110 ℃	1 hour	No	Full
2	110 ℃	1 hour	Yes	Full
3	100 ℃	3 hours	No	~50%
4	100 ℃	3 hours	Yes	~50%
5	90 ℃	72 hours	No	A few bubbles inside the polymer
6	90 ℃	72 hours	Yes	A few bubbles mainly on the surface of the polymer

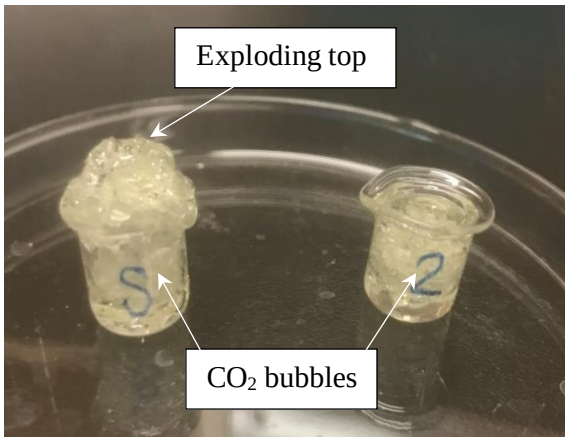

Figure 3.7 The result of Experiment 1 and 2. The left beaker labeled ‘S’ is the result of Experiment 1 and the right beaker labeled ‘2’ is the result of Experiment 2.

In Figure 3.7, the left beaker (the result of Experiment 1) showed that carbon dioxide was generated in the reaction and the sample contains many bubbles. The EAA/AUD resin was cured immediately, and the bubbles were contained in the polymer. Compared with Experiment 1, the result of Experiment 2 (Figure 3.7) did not have an exploding top. This is because the sample of Experiment 2 was placed in a vacuumed environment and part of the carbon dioxide generated was exhausted immediately during the reaction. Therefore, it can be concluded that the vacuumed environment is helpful for removing bubbles generated during the reaction. However, bubbles cannot completely be removed, because some bubbles get trapped during the polymerization of the resin. Even if the speed of the reaction was relatively slow at 90 ℃, there were still some bubbles trapped in the polymer (Figure 3.8).

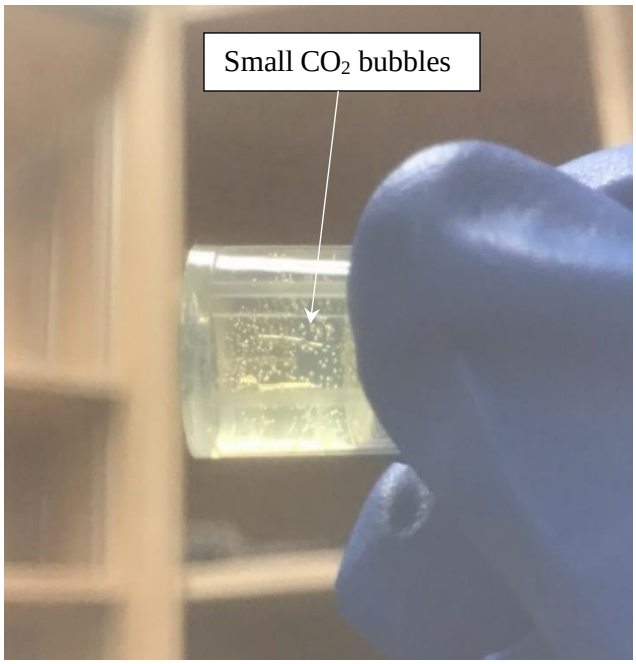

Figure 3.8 An EAA/AUD sample with small bubbles inside.

In conclusion, the speed of the decomposition of BPO can be controlled by lowering the reaction temperature, and the vacuumed environment helps exhaust bubbles out of the polymer. However, the method of thermal curing with BPO cannot completely clear the bubbles.

3.2.3 The EAA/AUD polymer with the redox initiator method

For the curing of the EAA/AUD resin, free radicals are needed for the curing process. Apart from the decomposition of peroxide that can release free radicals, redox reactions can also release free radicals. N,N-Dimethylaniline (DMA) and BPO are commonly used as the reduction agent and the oxidant to have a redox reaction, which generate free radicals for curing. To solve the CO_2 bubble problem in Section 3.2.2, the redox reaction was tried to cure the EAA/AUD resin.

The experiment of curing the EAA/AUD resin with a redox initiator was conducted with the following specification:

- **Method**: Redox initiator method.
- **Material**: 1.5 g epoxy aliphatic acrylate (EAA), 0.5 g aliphatic urethane diacrylate (AUD).
- **Redox initiator**: 9 mg DMA and 20 mg BPO.

The experiment process is as follows (Figure 3.9):

(1) Add 1.5 g EAA and 0.5 g AUD into the beaker A, and the same amount into the beaker B.
(2) Place the beaker A and B on a hotplate at 60 ℃ and stir for 10 minutes.
(3) Add 9 mg DMA into the beaker A and stir until completely dissolved. Add 20 mg BPO into the beaker B and stir until completely dissolved.
(4) Mix the beaker A and B into the beaker C and stir with a magnetic stir bar for 1 minute.
(5) Place the beaker C on the hotplate at 60 ℃ for 3 hours.

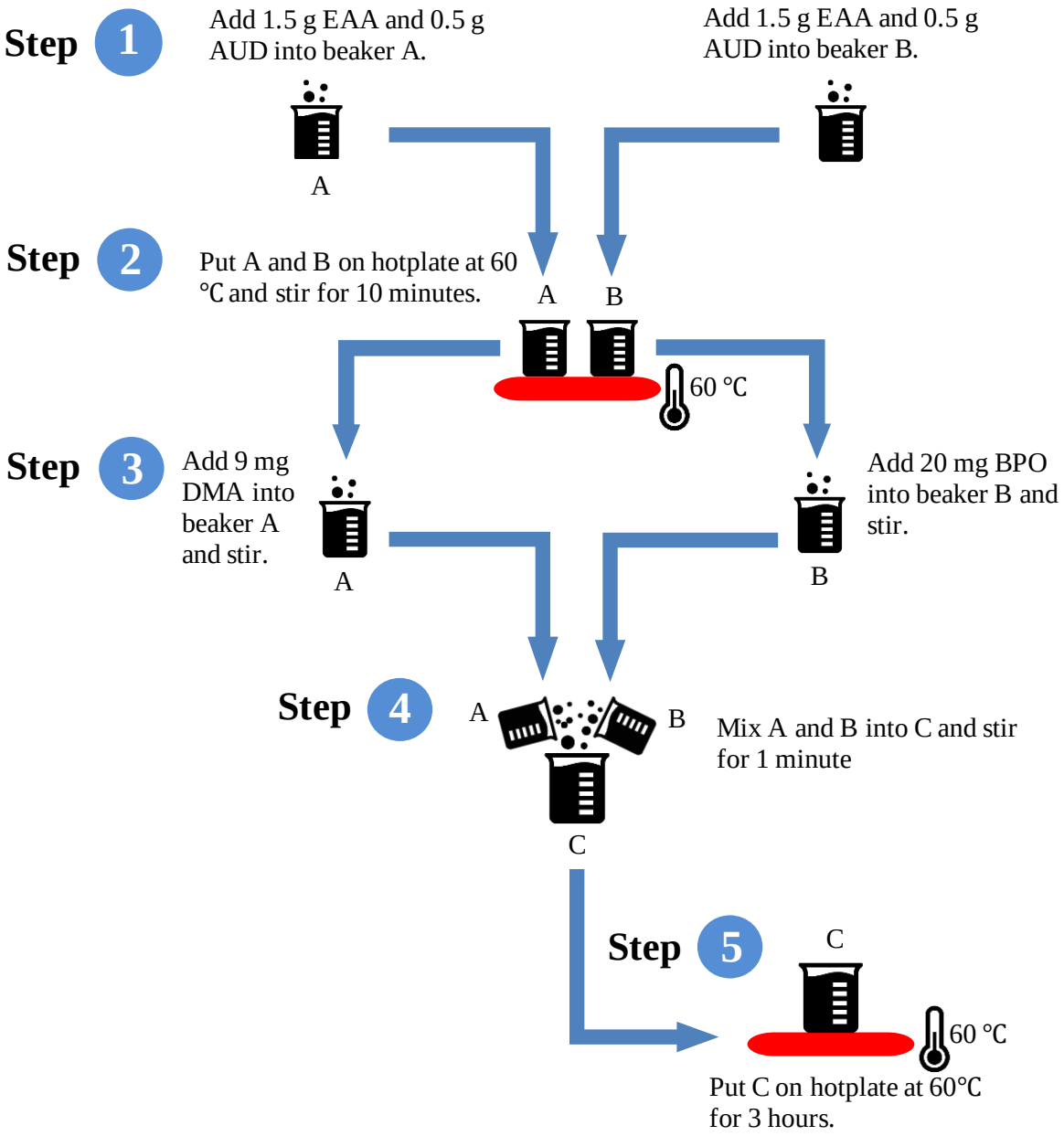

Figure 3.9 The curing procedure of the redox initiator method.

The result showed that this method was feasible for curing the EAA/AUD resin (Figure 3.10). The EAA/AUD resin was cured without bubbles inside.

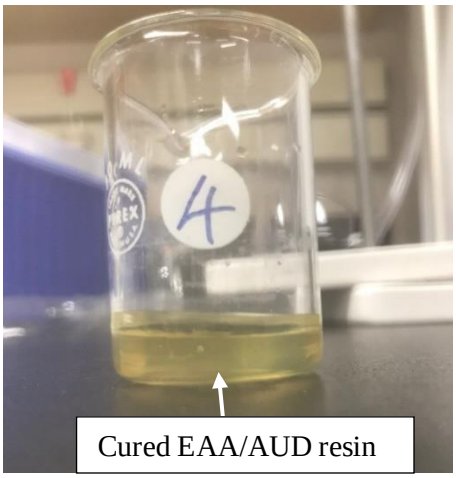

Figure 3.10 The cured EAA/AUD resin by redox initiator method.

Based on the procedure of the redox initiator method (Figure 3.9), MWCNTs were put into the EAA/AUD resin between Step 2 and Step 3. The procedure of adding MWCNTs is as follows:

(1) Take 800 mg solution from the beakers A and B into two sealable plastic containers, named 'X' and 'Y', respectively. (the beakers A and B are referred to A and B in Figure 3.9)

(2) Add 12 mg MWCNT and 8 mg SDS into the container X and the same amount into the container Y. Sonicate the containers X and Y with an ultra-sonification probe (Branson sonifier 150) for 5 minutes.

(3) Seal the plastic containers X and Y and place them in the ultrasonic cleaner (Branson 3510) for 3 hours with the water bath temperature at 60 ℃.

After the MWCNTs were dispersed in the containers X and Y, Step 3 was adding 3.6 mg DMA into the container X and adding 8 mg BPO into the container Y. Step 4 is mixing the containers X and Y into the beaker C and stirring for 1 minute (the beaker C is referred to C in Figure 3.9). Step 5 remained unchanged.

There are three remarks for the fabrication procedure. First, the temperature of the EAA/AUD resin should be kept at 60 ℃ to increase the fluidity of the resin and help dissolve the additives. The lower temperature may cause incompletely dissolve, and higher temperature may cause the fast decomposition of BPO before the redox reaction. Second,

when placing the plastic container into the ultrasonic cleaner, the liquid level inside the container should be lower than the liquid level of the water bath. Third, SDS was added as the surfactant to help the distribution of MWCNT.

The samples with different contents of MWCNT and SWCNT were fabricated with this method for comparison. For testing, a PDMS soft mold was used. The resin in Step 4 after mixing was poured into the PDMS mold instead of the beaker C. Then the PDMS mold with the resin was placed in an oven at 60 ℃ for 3 hours. Figure 3.11 shows the PDMS mold with the MWCNT filled EAA/AUD composite. After curing, the MWCNT filled EAA/AUD composite had a radius of 1 mm and thickness of 1.5 mm. A homemade measurement tool was used to test the force applied and the resistance change. The homemade measurement tool is composed of a micrometer, four-point resistance measurement probes, a force sensor, and a frame (Figure 3.12). The deformation of the MWCNT filled EAA/AUD composite was measured by the micrometer. The resistance of the composite was measured by four-point probes, and the signal was sent to JANDEL RM3000 test unit. The force applied on the composite was measured by a force sensor (Figure 3.12) along with a self-programed software application.

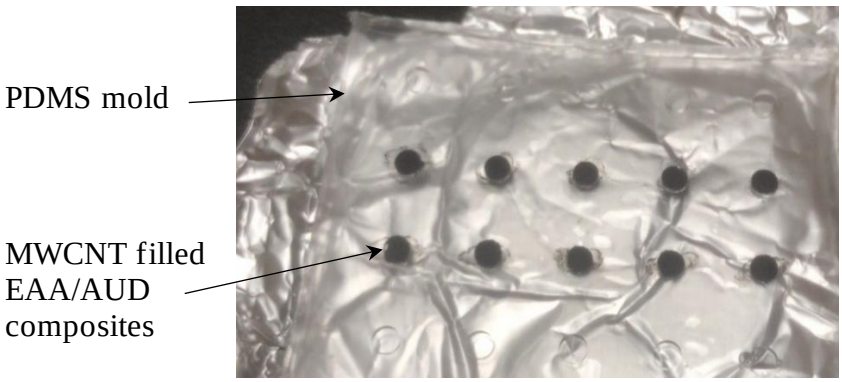

Figure 3.11 The PDMS mold with MWCNT filled EAA/AUD composites.

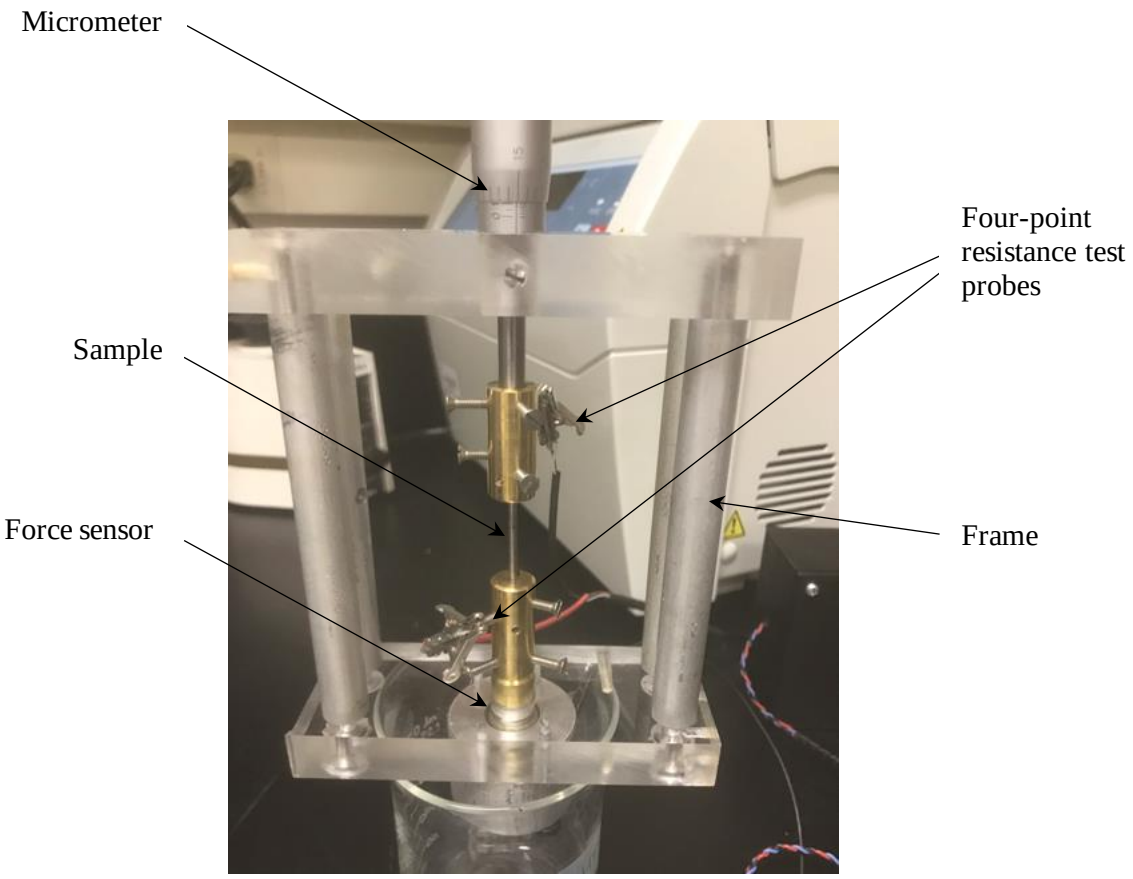

Figure 3.12 The homemade measurement tool.

By means of the redox initiator method and the set of measurement tools, SWCNT and MWCNT were filled into the EAA/AUD polymer with different contents for testing of the tactile sensing ability. For the SWCNT filled EAA/AUD composites, 1 wt%, 2 wt%, and 5 wt% of SWCNT dosage, had been fabricated and tested for the resistance. The EAA/AUD composites filled with 1 wt% and 2 wt% SWCNT were not conductive, and the composites filled with 5 wt% SWCNT were conductive. Therefore, the percolation threshold of the SWCNT filled EAA/AUD composite was between 2 wt% and 5 wt%. The EAA/AUD composites filled with 5 wt% SWCNT were further tested for its tactile sensing performance (Figure 3.13). For the MWCNT filled EAA/AUD composite, the result was like the SWCNT filled EAA/AUD composite. The EAA/AUD composites filled with 1 wt% and 2 wt% were not conductive. The EAA/AUD composites filled with 5 wt% were conductive. The performances of the EAA/AUD composites filled with 5 wt% MWCNT are shown in Figure 3.14. Table 3.4 and Table 3.5 show the resistance change and

deformation when a force is applied onto the 5 wt% SWCNT filled EAA/AUD composite and the 5 wt% MWCNT filled EAA/AUD composite, respectively.

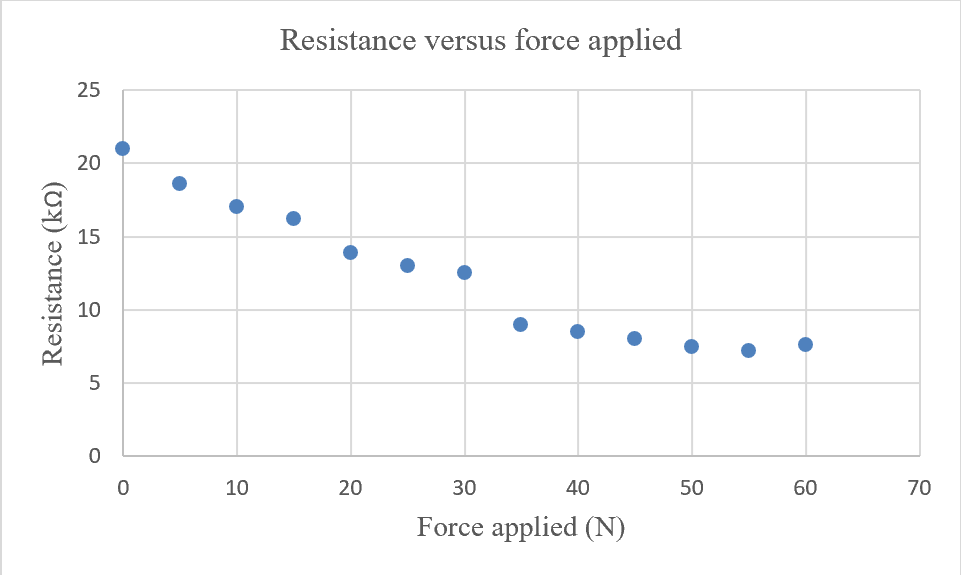

Figure 3.13 The resistance change of the 5 wt% SWCNT filled EAA/AUD composite.

Table 3.4 The force applied, resistance, and thickness of the 5 wt% SWCNT filled EAA/AUD composite.

Force applied (N)	Resistance (kΩ)	Thickness (mm)
0	21	1.625
5	18.6	1.623
10	17	1.619
15	16.2	1.611
20	13.9	1.607
25	13	1.602
30	12.5	1.598
35	9	1.592
40	8.5	1.587
45	8	1.582
50	7.5	1.577
55	7.2	1.569
60	7.6	1.560

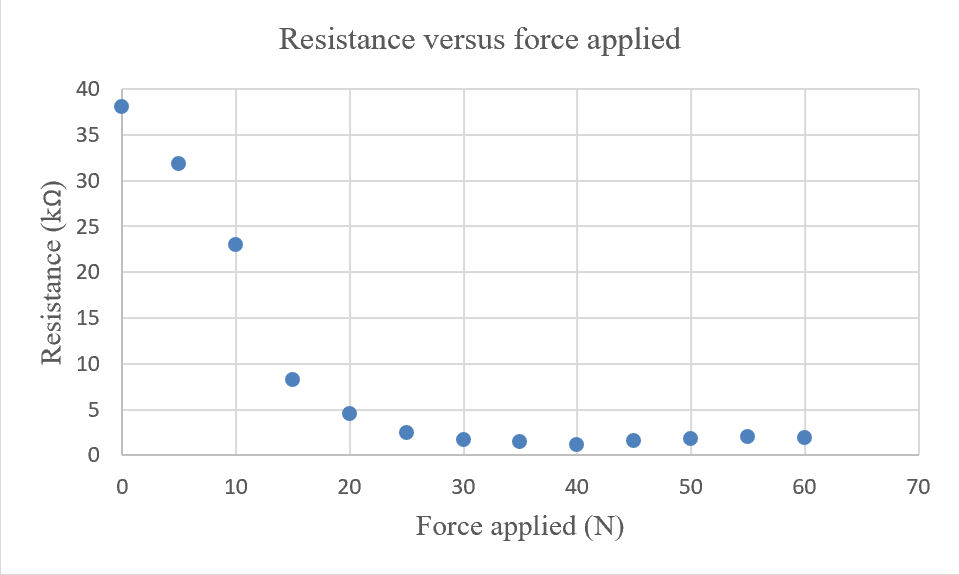

Figure 3.14 The resistance change of the 5 wt% MWCNT filled EAA/AUD composites.

Table 3.5 The force applied, resistance, and thickness of the 5 wt% MWCNT filled EAA/AUD composites.

Force applied (N)	Resistance (kΩ)	Thickness (mm)
0	38	1.463
5	31.8	1.459
10	23	1.452
15	8.2	1.449
20	4.5	1.432
25	2.42	1.423
30	1.7	1.419
35	1.5	1.415
40	1.1	1.409
45	1.6	1.404
50	1.8	1.399
55	1.96	1.395
60	1.9	1.389

The testing results showed that the developed single tactile sensor is acceptable. For the 5 wt% SWCNT filled EAA/AUD composite, it has a longer linear range of resistance change compared with the 5 wt% MWCNT filled EAA/AUD composite. The 5 wt% MWCNT filled EAA/AUD composite has a relatively high sensitivity when the applied force is lower than 20 N. The gauge factor of the 5 wt% MWCNT filled EAA/AUD composite is 57 and the gauge factor of the 5 wt% SWCNT filled EAA/AUD composite is 28. The performance difference between the EAA/AUD composite filled with 5 wt% SWCNT and 5 wt% MWCNT may be caused by the dispersing effectiveness and the different physical properties of SWCNT and MWCNT, such as gravity, electrical conductivity, and aspect ratio. In conclusion, the MWCNT or SWCNT filled EAA/AUD composite can work as a single tactile sensor and have a relatively high gauge factor (28~57).

One important shortcoming with this fabrication method is the repeatability. For the 5 wt% MWCNT filled EAA/AUD composite, 7 groups of samples were fabricated, and each group had 10 samples. For each group, 6 samples were selected for testing. In the 42 samples being tested, the resistances of 26 samples were in the range of 35.46 kΩ to 43.34 kΩ, which was 10% error of the average value 39.4 kΩ. This means that only 61.9% of the samples fabricated would have a relatively similar resistance ($\pm$10% error to the average value). It is worth mentioning that to a tactile sensing system (i.e., a network of tactile sensors), the repeatability of a single tactile sensor is a significant factor to a reliable performance of the tactile sensing system.

The foregoing variations in the performance of the carbon nanomaterial filled EAA/AUD composite may be caused by the degree of dispersion. The resin solution of EAA/AUD has low fluidity and distributing the carbon nanomaterials into the resin solution is difficult. On one hand, the resin solution needs to be heated to increase its fluidity. On the other hand, the decomposition of BPO will speed up with the increased temperature. Therefore, the resin solution was heated to 60 ℃ after multiple trials to have a balanced effect on the fluidity and decomposition speed. The restriction of the temperature makes the dispersion of carbon nanotubes difficult to control. Different dispersion degrees can lead to different performances of single tactile sensors.

In conclusion, the redox initiator method can be used to fabricate the single CNPC tactile sensor, but not suitable for tactile sensing systems concerned by this dissertation.

3.3 Carbon nanomaterial coated PDMS tactile sensors

For the coating method, a PDMS substrate was used. The PDMS substrate was designed with circular grooves for the coating materials and rectangle grooves for placing wires (Figure 3.15). The fabrication procedure is as follows (Figure 3.16):

(1) Add 5 mg MWCNT and 1mg SDS into 25 ml DCM solution.
(2) Place an ultra-sonification probe (Branson sonifier 150) into the solution to help disperse the MWCNT for 10 minutes.
(3) Use a spray gun and compressed nitrogen (15 PSI) to spray MWCNT solution on the PDMS substrate (Figure 3.17).

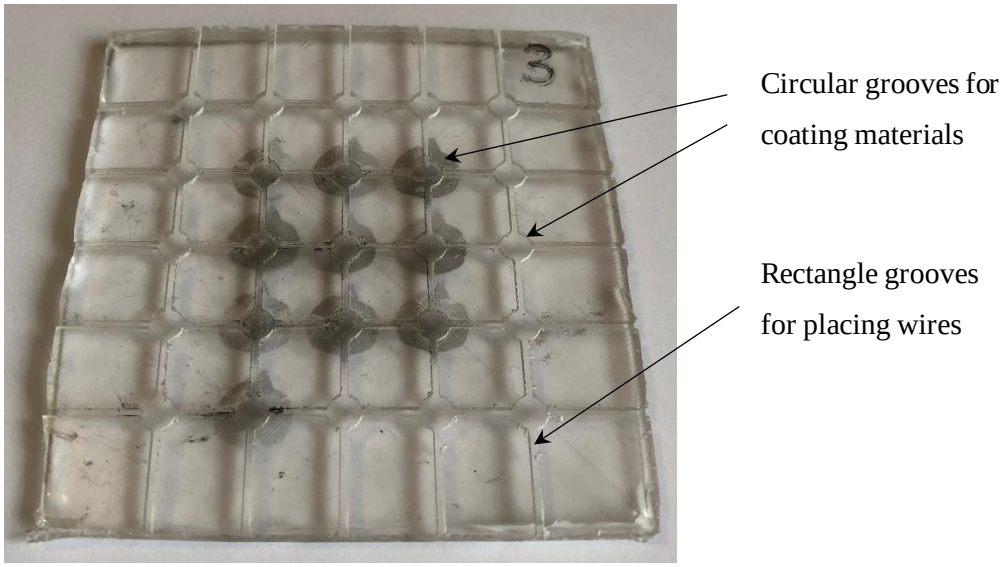

Figure 3.15 The PDMS substrate for coating method

It is noted that once the solution was ultrasonicated, the solution should be sprayed immediately to avoid the subsiding and bundling of the MWCNTs. The density of the carbon nanomaterials was determined by the number of drops sprayed and the distance between the spray gun and the substrate. The distance between the spray gun and the coating surface was set to 10 cm according to the instruction of the spray gun facility. The

density of the carbon nanomaterial was controlled by the number of drops sprayed (0.1 ml per drop using a pipette).

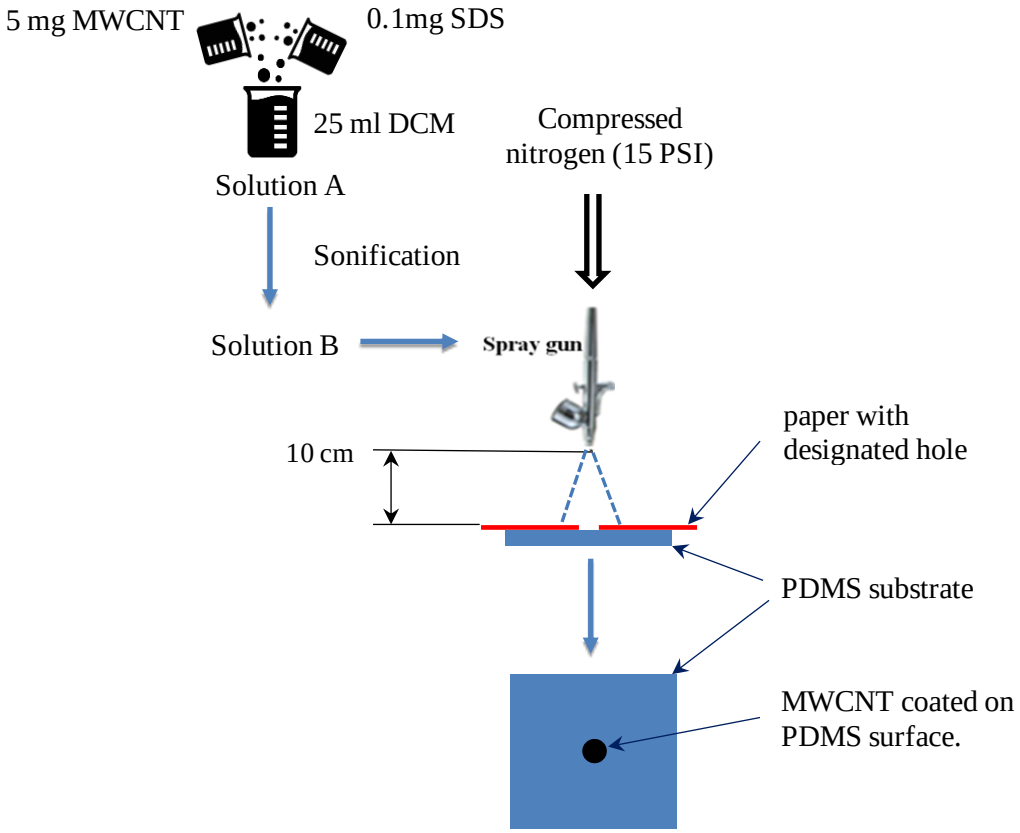

Figure 3.16 The procedure of coating method.

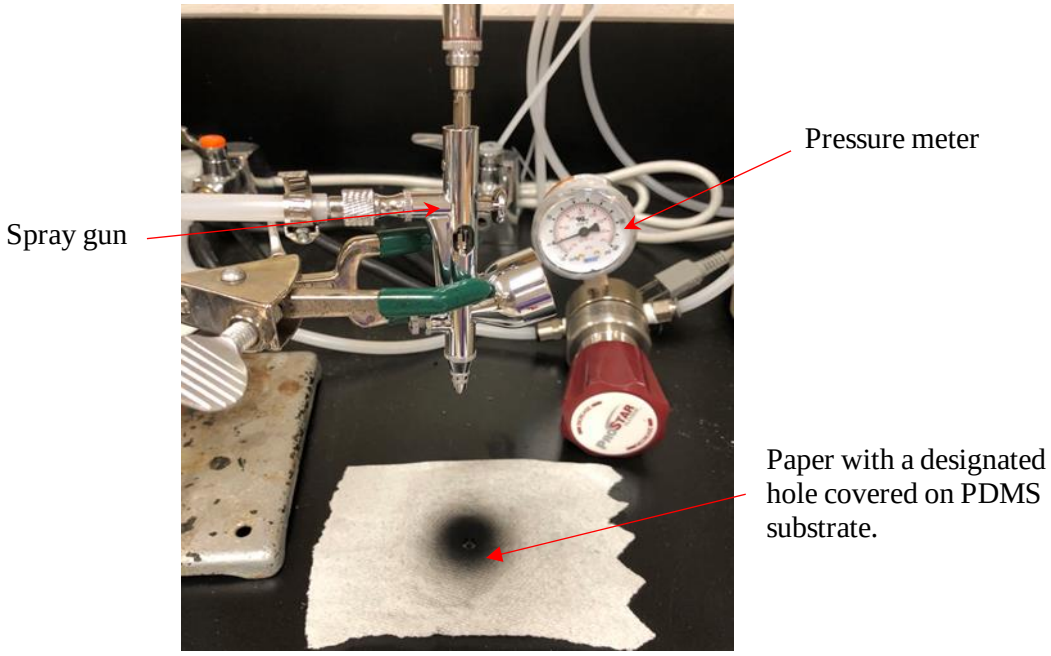

Figure 3.17 The coating procedure using a spray gun

After multiple trials, 91.3 % of the single tactile sensors were in the ±10 % error range of the average value. Therefore, the repeatability of this method was better than the redox initiator curing method. For the changeability of Young's modulus, it can be achieved by the polymer substrate, e.g., PDMS. The elastic property of PDMS is dependent on the mixing ratio of base polymer and cross-linking agent, curing temperature and time (Roh et al., 2016).

3.4 Conductance of the MWCNT coated PDMS tactile sensor

The coated MWCNT tactile sensor was designed in a circular shape considering the non-directional feature. In the content of a circular shape, it is unknown whether the MWCNT network follows the Ohm's Law at the macro level. Therefore, the resistance between two contacts on the rim of a conductive disk was calculated. Then, the resistance of the tactile sensor was measured. A set of MWCNT coated PDMS tactile sensors were fabricated with 10 drops of spraying volume (0.1 ml per drop) for testing.

3.4.1 The resistance of a disk

For a conductive disk of radius a, thickness $t \ll a$, and conductivity σ, calculate the resistance between two contacts on the rim, see Figure 3.18. The contacts have a small length of δ around the circumference. The distance between two contacts is $d \gg \delta$.

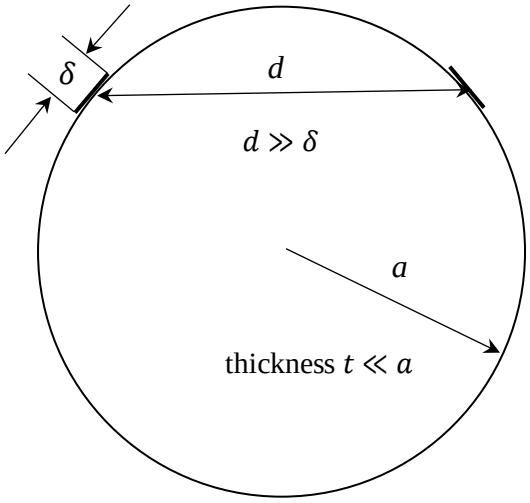

Figure 3.18 The schematic of the conductive disk. Adapted from (Mcdonald, 2000).

When a potential difference V is applied between the two contacts, the current I flows from one contact to another. As the thickness $t \ll a$, the current flow, electric field, and the electric potential are all two-dimensional. The electric field from the wire of charge density λ has magnitude

$$E_1 = \frac{2\lambda}{r_1} \tag{3-1}$$

r_1 refers to the distance between the wire and the observer. The electric potential is

$$\emptyset_1 = 2\lambda ln\frac{r_1}{r_0} \tag{3-2}$$

r_0 is a constant integration. Therefore, the potential of charge density $-\lambda$ is similarly

$$\emptyset_2 = -2\lambda ln\frac{r_2}{r_0} \tag{3-3}$$

r_2 refers to the distance between the observer and the other wire. The potential at an arbitrary point is

$$\emptyset = \emptyset_1 + \emptyset_2 = 2\lambda ln\frac{r_1}{r_2} \tag{3-4}$$

Assume that the contacts are fully conductive wires of radius $\delta/2$, as shown in Figure 3.19. The potential of the contact 2 is

$$\emptyset(contact\ 2) = 2\lambda ln\frac{d-\delta/2}{\delta/2} \tag{3-5}$$

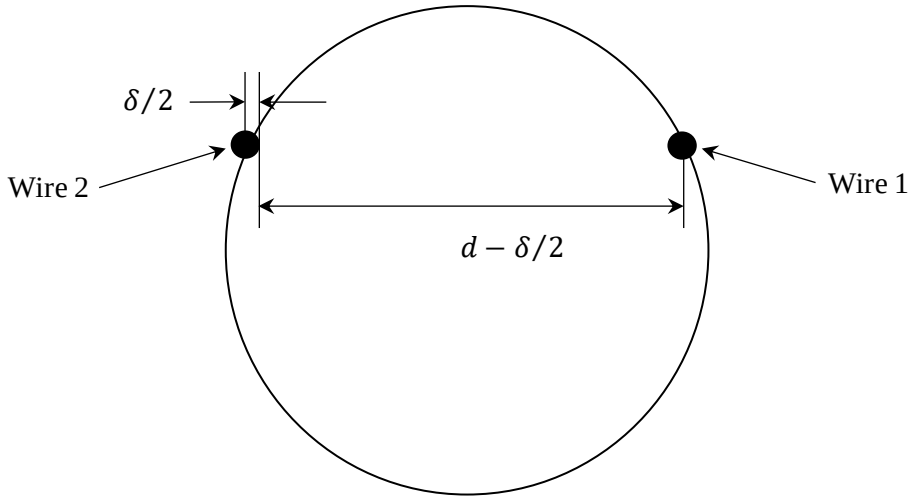

Figure 3.19 The schematic of conductive wires and conductive disk. Adapted from (Mcdonald, 2000).

The potential at the surface of the contact 1 is

$$\emptyset(contact\ 1) = -2\lambda ln\frac{d-\delta/2}{\delta/2} \tag{3-6}$$

The potential difference between the two contacts is

$$V = 4\lambda ln\frac{d-\delta/2}{\delta/2} \tag{3-7}$$

To calculate the current I flowing between two contacts, the current density J is introduced. For the calculation convenience, a cylindrical surface of radius r, that is $\delta/2 < r \ll d$, centered on each of the contacts, is assumed. Therefore, the electric field is

$$E = \frac{2\lambda}{r} \tag{3-8}$$

The current density $J = \sigma E$. The relevant area of the surface is πrt. The current I is

$$I = \pi rt \times \sigma \times \frac{2\lambda}{r} = 2\pi\sigma\lambda t \tag{3-9}$$

Therefore, the resistance R is

$$R = \frac{V}{I} \approx \frac{4\lambda ln\frac{d-\delta/2}{\delta/2}}{2\pi\sigma\lambda t} = \frac{2}{\pi\sigma t} In\frac{d-\delta/2}{\delta/2} \tag{3-10}$$

3.4.2 Validation of the single tactile sensor

The resistance of a disk is independent of the radius of the disk. To testify that the conductance of the tactile sensor follows the Ohm's Law, the resistances were tested from different directions and contacts of the circle, see Figure 3.20.

(a) Top view of the MWCNT coated PDMS

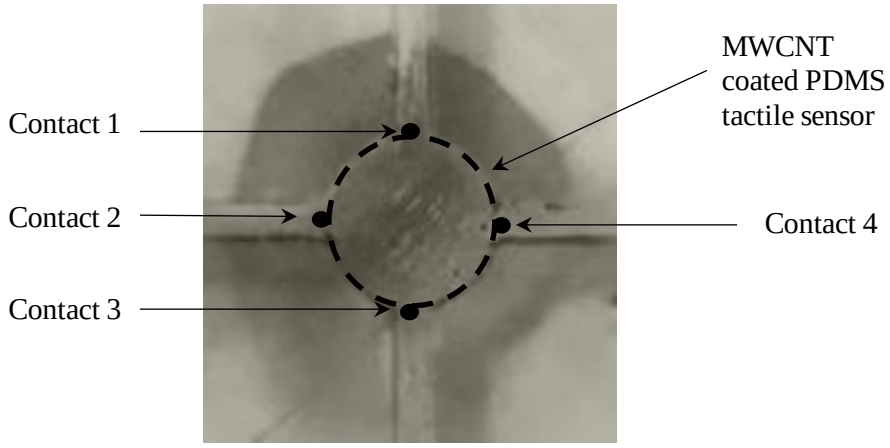

(b) Front view of the MWCNT coated PDMS

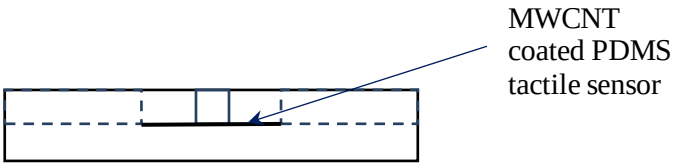

Figure 3.20 The contacts for the tactile sensor.

According to Section 3.4.1 the resistance between the contact 1 and 2 is

$$R_{12} = \frac{2}{\pi\sigma t} In \frac{d_{12}-\delta/2}{\delta/2} \tag{3-11}$$

R_{12} refers to the resistance between the contact 1 and the contact 2 and d_{12} refers to the distance between the contact 1 and the contact 2. Therefore, if the MWCNT network is coated evenly on the surface of the polymer substrate and over the percolation threshold, R_{xy} should equals to R_{yx}. The ratio of the resistances is

$$\frac{R_{ab}}{R_{cd}} = \frac{\frac{2}{\pi\sigma t} In \frac{d_{ab}-\delta/2}{\delta/2}}{\frac{2}{\pi\sigma t} In \frac{d_{cd}-\delta/2}{\delta/2}} = In \frac{2(d_{ab}-d_{cd})}{\delta} \quad (3\text{-}12)$$

Measurement method and instrument: A DC power supply and an oscilloscope were used. The 30V voltage was supplied for the measurement. In total, 9 tactile sensors were selected. For each tactile sensor, the resistance between the contact 1 and the contact 2, 1 and 3, 2 and 4, 3 and 1 were measured 10 times to get an average value.

3.4.3 Results and discussions

Considering the differences of resistance values between the five selected tactile sensors, the resistances measured were compared relatively for each tactile sensor. For $\frac{R_{13}}{R_{12}}$, the theoretical value is 1.545 according to Equation (3-12) The experiment value measured from 9 tactile sensors are shown in Figure 3.21.

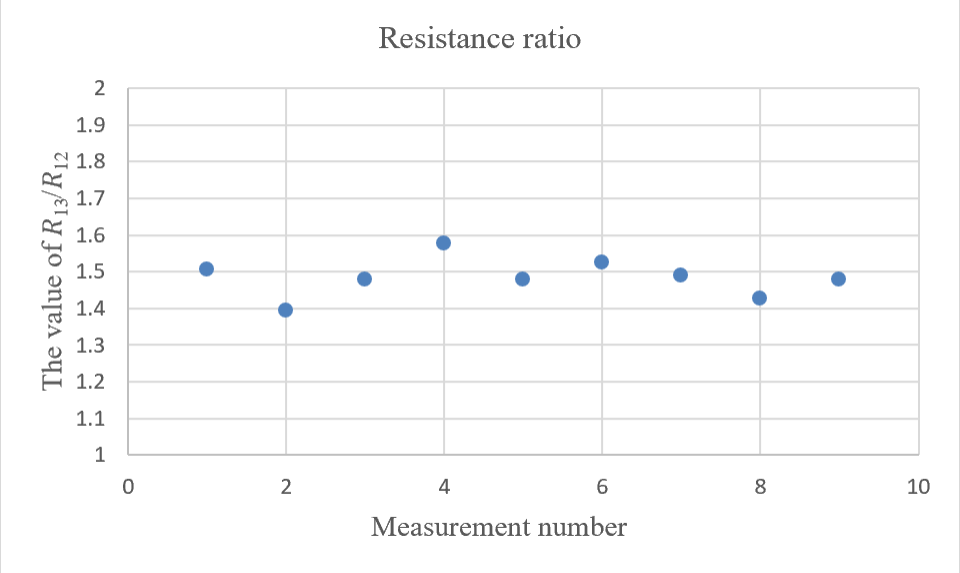

Figure 3.21 The value of $\frac{R_{13}}{R_{12}}$.

For $\frac{R_{13}}{R_{24}}$, the theoretically value should be 1 as the R_{13} should equal to R_{24}. The experiment value measured from 9 tactile sensors are shown in Figure 3.22.

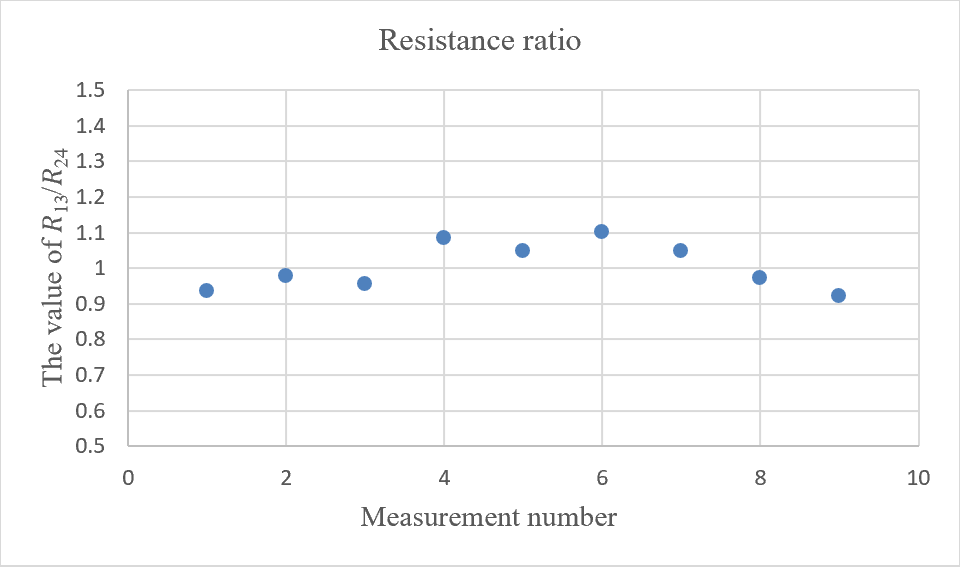

Figure 3.22 The value of $\frac{R_{13}}{R_{24}}$.

Also, for $\frac{R_{13}}{R_{31}}$, the theoretically value should be 1 as the R_{13} should be equal to R_{31}. The experiment value measured from 9 tactile sensors are shown in Figure 3.23.

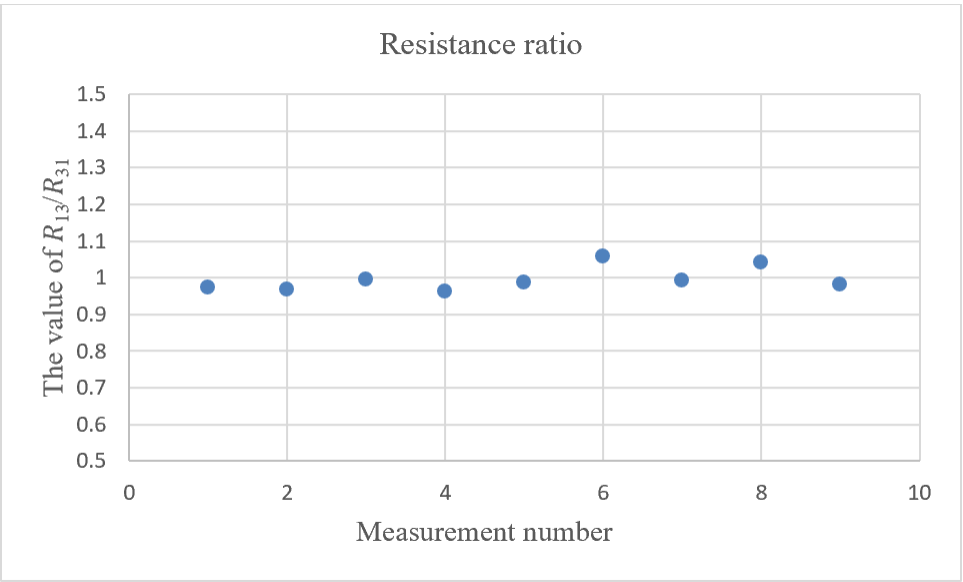

Figure 3.23 The value of $\frac{R_{13}}{R_{31}}$.

The results show that the MWCNT coated tactile sensor follows the Ohm's Law. Therefore, the sensor can be viewed as a regular resistor in calculating the resistance when different contacts of a single tactile sensor are connected in the sensor network. Also, the different

connections of tactile sensor, for example the connection of the contacts 1 and 2 or 1 and 3, enable the adaptability of the sensor network pattern.

The validation of the CNPC tactile sensor is important for the sensor network. The sensor network may include parallel circuits and series circuits. The validation proves that Ohm's Law is valid to the sensor network.

3.5 The coating thickness and the resistance of the MWCNT/PDMS tactile sensor

For different applications, different resistances of the MWCNT/PDMS tactile sensors are needed. Different resistances can be achieved by different thicknesses of the CNT on the PDMS substrate. The thickness is further translated to the number of drops of the CNT solution onto the PDMS substrate. Figure 3.24 shows the relationship of the number of drops with respect to the resistance.

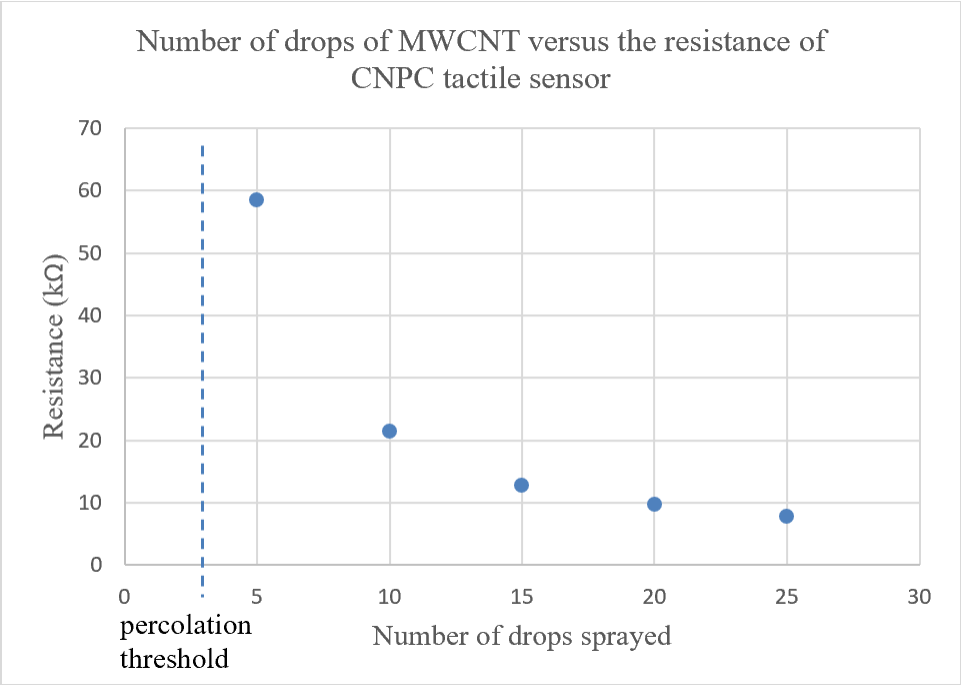

Figure 3.24 Number of drops of MWCNT solution versus the resistance of CNPC tactile sensor.

From Figure 3.24, it can be found that the resistance of the CNPC tactile sensor decreases with the increase of the number of drops of the MWCNT solution. When the number of drops is under 10, the MWCNT forms conductive pathways rapidly from none to a relatively dense condition. In this case, the resistance of the CNPC tactile sensor decreases quickly. When the number of drops is over 10, the resistance of the CNPC tactile sensor decreases at a slow speed and tends to reach a stable value. This phenomenon is because stable conductive pathways have already been formed with respect to 10 drops of the

MWCNT solution and more drops have less influence on the resistance. The resistance of the CNPC tactile sensor is approaching a stable value. This value can be determined by the purity of the MWCNT, the volume content of surfactant, and the surface roughness of the PDMS substrate.

3.6 Gauge factor and the deformation-resistance curve

To obtain the gauge factor and the relationship between the deformation and the resistance of the MWCNT/PDMS tactile sensor, another set of experiments was conducted. A MWCNT/PDMS tactile sensor was placed on cylinders with different radius, see Figure 3.25.

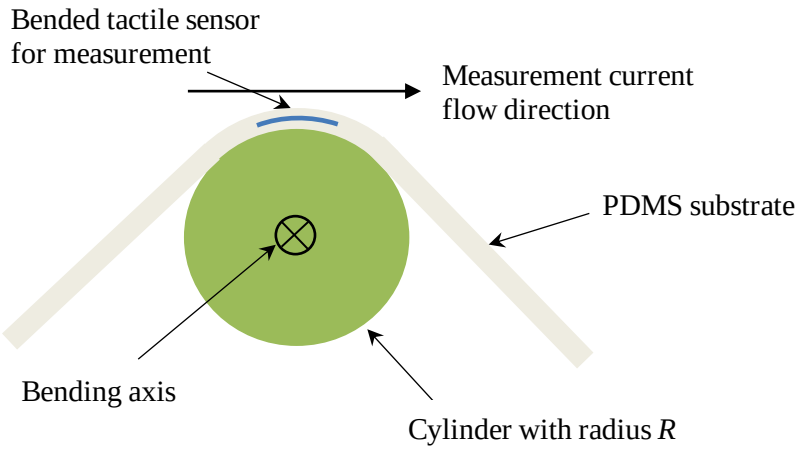

Figure 3.25 Schematic of pre-curved tactile sensing system

The cylinders with radius of 137 mm, 28.6 mm, 17.5 mm, and 5.5 mm were used (stick, cup, bottle, etc.). The results were an average value of the resistances got from 5 repetitive measurements (Figure 3.26). When the CNPC tactile sensor was placed on the surface with the radius of 5.5 mm, the CNPC tactile sensor was not conductive, so the radius of curved surfaces that work with the developed CNPC sensor must be larger than 5.5 mm. The results show the CNPC tactile sensor can be working when placing on the curved surface with the radius larger than 17.5 mm.

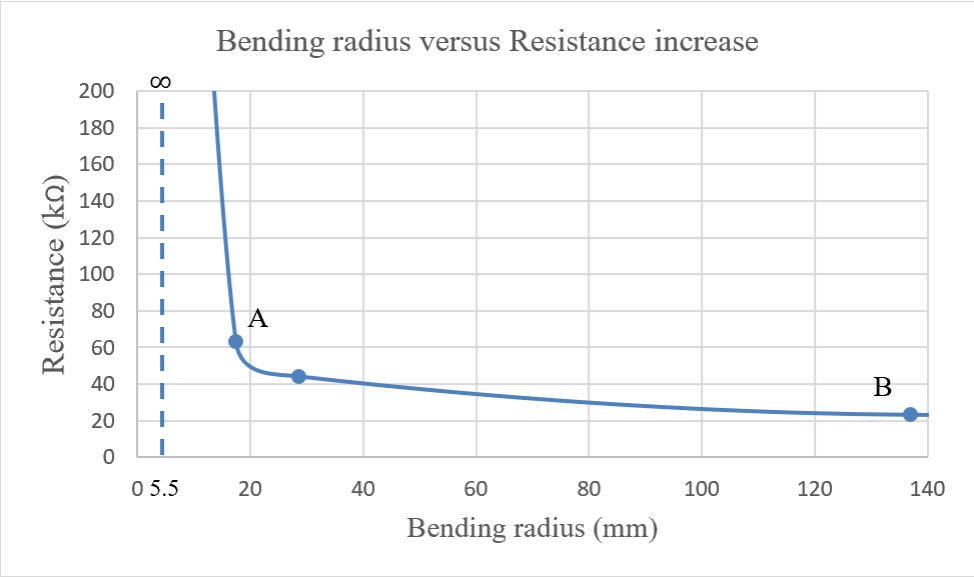

Figure 3.26 Resistance of MWCNT/PDMS tactile sensors with different radiuses.

From Figure 3.26, the point A and B are selected for calculating the gauge factor. For the point A, the bending radius is 17.5 mm, and the resistance is 63 kΩ. For the point B, the bending radius is 137 mm, and the resistance is 23 kΩ. The resistance difference is 40 kΩ. The length difference can be calculated based on the curve length (Figure 3.27). It is assumed that the surface contacting with the cylinder is undeformed.

$$\frac{l_0}{R_0} = \frac{l_0+\Delta l}{R_0+t} \tag{3-13}$$

l_0 is 4 mm. t is 2 mm. R_0 is the bending radius. The gauge factor is calculated as 11.9.

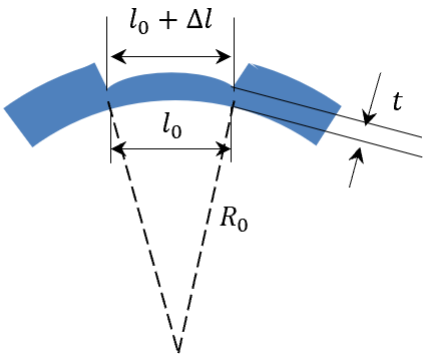

Figure 3.27 The schematic figure of the calculation of gauge factor. R_0: the bending radius; l_0: the initiator diameter of the single tactile sensor; Δl: the length difference

when bended; t: the distance between the surface of the single tactile sensor and the bottom surface of the substrate.

3.7 Conclusions

In this chapter, four different methods of fabricating CNPC single tactile sensors were discussed. The following conclusions can be drawn.

(1) The photo initiator method for curing the EAA/AUD resin can only make a thin layer of polymer composites filled with carbon nanomaterials. This is because the carbon nanomaterials distributed in the polymer resin would block the UV light such that only a thin layer on the surface can be cured.

(2) With the thermal initiator method for curing the EAA/AUD resin, a relatively high reaction temperature can improve the fluidity of the resin and thus facilitate the dispersion of the carbon nanomaterials into the resin solution; however, the thermal initiator BPO will release carbon dioxide, which forms bubbles in the polymer composite. By placing the whole fabrication system in a vacuumed environment and by slowing down the reaction speed, bubbles can but not completely be removed.

(3) The main benefit of the redox initiator method for curing the EAA/AUD resin is to fabricate the carbon nanomaterial filled composite free of bubbles. 5 wt% MWCNT filled EAA/AUD tactile sensor was fabricated with the gauge factor of 57. 5 wt% SWCNT filled EAA/AUD tactile sensor was fabricated with the gauge factor of 28. However, with this method, it is difficult to disperse carbon nanomaterials evenly inside the resin solution because of the low fluidity of the resin, which is further because of a relatively low temperature in the fabrication process. Indeed, the repeatability of this method is poor (about 10% uncertainty).

(4) The coating method remains most robust in terms of the quality of CNPCs. Compared with the first three methods, which is in essence to disperse carbon nanomaterials into the composite, coating the carbon nanomaterials on the polymer surface is a reliable approach to constructing a CNPC tactile sensor. It is worth

mentioning that the density of the carbon nanomaterials is in some sense of the 3D structure, which is controlled by the number of drops sprayed on the substrate.

(5) For the MWCNT/PDMS tactile sensor constructed with the coating method, the conductance of the sensor follows Ohm's Law. The relationship between the coating thickness of MWCNTs and the resistance of the sensor is significant, so the construction of the sensors with varying gauge factors and resolutions is possible. The gauge factor of the prototype of the sensor with 10 drops of the coating volume is 11.9, which is adequate according to Table 2.4.

CHAPTER 4
SYSTEMATIC DESIGN OF A CNPC TACTILE SENSING SYSTEM

4.1 Introduction

In this chapter, design of CNPC tactile sensing system or senor network is discussed. The goal of the design is to make a robust and resilient sensor network. To make the design more systematical, two design theories, namely Axiomatic Design Theory (ADT) and ADaptable Design Theory (ADDT) are applied to achieve this goal. The definition of concept design follows that for general products or devices; namely the concept design is expected to determine principles a device (e.g., sensor network) follows. The definition of embodiment design follows that for general products or devices; namely the embodiment is expected to determine the connectivity of sensors in the network, size, and shape of the network.

4.2 The coating method versus the distribution method for HuBots

The coating method and distribution method are two methods for making CNPC sensors (Chapter 3). This section presents an analysis and comparison of the two methods in terms of their better suitability in the context that they are put on a substrate and connected into a network, i.e., a skin wrapped onto a HuBot. Axiomatic design theory (ADT) is employed for aiding this analysis.

Axiomatic design theory (ADT) is a systematic design methodology (Suh, 1998; Fan et al., 2015). Let us denote FR for functional requirement and DP for design parameter. DPs are supposed to fulfil FRs. The correspondence of DPs and FRs can be represented by a correspondence matrix, see Figure 4.1. ADT has two axioms: Axiom I and Axiom II. Axiom I says the coupled design should be avoided. Axiom II says the best design among all the designs that meet Axiom I is the one with the least amount of information content (Fan et al., 2015). In this dissertation, only Axiom I is relevant, because the number of design alternatives is only two. Details of ADT can be found in Appendix B.

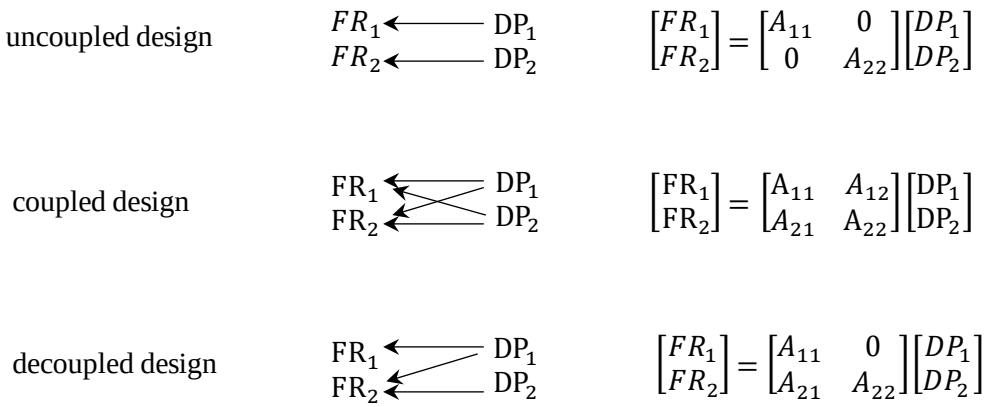

Figure 4.1 The relationship of FR and DP of the uncoupled design, coupled design, and decoupled design.

4.2.1 ADT analysis of the network of sensors made with the distribution method

For the CNPC tactile sensor that is built with the distribution method (i.e., dispersing carbon nanomaterials into the polymer solution), FRs are defined as follows:

- FR1: to have tactile sensing ability.
- FR2: to have low stiffness (close to human skin).

FR1 and FR2 are further decomposed to:

- FR11: to have resistance change when CNPC deformed.
- FR12: to generate deformation when force applied on CNPC.
- FR13: to collect data from the tactile sensors.
- FR14: to have low stiffness substrate.

DPs are proposed as follows:

- DP1: carbon nanomaterials polymer composite, to fulfill FR1.
- DP2: polymer substrate, to fulfill FR2.

DP1 and DP2 are further decomposed to:

- DP11: carbon nanomaterials conductive pathways for CNPC, to fulfill FR11.

- DP12: polymer matrix for CNPC, to fulfill FR12 and FR14.
- DP13: soft wires to form electrical circuits, to fulfill FR13.
- DP14: polymer substrate, to fulfill FR14 and FR12.

The correspondence of FRs and DPs can be represented by

$$\begin{Bmatrix} FR11 \\ FR12 \\ FR13 \\ FR14 \end{Bmatrix} = \begin{bmatrix} \times & & & \\ & \times & & \times \\ & & \times & \\ & \times & & \times \end{bmatrix} \begin{Bmatrix} DP11 \\ DP12 \\ DP13 \\ DP14 \end{Bmatrix} \quad (4\text{-}1)$$

From Eq. (4-1) it can be found that DP12 and DP14 are coupled with respect to FR12 and FR14, which means that the concept design violates Axiom I of ADT. A further analysis can find that with this design, the polymer matrix distributed with carbon nanomaterials and the polymer substrate have an overlapping function (i.e., the function to change the conductive path established by the carbon nanomaterials in the polymer given an applied force). More specifically, when a force is applied to the substrate polymer, it would first generate deformation and then transfer it to the nearest sensor on the network, and subsequently cause the deformation of the polymer of the CNPC sensor. As such, the deformation on the polymer of the CNPC sensor does not reflect the force applied on the sensor network only, and this means the information from the CNPC sensor on the network does not represent the force applied only. To resolve this confounding effect on the CNPC sensor, algorithms to resolve this confounding effect are needed, which complicate the sensing system. Therefore, the distribution method for constructing CNPC tactile sensors for HuBots is not suitable as opposed to the coating method (see justification in the next section).

4.2.2 ADT analysis of the network of sensors made with the coating method

For the CNPC tactile sensor that is built with the coating method (i.e., coating carbon nanomaterials onto the surface of a polymer substrate). The definition of FRs in Section 4.2.1 is still valid. DPs with the coating method are proposed as follows:

- DP1: carbon nanomaterials polymer composite, to fulfill FR1.
- DP2: polymer substrate, to fulfill FR2 and FR14.

DP1 and DP2 are further decomposed to:

- DP11: carbon nanomaterials conductive pathways for CNPC, to fulfill FR11.
- DP12: polymer substrate, to fulfill FR12.
- DP13: soft wires to form electrical circuits, to fulfill FR13
- DP14: DP12.

The correspondence of FRs and DPs can be represented by

$$\begin{Bmatrix} FR11 \\ FR12 \\ FR13 \\ FR14 \end{Bmatrix} = \begin{bmatrix} \times & & \\ & \times & \\ & & \times \\ & \times & \end{bmatrix} \begin{Bmatrix} DP11 \\ DP12 \\ DP13 \end{Bmatrix} \tag{4-2}$$

From Eq. (4-2), it can be found that DP12 meets both FR12 and FR14 at the same time and thus, the design is a decoupled design, which means that the design meets Axioms I of the ADT. A further analysis shows that because one polymer material has two uses at the same time: the substrate for the CNPC and the substrate for the network of sensors. Otherwise, the design is redundant design with potential conflicts. In fact, the concept design with the coating method implies a following procedure to construct the CNPC tactile sensing system (i.e., a network of CNPC tactile sensors): (1) make a substrate on a HuBot, and (2) coat carbon nanomaterials onto the substrate (Figure 4.2). The carbon nanomaterials are coated on the concave surface in Figure 4.2, because the concave surface can prevent the coating layer from being destroyed more easily than the convex surface. From the foregoing discussion, it can be concluded that the coating method for constructing CNPC tactile sensors for HuBots is more suitable than the distribution method.

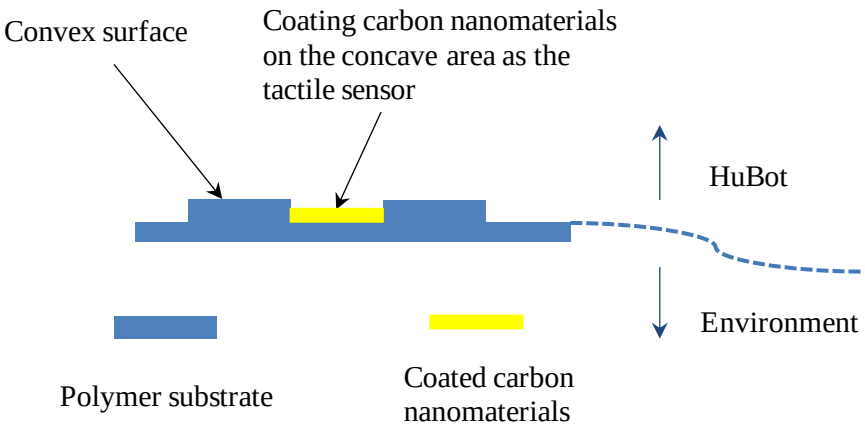

Figure 4.2 The structure of the CNPC tactile sensing system guided by ADT.

4.3 Concept design of the CNPC tactile sensor network

The above analysis in Section 4.2 shows that the coating method is preferred for HuBots in this dissertation. The task of the concept design involves the following: (1) to determine the elements of the CNPC tactile sensing system, (2) to determine the topology of the CNPC tactile sensing system, (3) to determine the method and structure to achieve the adaptability of the CNPC tactile sensing system.

HuBots are in a variety in terms of the shape and size of their body. The skin that is supposed to wrap up the body of HuBot is required to be adaptable – i.e., the skin is adjustable to satisfying any new requirement. The new requirement includes not only the shape and size of the body of a robot but also the measurement features (e.g., gauge factor, range of force signals, etc.). Nevertheless, new requirements are "extendable" in that new required features will not compromise the validity of the existing required features. A design methodology in literature called "adaptable design" is suitable to this situation, and therefore is chosen to develop a network of CNPC sensors made with the coating method.

4.3.1 Adaptable design theory

Adaptable design is a design approach that aims to enable product adaptability and subsequently facilitate product reuse (Gu et al., 2004). The primary idea to achieve this

aim with adaptable design is to develop a product requirement model which is extendable to incorporate future required features on a new product, and to develop a product structure such that a new product can be built by adding new structural features to the structure of the existing product or modifying the existing structural feature. According to (Hashemian, 2005), the adaptable design methodology contains four phases. The first phase is Specific Adaptable Design, which is a design process that the information of future requirements is available. For example, the tactile sensing system is expected to work for different sizes and shapes of surfaces in future. The second phase is General Adaptable Design phase, which a design process that future requirements are is uncertain. The third phase is Development and Hierarchy, two of which make sense to a system that needs to be decomposed into sub-systems. In this dissertation, the third phase and fourth phase are combined as the CNCP tactile sensing system is considered as one system (i.e., no sub-systems; thus, no hierarchy in the structure).

4.3.2 Adaptable design of CNPC tactile sensing systems

4.3.2.1 Phase 1: Specific Adaptable Design

Step 1: Define the original design problem (FRs). As discussed in Section4.2, the original design requirements are represented as:

- FR11: to have resistance change when CNPC is deformed.
- FR12: to generate deformation when force is applied on CNPC.
- FR13: to collect data from the tactile sensors.
- FR14: to have a low stiffness substrate.

Step 2: Identify the set of target adaptation tasks (Sp). As discussed in Chapter 2, tactile sensing systems have different gauge factors, which can be chosen to meet different sensitivities of different parts of a human collaborative robot. Further, a different area of a human collaborative robot is expected to work for different loads and different resolutions to CNPC tactile sensors. For example, the hands (or paws) of a HuBot are expected to work with relatively low loads and high resolutions, while the arms of the HuBot are expected with a heavy duty and low resolution. As such, the adaptivity of the sensing range, sensitivity and resolution of a tactile sensing system is needed, which leads to the proposal of the following target adaptation tasks:

- Sp1: the resistance change is adaptable to achieve different sensibility.
- Sp2: the deformation range is adaptable to achieve different sensing range.
- Sp3: the network structure is adaptable to achieve different resolution.

Step 3: Develop a functional structure that includes both original FRs and the adaptable Functional requirements. The original functional requirements and the adaptable task requirements are merged to evolve into a new set of functional requirements, namely the evolved functional requirements (E-FR) (Figure 4.3). The E-FRs are listed as follows:

- E-FR11: to have resistance change when CNPC is deformed.
- E-FR12: to generate deformation when force is applied on CNPC.
- E-FR13: to collect data from the tactile sensors.
- E-FR14: to have a low stiffness substrate.
- E-FR15: the resistance change is adaptable to achieve different sensibility.
- E-FR16: the deformation range is adaptable to achieve different sensing range.
- E-FR17: the network structure is adaptable to achieve different resolution.

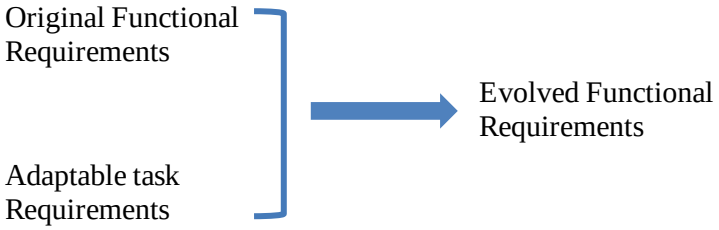

Figure 4.3 The relationship between the Evolved Functional Requirement, Original Functional Requirement, and Adaptable Task Requirement.

Step 4: Design the physical structure of the product according to the combined functional requirements. As discussed in Section 4.2, the structure is based on coating carbon nanomaterials on the surface of a polymer substrate. Therefore, the evolved design parameters are proposed as follows:

- E-DP1: carbon nanomaterials conductive pathways for CNPC, to fulfill E-FR11.
- E-DP2: polymer substrate, to fulfill E-FR12 and E-FR14.
- E-DP3: soft wires to form electrical circuits, to fulfill E-FR13.
- E-DP4: the amount of coated carbon nanomaterials is adjustable, to fulfill E-FR15.
- E-DP5: the material of polymer substrate is selectable for different Young's Modulus, to fulfill E-FR16.
- E-DP6: the network of sensors is adaptable for different patterns, to fulfill E-FR17.

Therefore, in terms of the E-DPs listed, the physical structure of the tactile sensing system is designed as shown in Figure 4.4. To connect the single tactile sensors, grooves are designed for applying the soft conductive wires. Measurement circuits can connect through the measurement portals to measure the resistance of single or groups of CNPC tactile sensors.

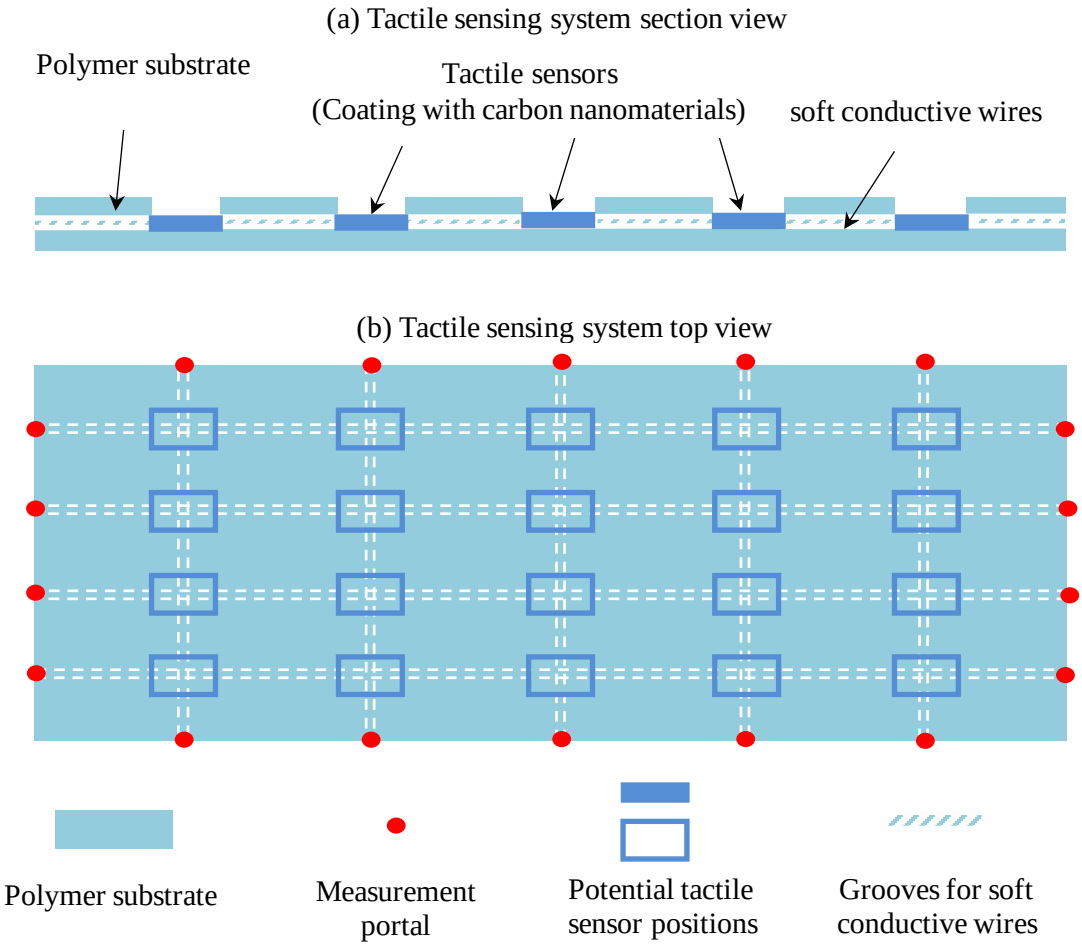

Figure 4.4 The structure of the tactile sensing system.

According to this structure, there would be different adaptable patterns for tactile sensors (Figure 4.5). The grooves for soft conductive wires can offer different measurement circuits for data collection. Access to different measurement portals into the measurement circuit can get the resistance of single or multiple CNPC tactile sensors.

(a) Evenly distributed low-resolution pattern

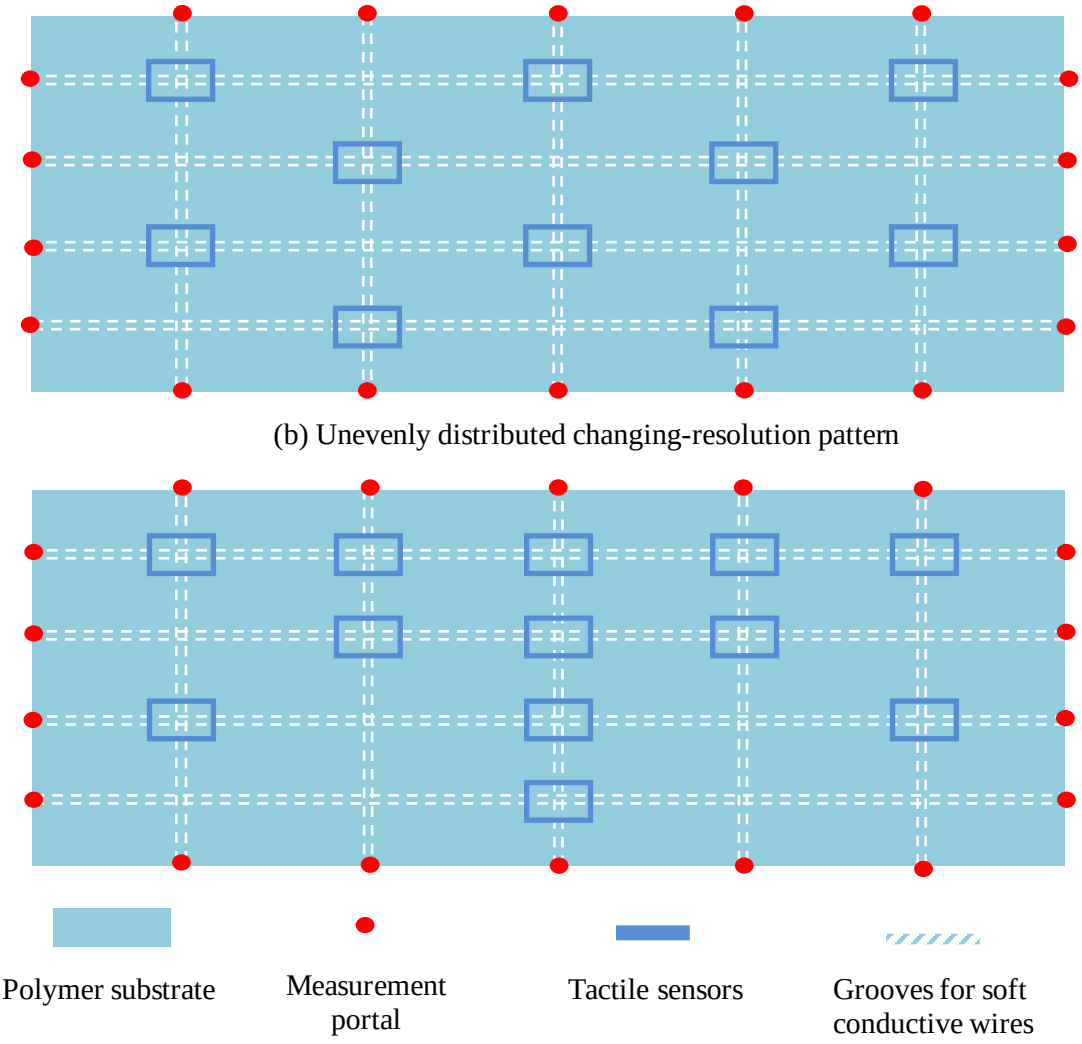

Figure 4.5 Different patterns of adaptable sensor network.

Further, the tactile sensors and polymer substrate are adaptable. Changing the volume of carbon nanomaterials coated would change its sensitivity. Changing the polymer type would have different Young's modulus.

4.3.2.2 Phase 2: General Adaptable Design

In this phase, non-sufficient adaptive tasks are considered as many as possible to meet the requirements of future unexpected adaptable applications. The system is expected to be designed as functional modules, and functional modules should be self-sufficient as possible (Hashemian, 2005).

As discussed in Section 4.3.2.1, the shape, size, and network pattern of the polymer substrate are adaptable. Therefore, the adaptability on the plane of the sensor network is relatively high for different applications. For the general adaptable application, another adaptability can be explored in terms of thickness. Adding more layers can expand the sensing range of the tactile sensing system. Once the first layer of the tactile sensing system achieved its maximum sensing range, the deformation of the first layer polymer substrate would be transferred to the second layer. The second layer of the tactile sensing starts working when the force keeps increasing. The intrinsic principle of this design is like the rocket booster which has two or three stages. For a two-stage rocket booster, when the first stage of the booster resource is exhausted, the second stage of the booster resource would be triggered to expand the working range. Similarly, for a two-layer tactile sensing system, when the force applied exceeds the sensing range of the first layer of the tactile sensing system, the deformation would then transfer to the second layer, and the second layer of the tactile sensing system would start to work (Figure 4.6).

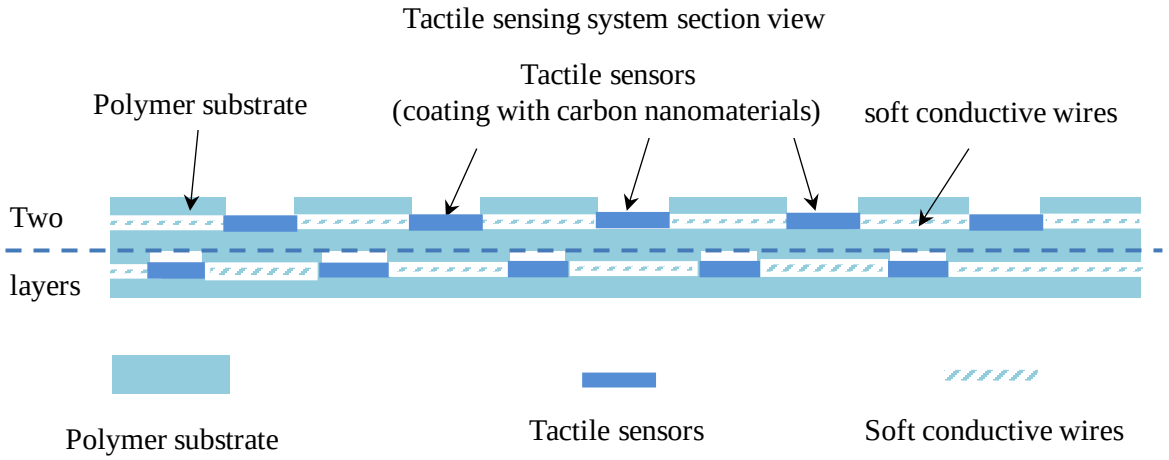

Figure 4.6 The section view of the tactile sensing system structure.

4.3.2.3 Phase 3: Development and Hierarchy

In this phase, subsystems or modules are maintained and developed independently. The connection between modules should be developed in this phase. Standard interfaces between modules are preferred to increase the interchangeability and adaptability. For a complicated system, the foregoing adaptable design procedures can be applied for each subsystem or module. A hierarchy structure is achieved by dividing an overall design into assemblies. In this dissertation, there is no complicated subsystem to form a hierarchy design structure. However, the interface between different layers needs to be designed to increase its interchangeability and adaptability, which is a routine mechanical design.

The interface between modules of the tactile sensing system mainly has two functions. One is to mount the upper layer on the lower layer to avoid the relative movement. The other one is to transfer the deformation. The interface between two layers is designed as shown in Figure 4.7. The mounting columns are designed as the same shape of the grooves coated with carbon nanomaterials so that the mounting columns can embed with the grooves. Therefore, the second layer can be mounted on the first layer and the deformation can be transferred to the second layer through the mounting columns.

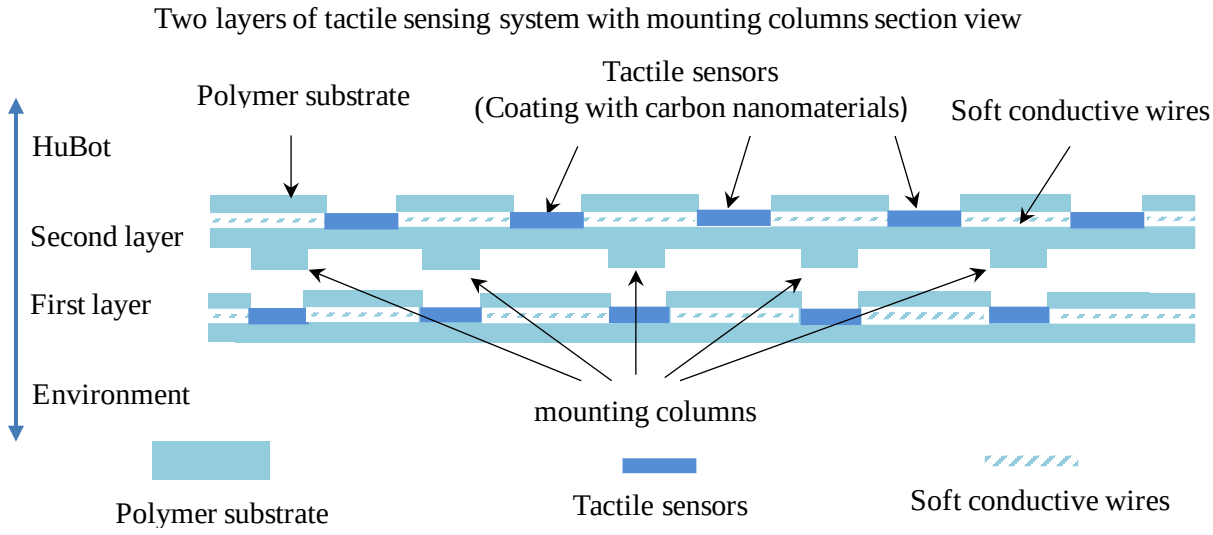

Figure 4.7 The mounting columns.

4.4 Embodiment design of the tactile sensing system

As the structures of the tactile sensing system have been determined, the embodiment design is needed for the specific shape and size of each feature of the structure. However, to keep the adaptability of the tactile sensing system, only a size range, suggested value, or selection criteria will be provided of each feature.

4.4.1 The polymer substrate

The overall size and shape of the polymer substrate does not have specific limitations. It can be designed as a round thin film to cover the elbow of a humanoid robot or a small rectangular film to cover the finger of a humanoid robot. However, several key values are important during the design of the polymer substrate, see Figure 4.8. The followings are the notes for the selection of size values that obtained from experiments.

(1) The thickness of the polymer substrate should be greater than 1 mm. Otherwise, it may not be able to completely remove the polymer substrate from the 3D printing mold or the features of the polymer substrate may not be as accurate as it should be, for example the grooves for coating MWCNTs or soft conductive lines.
(2) The grooves reserved for coating MWCNTs as tactile sensors are better designed as circulars to make it non-directional.
(3) The grooves reserved for soft conductive wires should be at least 0.5mm wide and 0.5 mm deep to contain enough amount of soft conductive materials.

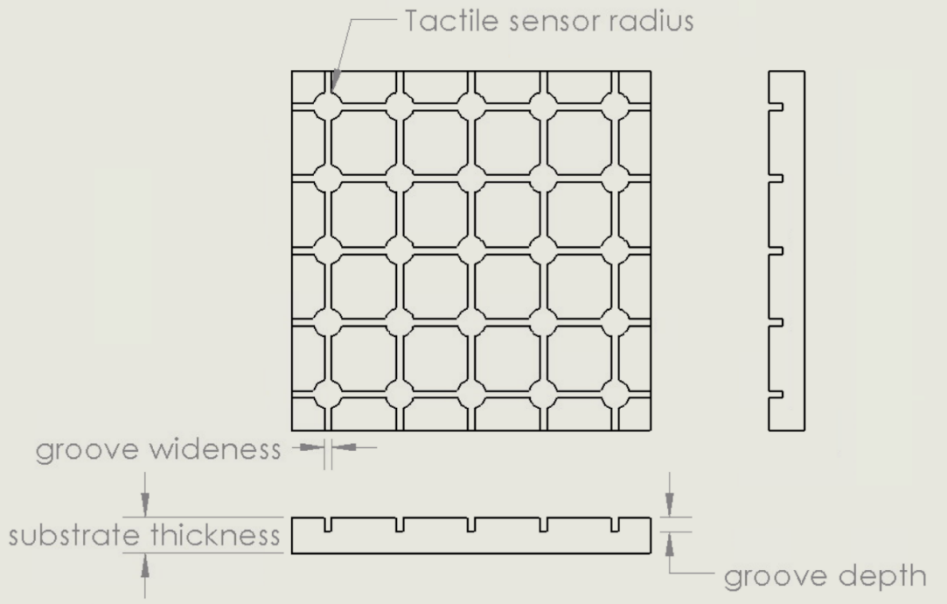

Figure 4.8 The several key sizes of the polymer substrate.

4.4.2 The tactile sensor, the sensor network, and the soft conductive wire

The coating area of the MWCNTs is restricted by the grooves reserved on the polymer substrate. The coating density of the MWCNTs is controlled by the spraying volume. A table related to the spraying volume and the resistance of the MWCNT network is expected for future reference. The sensor network is designed according to the resolution requirement. It is suggested to distribute the tactile sensors evenly for the same resolution requirement. There are several notes for the detailed design of the tactile sensor, sensor network, and the soft conductive wire.

(1) The sensor network should be designed with extra margin to provide adaptability.
(2) For the tactile sensors in the same network, it is suggested to coat the same density of the MWCNTs so that they have the same sensitivity theoretically.
(3) For the soft conductive wire, it is suggested to keep the same distance between neighboring tactile sensors so that they have the same resistance.

4.5 Summary

This chapter presented a systematic design approach to a CNPC tactile sensing system or a robotic skin for HuBots. Application of Axiomatic Design Theory, particularly its Axiom I of this theory, led to the conclusion that the coating method for constructing a CNPC tactile sensor and then the network of such sensors is the better than the distribution method. After that, Adaptable Design Theory was employed to develop the systematic design approach to the network of CNPC tactile sensors (or the robotic skin) constructed with the coating method so as to enable the design of the robotic skin for all HuBots, characterized by different bodies, shapes, sizes, and gauge factors, and resolutions. The approach has two phases: concept design phase and embodiment design phase (their definition is consistent with the general design theory (Pahl et al., 2007).

CHAPTER 5
CASE STUDY

5.1 Introduction

This chapter presents a case study to demonstrate and illustrate the effectiveness of the systematic design approach proposed in Chapter 4. The case study is about construction of a robotic skin for a hypothetical HuBot. Section 5.2 presents the specification of design requirements. Section 5.3 presents the material selection and detail design. Section 5.4 discusses the fabrication of the design. There is a conclusion in the last section.

5.2 Design requirements

The design requirements are given in Table 5.1. In this case study, the cost is not concerned for simplicity. The specific quantitative information for Young's modulus is not concerned but assumed that Young's modulus of the robotic skin is close to that of human skin and body.

Table 5.1 Design requirements of the case study.

Design requirements	Parameter
Sensing coverage area	50 mm × 50 mm
Number of sensors	25 sensors in total
Uniform sensitivity	Yes
Gauge factor of single CNPC tactile sensor	10~15
Hardness of the substrate	No specific value, close to human skin
Thickness	3 mm
Cost	No specific value
Fabrication	Industrial mass production if possible

5.3 Material selection and detail design

According to the structure of the CNPC tactile sensing system proposed in Section 4.4, the technical specifications are met by determining the sizes and features (Figure 5.1). The coverage area for a HuBot determines the substrate size. The number of sensors and coverage area together determine the sensor network configuration. The hardness of the substrate determines the material of the polymer substrate. The requirement of the gauge factor of the tactile sensing system can be met by the polymer substrate and the carbon nanomaterials coated.

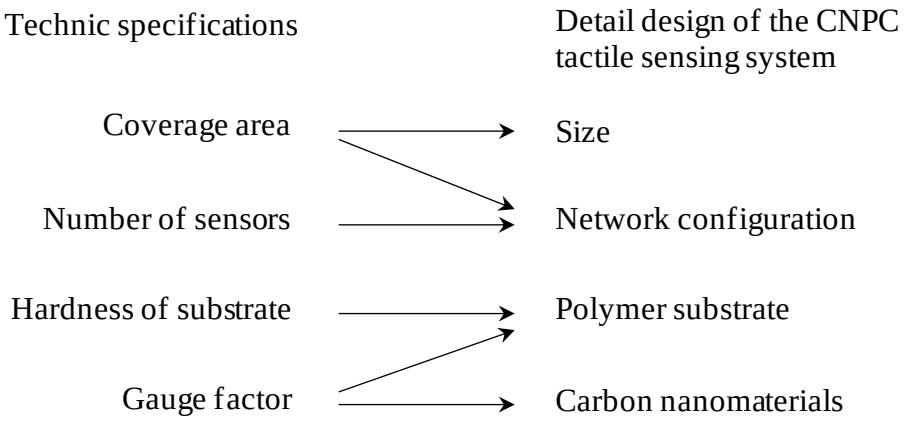

Figure 5.1 The relationship between the technic specifications and detail design of the CNPC tactile sensing system.

5.3.1 Material selection

For the polymer substrate, the requirement is that the hardness of the polymer should be similar to the human skin. The polymer substrate has two functions: serving as the soft substrate and generating deformation for tactile sensing. The first function is related to the hardness requirement and the second function is related to the sensitivity (gauge factor) of the tactile sensing system. It is noted that a specific sensitivity of a CNPC tactile sensor can be achieved by adjusting the volume of carbon nanomaterials coated on the polymer substrate according to the conclusion of Chapter 3. Therefore, the selection of the material of the polymer substrate is expected to first meet the hardness requirement.

The hardness of human skin varies with the age and the location on the body. Normally, the hardness of human skin is varying between Shore A 20 to 45 (Muthu, 2007). Considering the requirement is that the hardness of the polymer substrate is close to human skin, there are many polymers suitable to this range of Shore A hardness. Another concern of the selection of the polymer substrate is the fabrication cost. The shape and size of the polymer substrate vary from one application to another. The polymer substrate should be fabricated to different shapes and sizes in an easy and cost-effective method. There are many types of polymers are readily suitable to the requirements of hardness range and fabrication method, e.g., PDMS, silicone rubber, Polychloroprene rubber, etc. PDMS was selected as the polymer substrate for multiple benefits of it: (1) simple and inexpensive fabrication method; (2) good contour accuracy; (3) low production cost; (4) easy bonding to other substrates (Roh et al., 2016) (McDonald et al., 2000) (Schneider et al., 2009). PDMS is a commercially available elastomer and can be molded to different shapes and sizes.

For the carbon nanomaterials, SWCNT, MWCNT, and graphene are typically used as coating materials. To reduce the fabrication difficulty and achieve the evenly distribution, MWCNT was selected (Nurazzi et al., 2021). Miao (2013) introduced a coating method with a spraying gun and proved its effectiveness, which was employed in this dissertation.

For the soft conductive wire, it should be elastic and do not have resistance change when deformed or the resistance change is relatively small compared with the resistance change of the tactile sensor when deformed. Carbon conductive paste from MG Chemical (Product number 847) was selected as the soft wire material. It has relatively low resistivity, $23\ \Omega \cdot m$. It can maintain its shape after applied in the grooves of the polymer substrate and deformed with the polymer substrate.

5.3.2 Embodiment design

The structure is based on the one proposed in Section 4.4. Per the design requirements, the tactile sensing system is a 50 mm × 50 mm square film with thickness of 3 mm. There are

in total 25 sensors distributed over the substrate. Therefore, each sensor occupied a 10 mm × 10 mm square and is located at the center of the square (Figure 5.2). The size of the sensor was designed as a circular with a diameter of 4 mm and a depth of 1.5 mm. The circular shape makes it non-directional to receive deformation around.

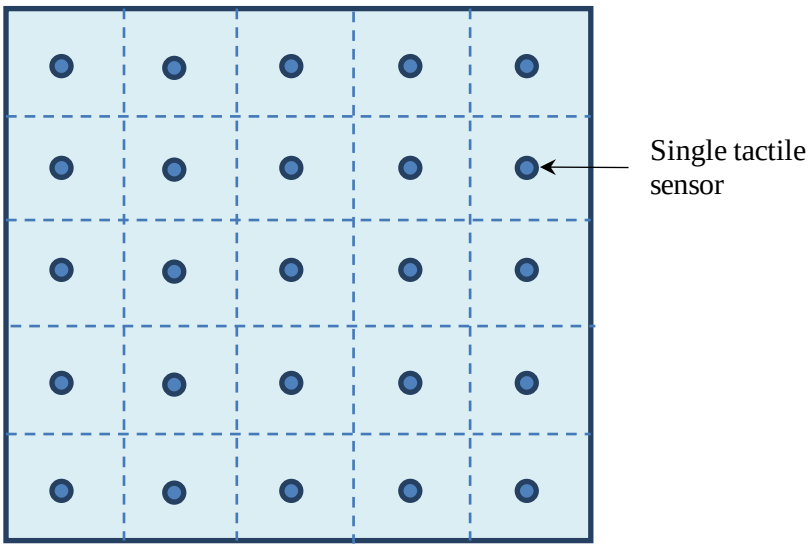

Figure 5.2 The distribution of the CNPC tactile sensors

It is noted that the gauge factor of the single CNPC tactile sensor for this example system is from 10 to 15 (Table 5.1). The coating volume 10 drops (0.1 ml per drop using a pipette) of MWCNT on the PDMS substrate was determined, which can achieve the gauge factor of 11.9 based on the results obtained in Section 3.6. The schematic diagram of the prototype is shown in Figure 5.3.

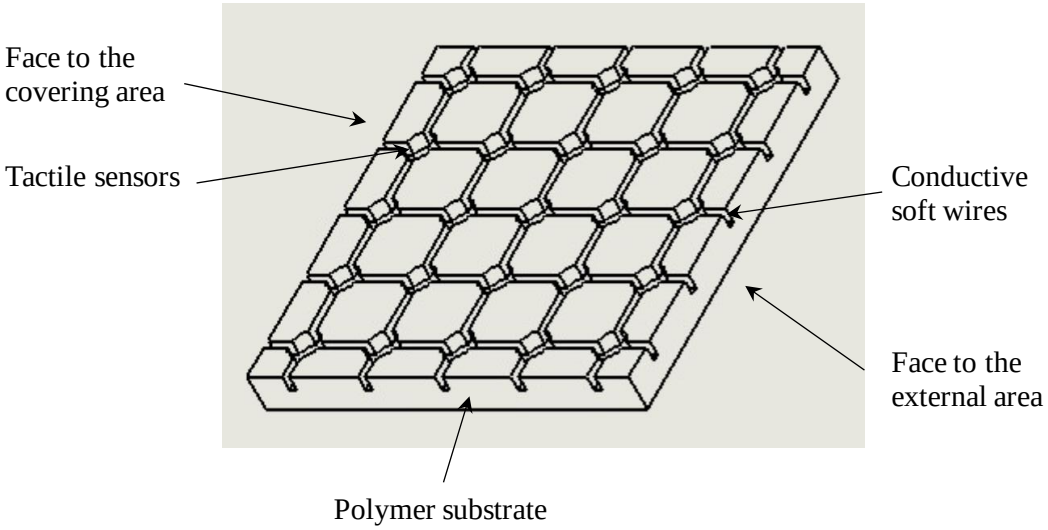

Figure 5.3 Structure of the tactile sensing system.

5.4 The fabrication procedure

The fabrication procedure for the tactile sensing system includes two steps. Step 1: the fabrication of PDMS substrate; Step 2: fabrication of the CNPC tactile sensors. The fabrication of the CNPC tactile sensors contains the coating of carbon nanomaterials and placing soft conductive wires into the grooves. Figure 5.4 shows the entire fabrication procedure, and details of each step are discussed in the following.

5.4.1 Step 1: Fabrication of the PDMS substrate

To achieve the adjustability, scalability, and fast fabrication, an easily accessible mold is needed for the PDMS substrate. 3D printing for the mold was considered. However, two problems occurred when finding a suitable 3D printing material for the mold.

The first problem is that the thermal expansion of the 3D printing mold should be limited in a certain range that would not affect the shape of PDMS substrate. The curing time of PDMS decreases with the increase of curing temperature (The Dow Chemical Company, 2017). It needs 48 hours to cure the PDMS when the temperature is 25 ℃, while only 10 minutes at 150 ℃. The 3D printed mold may not stand the high temperature. Therefore, a

trade-off was taken between the time and curing temperature. After dozens of trials, Polylactic Acid (PLA) was chosen to be the material of the 3D printed mold. The curing temperature was set to 60 ℃ for 10 hours to cure the PDMS. The PLA mold was expected to have mild deformation only, which will not affect the shape of PDMS when heated to 60 ℃ for curing.

The other problem is the detach of the PLA mold and the PDMS substrate. After curing, the PDMS substrate is attached with the PLA mold. The minor features would be destroyed when removing the PDMS substrate from the PLA mold without a releasing agent. Silanization was used to produce a passivation of the surface to help release the PDMS from the PLA substrate.

The fabrication process is as follows:

(1) 3D modelling of the PDMS substrate mold.
(2) 3D printing the mold.
(3) Silanization treatment of the mold surface.
(4) Mixing PDMS base polymer and cross-linking agent (1:10) together.
(5) Debubble the mixing liquid in a vacuumed environment.
(6) Pouring the PDMS liquid on the mold.
(7) Putting the mold with PDMS liquid in an oven at 60 ℃ for 10 hours.
(8) Remove the PDMS from the mold.

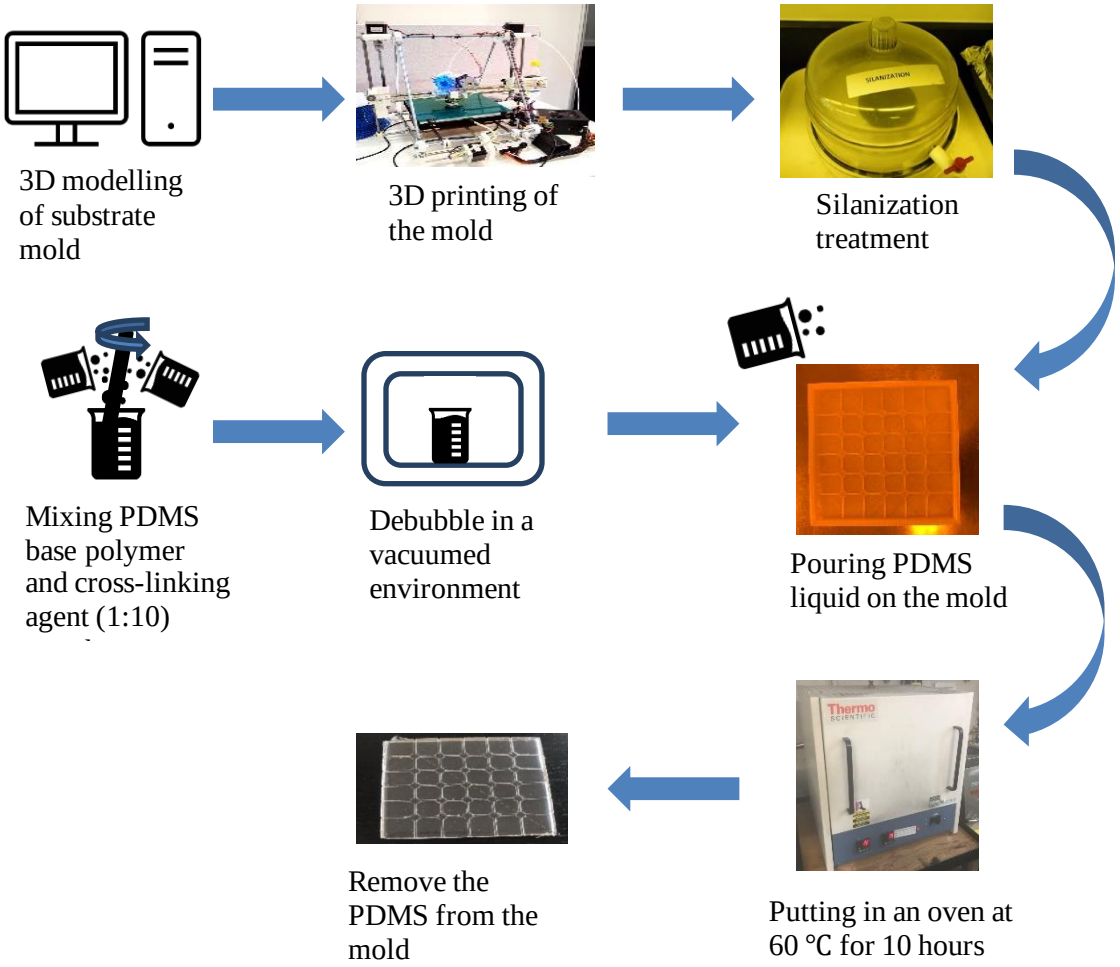

Figure 5.4 The fabrication process of the PDMS substrate.

5.4.2 Step 2: Fabrication of the CNPC tactile sensors

After getting the PDMS substrate, the tactile sensor network is fabricated upon the PDMS substrate, see Figure 5.5. To coating the MWCNT on the surface of the substrate, the dichloromethane (DCM) was used as the solvent, 1 wt.% Sodium dodecyl sulfate (SDS) was added as the surfactant, and a spray gun supplied with pressured nitrogen was employed. To avoid the bundling of the MWCNTs, a powerful ultra-sonification probe was used (Branson sonifier 150). The amount of MWCNT that sprayed was controlled by the volume of the MWCNT/DCM solution. After spraying the MWCNT, carbon conductive paste was used as the soft conductive wiring to connect the sensing network.

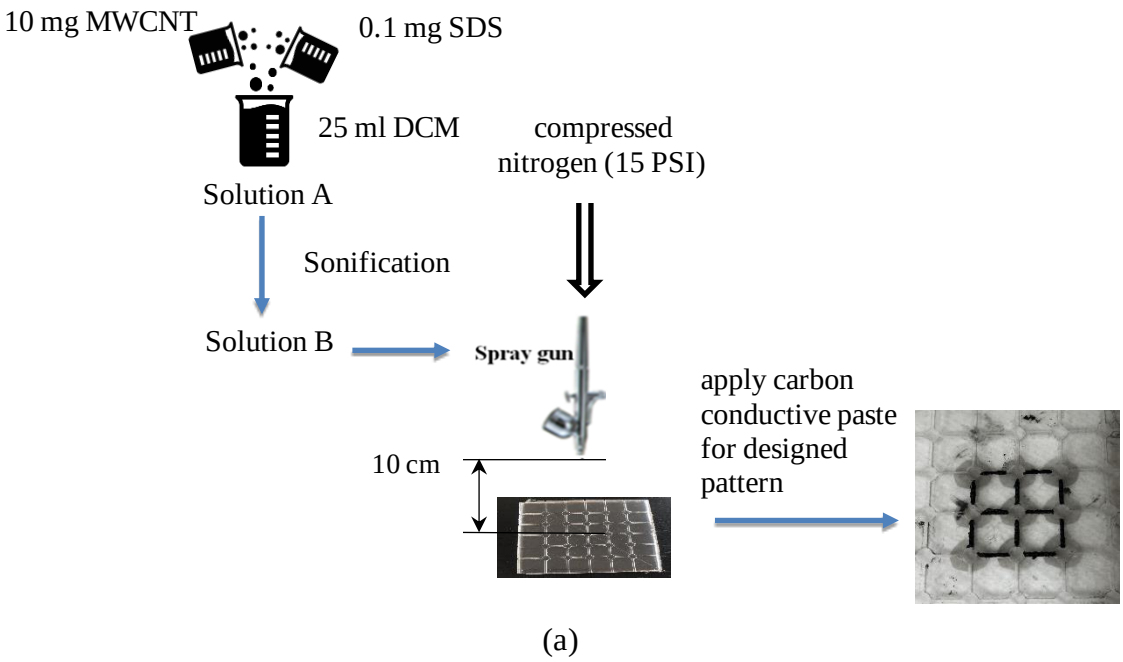

(a)

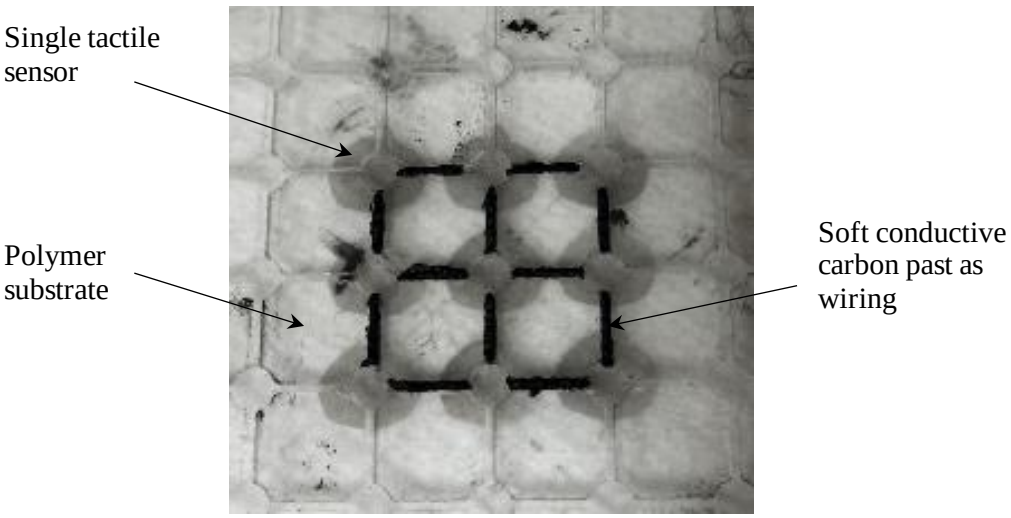

(b)

Figure 5.5 (a) the fabrication procedure of the tactile sensing system; (b) the prototype of the CNPC tactile sensing system with a 3 by 3 sensor network.

It is noted that the diameter of the coating area is 2 mm larger than the designed circular groove. This is because the overlapping of the coating area and the conductive wires can

minimize the contact resistance. After the conductive wires were applied, the actual coating area that has the piezo resistance response is not changed (i.e., the circular groove).

5.5 Validation of the CNPC tactile sensing system

The gauge factor of the CNPC tactile sensing system is defined as the gauge factor of the single CNPC tactile sensor. The resolution of the CNPC tactile sensing system is one single sensor per 1 cm square. The resolution of the single CNPC sensor is measured with the specific thickness of polymer substrate of the CNPC tactile sensing system.

5.5.1 The gauge factor of the single tactile sensor

Figure 5.6 shows a setup of the testbed to validate the robotic skin as fabricated. In Figure 5.5, a DC power supply was connected to the CNPC tactile sensing system. An amplifier probe was used together with an oscilloscope to measure the electric current in the measurement circuit.

The gauge factor was measured by applying the CNPC tactile sensing system on a curved surface and calculating the resistance change and the length change. The gauge factor was measured as 12.7, which is close to the reference value 11.9 in Section 3.6. This error was likely caused by the fabrication error and measurement error.

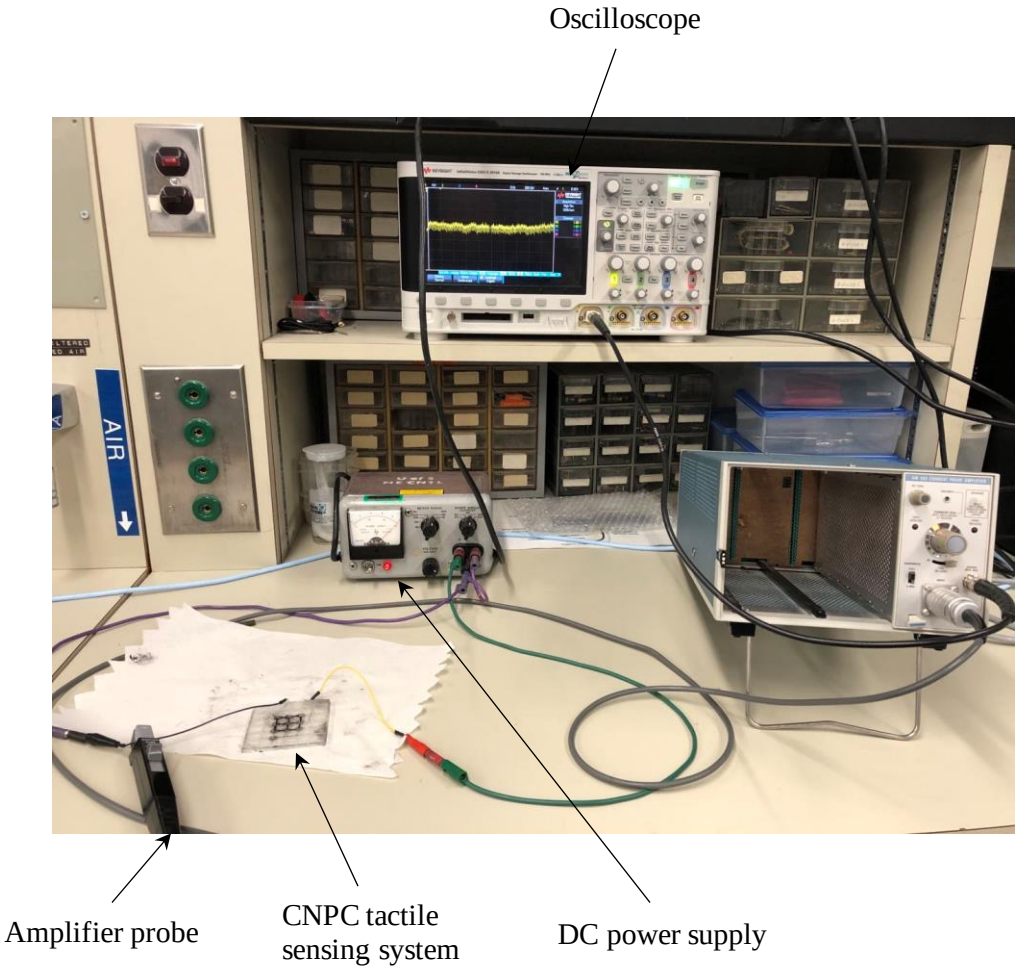

Figure 5.6 The validation of the CNPC tactile sensing system.

5.5.2 The resolution of the single tactile sensor

To measure the resolution of the single tactile sensor, a set of metal balls were chosen as the loading to create the deformation. The set of metal balls includes 5 stainless steel balls with radiuses of 5/32 inch (3.97 mm), 5/16 inch (7.94 mm), 7/16 inch (11.11 mm), 9/16 inch (14.29 mm), and 3/4 inch (19.05 mm) and were available in the market. Their weights are listed in the Table 3.4.

Table 5.2 The radiuses and weights of the metal balls.

Metal ball weight	Radius	Weight
No. 1	5/32 inch (3.97 mm)	0.5 g
No. 2	5/16 inch (7.94 mm)	3.6 g
No. 3	7/16 inch (11.11 mm)	8.4 g
No. 4	9/16 inch (14.29 mm)	12.3 g
No. 5	3/4 inch (19.05 mm)	28.5 g

Measurement method: A specific metal ball was placed on the surface of the single tactile sensor (Figure 5.7). A multimeter was used to measure the resistance before and after the metal ball is placed. An average value was obtained from 5 repetitive measurements.

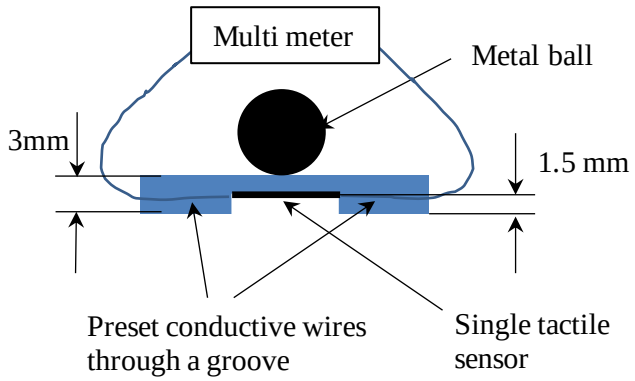

Figure 5.7 The measurement of resolution of single tactile sensor.

Because of the signal noise, measurement error, and the fabrication error, the resolution is varying in a range between 0.12 N and 0.28 N, which are the weights of No. 4 metal ball and No. 5 metal ball.

5.6 Conclusion

This chapter presented the design, fabrication, and testing of a prototype of a robotic skin for HuBots. The prototype was designed by following the systematic design approach presented in Chapter 4 and fabricated by following the experience described in Chapter 3, particularly with the coating method for the CNPC sensor along with the 3D printing of the PDMS substrate. The prototype was successfully built with the following

characteristics: (1) the area covered being curved with the curvature of a minimum radium of 28.6mm, (2) the covered area being 25 cm^2, (3) the gauge factor being 12.7 within the required gauge factor range, and (4) the resolution being one sensor per 1 cm^2. The error of the gauge factor is likely attributed to the fabrication error especially 3D fabrication of the mold of PLA and peeling of the PDMS substrate from PLA molding. This seems to be a limiting factor with the 3D printing technique for this application. Finally, the successful building of the prototype has also demonstrated the effectiveness of the proposed design approach with this dissertation, presented in Chapter 4.

The fabrication of the tactile sensing system includes two steps. The first is the fabrication of the PDMS substrate. It is related to the shape and size of the substrate and the pattern of the sensing network. The 3D printing technique makes it easy and fast for different changes. The second step is the fabrication of the CNPC tactile sensors. It includes the coating of carbon nanomaterials and placing soft wirings. The coating thickness of the carbon nanomaterials is controlled by the volume sprayed.

CHAPTER 6
CONCLUSIONS AND RECOMMENDATIONS FOR FUTURE WORK

6.1 Overview and conclusions

The carbon nanomaterials and polymers can be used for soft tactile sensors as well as networks of sensors (or robotic skins) for HuBots. An effective combination of them has been studied in literature. There are potentially two types of CNPC tactile sensors, namely (1) the carbon nanomaterial filled polymer composite tactile sensor and (2) the carbon nanomaterial coated polymer film tactile sensor. The technology for constructing CNPC tactile sensors was not matured enough. Further, fabrication of networks of force tactile sensors for applications other than HuBots has been studied in literature, but there is no systematic design approach available in literature for networks of CNPC tactile sensors with consideration of their manufacturability.

The overall objective of this dissertation was to advance the design and manufacturing technology for constructing robotic skins for HuBots. The following three specific objectives were defined to achieve the overall objective: (1) To advance the technology for constructing CNPC tactile sensors with adaptable Young's modulus for HuBots. (2) To develop a systematic design approach for a CNPC tactile sensing system such that the design process starts with the technical specification of requirements and ends at the specification of a skin sensor system for HuBots. (3) To construct a prototype of the CNPC tactile sensing system, which can adapt to different sizes and shapes of surfaces of a Hu Bot, and to demonstrate the effectiveness of the design approach developed in Objective (2).

The experimental study of constructing CNPC tactile sensors with two categories of methods (i.e., distributing carbon nanomaterials into a polymer solution called the distribution method, carbon nanomaterials onto the surface of a polymer called the coating method) was conducted. Three possible ways for distributing carbon nanomaterials into a particular polymer solution, which consists of two materials (EAA, AUD), were studied.

Development of a systematic design approach to networks of CNPC tactile sensors by applying general design theories and methodologies, specifically axiomatic design theory and adaptable design methodology, was attempted. Prototyping of a robotic skin on a hypothetical HuBot was conducted.

The following conclusions can be drawn from this study. (1) With respect to Objective (1), it is possible to make MWCNT or SWCNT filled EAA/AUD tactile sensor with the redox method with its reliability needing improvement. (2) With respect to Objective (2), (a) the coating method is better than the distribution method, as the latter is a coupled design, which increase the complexity of fabrication, and (b) a systematic design approach for the CNPC tactile sensing system or for HuBots is effective; in particular the design is adaptable to any HuBot in terms of different shapes, size, gauge factors, and resolutions. (3) With respect to Objective (3), a prototype of an adaptable CNPC tactile sensing system including CNPC tactile sensors is constructed with a reasonable accuracy in terms of achieving a required gauge factor.

6.2 Contributions

This dissertation has made contributions in the field of soft tactile sensors and soft sensor networks. First, some new knowledge has been generated regarding the feasibility for the distribution of carbon nanomaterials into the EAA/AUD polymer with the photo initiator curing method, thermal initiator curing method, and redox initiator curing method. This knowledge gives a limit of the distribution method. Second, a new type of CNPC tactile sensor has been fabricated, i.e., the 5 wt% MWCNT filled EAA/AUD polymer composite tactile sensor with gauge factor of 57 and the 5 wt% SWCNT filled EAA/AUD polymer composite tactile sensor with gauge factor of 28. Third, the best fabrication method of CNPC tactile sensors and flexible sensor networks for HuBots has been given, i.e., the coating method. Fourth, a systematic design approach with reliable manufacturability to CNPC tactile sensors and flexible sensor networks for HuBots has been developed with a unique feature of the network being adaptable to new requirements. Last, a prototype of the network of CNPC tactile sensors has been made, which consists of 25 sensors and has

the coverage area of 25 cm^2, and gauge factor of 12.7. The resolution of the CNPC single tactile sensor is between 0.12 N and 0.28 N (metal ball test in Section 5.5).

6.3 Recommendations for future work

Future works are expected to improve the dissertation research.

First, the signal collection and processing system needs to be further developed, specifically reducing the number of circuits and improving the resilience of the sensing system. For the case study in Chapter 5, only a few tactile sensors are employed, and each tactile sensor is measured separately to get the direct result of the resistance change. When many tactile sensors are included, the signal collection and processing system would be sophisticated if each tactile sensor is connected in one circuit. To reduce the number of circuits, several tactile sensors can be contained in one measurement circuit. The resilience of the tactile sensing system is meant that if a specific tactile sensor changes to be non-conductive, the multiple pathways of circuits can keep working.

Second, a table of the coating density, the resistance, and gauge factor is needed to facilitate the design of CNPC tactile sensing system, determining the dosage of carbon nanomaterials. That is, given the expected initial resistance and gauge factor of the tactile sensors that can be fabricated by a specific coating method, to determine dosages of carbon nanomaterials based on the foregoing table.

Third, the self-healing polymer (Thakur & Kessler, 2015; Wu et al., 2008) may be used as the polymer substrate of the CNPC tactile sensing system or the polymer matrix of the single tactile sensor to increase its resilience. The CNPC tactile sensing system is designed to cover the body of HuBot, and the polymer substrate interacts with the environment. The damage of the CNPC tactile sensing system may happen if the substrate is scratched or cut. The self-healing polymer can self-heal such partial damages. It is worth mentioning that use of the self-healing polymer as the polymer matrix of the single tactile sensor was studied in (Tee et al., 2012). The main concern of using the self-healing polymer in the

CNPC tactile sensing system is the change of the mechanical and electrical properties of the substrate after self-healing, and thus the change of the performance of the sensor.

Fourth, the application of the soft CNPC tactile sensing system is expected to be explored. The soft CNPC tactile sensors and sensing systems could also be applied in remote surgery, exoskeleton, rehabilitation equipment, condition monitoring, etc. The key enabler for these applications is that the soft CNPC tactile system is a thin skin, capable of wrapping on curved bodies, e.g., surgical tool body, rehabilitation equipment body, etc. What the operators, e.g., physicians, hold the machine body, the sensor can measure the operators' pressure on the body, which may imply a mental state of the operators.

REFERENCES

Alamusi, Hu, N., Fukunaga, H., Atobe, S., Liu, Y., & Li, J. (2011). Piezoresistive strain sensors made from carbon nanotubes based polymer nanocomposites. *Sensors*, 11(11), 10691–10723. https://doi.org/10.3390/s111110691

Amjadi, M., Kyung, K. U., Park, I., & Sitti, M. (2016). Stretchable, skin-mountable, and wearable strain sensors and their potential applications: a review. *Adv. Funct. Mater.*, 26: 1678-1698. https://doi.org/10.1002/adfm.201504755

Amjadi, M., Pichitpajongkit, A., Lee, S., Ryu, S., & Park, I. (2014). Highly stretchable and sensitive strain sensor based on silver nanowire-elastomer nanocomposite. *ACS Nano*, *8*(5), 5154–5163. https://doi.org/10.1021/nn501204t

Amjadi, M., Yoon, Y. J., & Park, I. (2015). Ultra-stretchable and skin-mountable strain sensors using carbon nanotubes-Ecoflex nanocomposites. *Nanotechnology*, *26*(37), 375501. https://doi.org/10.1088/0957-4484/26/37/375501

Barnett, B., & Vaughan, W. E. (1947). The decomposition of benzoyl peroxide. *Ind. Eng. Chem., Anal. Ed* (17). https://pubs.acs.org/sharingguidelines

Bartlett, P. D., & Nozaki, K. (1947). The decomposition of benzoyl peroxide in solvents. II. ethers, alcohols, phenols and amines. *Journal of the American Chemical Society*, *69*(10), 2299–2306. https://doi.org/10.1021/ja01202a017

Bi, Z. M., Lang, S. Y. T., & Wang, L. (2008). Improved control and simulation models of a tricycle collaborative robot. *Journal of Intelligent Manufacturing*, 19(6), 715–722. https://doi.org/10.1007/s10845-008-0122-4

Biswas, S., Fukushima, H., & Drzal, L. T. (2011). Mechanical and electrical property enhancement in exfoliated graphene nanoplatelet/liquid crystalline polymer nanocomposites. *Composites Part A: Applied Science and Manufacturing*, *42*(4), 371–375. https://doi.org/10.1016/j.compositesa.2010.12.006

Boland, C. S., Khan, U., Backes, C., O'Neill, A., McCauley, J., Duane, S., … Coleman, J. N. (2014). Sensitive, high-strain, high-rate bodily motion sensors based on graphene-rubber composites. *ACS Nano*, *8*(9), 8819–8830. https://doi.org/10.1021/nn503454h

Boland, C. S., Khan, U., Ryan, G., Barwich, S., Charifou, R., Harvey, A., … Coleman, J. N. (2016). Sensitive electromechanical sensors using viscoelastic graphene-polymer

nanocomposites. *Science*, *354*(6317), 1257–1260. https://doi.org/10.1126/science.aag2879

Broadbent, S. R., & Hammersley, J. M. (1957). Percolation processes: I. crystals and mazes. *Mathematical Proceedings of the Cambridge Philosophical Society*, *53*(3), 629–641. https://doi.org/10.1017/S0305004100032680

Broza, G., Piszczek, K., Schulte, K., & Sterzynski, T. (2007). Nanocomposites of poly(vinyl chloride) with carbon nanotubes (CNT). *Composites Science and Technology*, *67*(5), 890–894. https://doi.org/10.1016/j.compscitech.2006.01.033

Bunde, A., & Dieterich, W. (2000). Percolation in composites. *Journal of Electroceramics*, *5*(2), 81–92. https://doi.org/10.1023/A:1009997800513

Bunde, A., Heitjans, P., Indris, S., Kantelhardt, J. W., & Ulrich, M. (2007). Anomalous transport and diffusion in percolation systems. *Diffusion Fundamentals*, 6(2007), 1–17.

Chang, T. H., Tian, Y., Li, C., Gu, X., Li, K., Yang, H., … Chen, P. Y. (2019). Stretchable graphene pressure sensors with Shar-Pei-like hierarchical wrinkles for collision-aware surgical robotics. *ACS Applied Materials and Interfaces*, *11*(10), 10226–10236. research-article. https://doi.org/10.1021/acsami.9b00166

Chen, Y., Yu, M., Bruck, H. A., & Smela, E. (2016). Stretchable touch-sensing skin over padding for co-robots. *Smart Materials and Structures*, *25*(5). https://doi.org/10.1088/0964-1726/25/5/055006

Cheng, M. Y., Tsao, C. M., Lai, Y. Z., & Yang, Y. J. (2011). The development of a highly twistable tactile sensing array with stretchable helical electrodes. *Sensors and Actuators, A: Physical*, *166*(2), 226–233. https://doi.org/10.1016/j.sna.2009.12.009

Choudhary, N., Hwang, S., & Choi, W. (2014). Carbon nanomaterials: a review. *Handbook of Nanomaterials Properties* (pp. 709–769). Berlin, Heidelberg: Springer Berlin Heidelberg. https://doi.org/10.1007/978-3-642-31107-9_37

Dai, Z., (2019). Improvement of general design theory and methodology with its application to design of a retractor for ventral hernia repair surgery [Master's thesis, University of Saskatchewan].

Dargahi, J., & Najarian, S. (2004). Human tactile perception as a standard for artificial tactile sensing--a review. *The International Journal of Medical Robotics + Computer*

Assisted Surgery : MRCAS, *1*(1), 23–35. https://doi.org/10.1002/rcs.3

Delozier, D. M., Watson, K. A., Smith, J. G., Clancy, T. C., & Connell, J. W. (2006). Investigation of aromatic/aliphatic polyimides as dispersants for single wall carbon nanotubes. *Macromolecules*, *39*(5), 1731–1739. https://doi.org/10.1021/ma051826u

Du, F., Guthy, C., Kashiwagi, T., Fischer, J. E., & Winey, K. I. (2006). An infiltration method for preparing single-wall nanotube/ epoxy composites with improved thermal conductivity. Journal of Polymer Science, Part B: Polymer Physics, 44(10), 1513–1519. https://doi.org/10.1002/polb.20801

Du, J., Zhao, L., Zeng, Y., Zhang, L., Li, F., Liu, P., & Liu, C. (2011). Comparison of electrical properties between multi-walled carbon nanotube and graphene nanosheet/high density polyethylene composites with a segregated network structure. *Carbon*, *49*(4), 1094–1100. https://doi.org/10.1016/j.carbon.2010.11.013

Engel, J., Chen, J., Chen, N., Pandya, S., & Liu, C. (2006). Multi-walled carbon nanotube filled conductive elastomers: materials and application to micro transducers. *MEMS*, 2006, 246–249.

Fan, L. X., Cai, M. Y., Lin, Y., & Zhang, W. J. (2015). Axiomatic design theory: Further notes and its guideline to applications. *International Journal of Materials and Product Technology*, *51*(4), 359–374. https://doi.org/10.1504/IJMPT.2015.072557

Fan, Z., Zhang, L., Tan, Q., Yao, X., Lin, B., Wang, Y., & Xiong, J. (2021). Wearable pressure sensor based on MXene/single-wall carbon nanotube film with crumpled structure for broad-range measurements. *Smart Materials and Structures*, *30*(3). https://doi.org/10.1088/1361-665X/abe030

Ghislandi, M., Tkalya, E., Schillinger, S., Koning, C. E., & De With, G. (2013). High performance graphene- and MWCNTs-based PS/PPO composites obtained via organic solvent dispersion. *Composites Science and Technology*, *80*, 16–22. https://doi.org/10.1016/j.compscitech.2013.03.006

Göger, D., & Wörn, H. (2007). A highly versatile and robust tactile sensing system. *Sensors, 2007 IEEE*, 2007, 1056-1059. https://doi.org/10.1109/ICSENS.2007.4388587

Grossiord, N., Loos, J., Regev, O., & Koning, C. E. (2006). Toolbox for dispersing carbon nanotubes into polymers to get conductive nanocomposites. *Chemistry of Materials*, *18*(5), 1089–1099. https://doi.org/10.1021/cm051881h

Gu, P., Hashemian, M., & Nee, A. Y. C. (2004). Adaptable design. *CIRP Annals - Manufacturing Technology*, *53*(2), 539–557. https://doi.org/10.1016/S0007-8506(07)60028-6

Hashemian, M. (2005). Design for adaptability [Doctoral dissertation, University of Saskatchewan]

He, Zhiping, Zhang, X., Chen, M., Li, M., Gu, Y., Zhang, Z., & Li, Q. (2013). Effect of the filler structure of carbon nanomaterials on the electrical, thermal, and rheological properties of epoxy composites. *Journal of Applied Polymer Science*, *129*(6), 3366–3372. https://doi.org/10.1002/app.39096

He, Zuoli, Zhou, G., Byun, J. H., Lee, S. K. B., Um, M. K., Park, B., … Chou, T. W. (2019). Highly stretchable multi-walled carbon nanotube/thermoplastic polyurethane composite fibers for ultrasensitive, wearable strain sensors. *Nanoscale*, *11*(13), 5884–5890. https://doi.org/10.1039/C9NR01005J

Hu, G., Zhao, C., Zhang, S., Yang, M., & Wang, Z. (2006). Low percolation thresholds of electrical conductivity and rheology in poly(ethylene terephthalate) through the networks of multi-walled carbon nanotubes. *Polymer*, *47*(1), 480–488. https://doi.org/10.1016/j.polymer.2005.11.028

Ji, Z., Zhu, H., Liu, H., Liu, N., Chen, T., Yang, Z., & Sun, L. (2016). The design and characterization of a flexible tactile sensing array for robot skin. *Sensors*, *16*(12), 2001. https://doi.org/10.3390/s16122001

Khan, M. O., Leung, S. N., Chan, E., Naguib, H. E., Dawson, F., & Adinkrah, V. (2013). Effects of microsized and nanosized carbon fillers on the thermal and electrical properties of polyphenylene sulfide based composites. *Polymer Engineering and Science*, *53*(11), 2398–2406. https://doi.org/10.1002/pen.23503

Knapp, B., & Kohl, P. A. (2014). Polymers for microelectronics. *Journal of Applied Polymer Science*, *131*(24), n/a-n/a. https://doi.org/10.1002/APP.41233

Kong, J. H., Jang, N. S., Huh, J. Y., Kim, S. H., & Kim, J. M. (2015). Piezoresistive polymer diaphragm sensor array using conductive elastomeric nanocomposite films for skin-mountable keypad applications. *Journal of Microelectromechanical Systems*, *24*(3), 626–633. https://doi.org/10.1109/JMEMS.2014.2338332

Kong, J. H., Jang, N. S., Kim, S. H., & Kim, J. M. (2014). Simple and rapid micropatterning

of conductive carbon composites and its application to elastic strain sensors. *Carbon*, *77*, 199–207. https://doi.org/10.1016/j.carbon.2014.05.022

Kong, K. T. S., Mariatti, M., Rashid, A. A., & Busfield, J. J. C. (2014). Enhanced conductivity behavior of polydimethylsiloxane (PDMS) hybrid composites containing exfoliated graphite nanoplatelets and carbon nanotubes. *Composites Part B: Engineering*, *58*, 457–462. https://doi.org/10.1016/j.compositesb.2013.10.039

Kumar, S., Sun, L. L., Caceres, S., Li, B., Wood, W., Perugini, A., … Zhong, W. H. (2010). Dynamic synergy of graphitic nanoplatelets and multi-walled carbon nanotubes in polyetherimide nanocomposites. *Nanotechnology*, *21*(10), 105702. https://doi.org/10.1088/0957-4484/21/10/105702

Li, J., Ma, P. C., Chow, W. S., To, C. K., Tang, B. Z., & Kim, J. K. (2007). Correlations between percolation threshold, dispersion state, and aspect ratio of carbon nanotubes. *Advanced Functional Materials*, *17*(16), 3207–3215. https://doi.org/10.1002/adfm.200700065

Li, J., Orrego, S., Pan, J., He, P., & Kang, S. H. (2019). Ultrasensitive, flexible, and low-cost nanoporous piezoresistive composites for tactile pressure sensing. *Nanoscale*, *11*(6), 2779–2786. https://doi.org/10.1039/c8nr09959f

Liao, S. H., Yen, C. Y., Weng, C. C., Lin, Y. F., Ma, C. C. M., Yang, C. H., … Hsiao, Y. H. (2008). Preparation and properties of carbon nanotube/polypropylene nanocomposite bipolar plates for polymer electrolyte membrane fuel cells. *Journal of Power Sources*, *185*(2), 1225–1232. https://doi.org/10.1016/j.jpowsour.2008.06.097

Lin, Y., & Zhang, W. J. (2005). A function-behavior-state approach to designing human-machine interface for nuclear power plant operators. *IEEE Transactions on Nuclear Science*, *52*(1 III), 430–439. https://doi.org/10.1109/TNS.2004.842728

Lu, N., Lu, C., Yang, S., & Rogers, J. (2012). Highly sensitive skin-mountable strain gauges based entirely on elastomers. *Advanced Functional Materials*, *22*(19), 4044–4050. https://doi.org/10.1002/adfm.201200498

Lu, X., Dou, H., Yang, S., Hao, L., Zhang, L., Shen, L., … Zhang, X. (2011). Fabrication and electrochemical capacitance of hierarchical graphene/polyaniline/carbon nanotube ternary composite film. *Electrochimica Acta*, *56*(25), 9224–9232. https://doi.org/10.1016/j.electacta.2011.07.142

Ma, P. C., Siddiqui, N. A., Marom, G., & Kim, J. K. (2010). Dispersion and functionalization of carbon nanotubes for polymer-based nanocomposites: A review. *Composites Part A: Applied Science and Manufacturing*. *41*(10), 1345-1367. https://doi.org/10.1016/j.compositesa.2010.07.003

Marsden, A. J., Papageorgiou, D. G., Vallés, C., Liscio, A., Palermo, V., Bissett, M. A., … Kinloch, I. A. (2018). Electrical percolation in graphene-polymer composites. *2D Materials*. 5(3), 32003. https://doi.org/10.1088/2053-1583/aac055

Martin, C. A., Sandler, J. K. W., Shaffer, M. S. P., Schwarz, M. K., Bauhofer, W., Schulte, K., & Windle, A. H. (2004). Formation of percolating networks in multi-wall carbon-nanotube-epoxy composites. *Composites Science and Technology*, *64*(15 SPEC. ISS.), 2309–2316. https://doi.org/10.1016/j.compscitech.2004.01.025

Mattmann, C., Clemens, F., & Tröster, G. (2008). Sensor for measuring strain in textile. *Sensors*, *8*(6), 3719–3732. https://doi.org/10.3390/s8063719

McDonald, J. C., Duffy, D. C., Anderson, J. R., Chiu, D. T., Wu, H., Schueller, O. J. A., & Whitesides, G. M. (2000). Fabrication of microfluidic systems in poly(dimethylsiloxane). *Electrophoresis*. 21: 27-40. https://doi.org/10.1002/(SICI)1522-2683(20000101)21:1<27::AID-ELPS27>3.0.CO;2-C

Mcdonald, K. T. (2000). Resistance of a Disk. https://www.hep.princeton.edu/~mcdonald/examples/resistivedisk.pdf

Miao, Y., Yang, Q., Chen, L., Sammynaiken, R., & Zhang, W. J. (2012). Modelling of piezoresistive response of carbon nanotube network based films under in-plane straining by percolation theory. *Applied Physics Letters*, *101*(6). https://doi.org/10.1063/1.4742893

Miao, Y., Chen, L., Lin, Y., Sammynaiken, R., & Zhang, W. J. (2011). On finding of high piezoresistive response of carbon nanotube films without surfactants for in-plane strain detection, *22*(18), 2155–2159. https://doi.org/10.1177/1045389X11426179

Miao, Y. (2013). *On understanding of piezoresistive response in carbon nanotube networks under in-plane straining* [Doctoral dissertation, University of Saskatchewan]. Retrieved from http://hdl.handle.net/10388/ETD-2013-11-1506

Miao, Y., Chen, L., Sammynaiken, R., Lin, Y., & Zhang, W. J. (2011). Optimization of

piezoresistive response of pure carbon nanotubes networks as in-plane strain sensors. *Review of Scientific Instruments*, *82*(12), 126104. https://doi.org/10.1063/1.3665959

Miao, Y., Yang, Q. Q., Sammynaiken, R., Zhang, W. J., Maley, J., Schatte, G., … In, I. (2013). Influence of aligned carbon nanotube networks on piezoresistive response in carbon nanotube films under in-plane straining. *Applied Physics Letters*, *102*(23), 233106. https://doi.org/10.1063/1.4808203

Min, C., Shen, X., Shi, Z., Chen, L., & Xu, Z. (2010). The electrical properties and conducting mechanisms of carbon nanotube/polymer nanocomposites: A review. *Polymer - Plastics Technology and Engineering*, *49*(12), 1172–1181. https://doi.org/10.1080/03602559.2010.496405

Muthu, J. E. R. P. (2007). Mechanics of silicon micro needle penetration in human cadaver sk[Master's thesis, Lehigh University]. https://asa.lib.lehigh.edu/Record/972044

Nurazzi, N. M., Asyraf, M. R. M., Khalina, A., Abdullah, N., Sabaruddin, F. A., Kamarudin, S. H., … Sapuan, S. M. (2021). Fabrication, functionalization, and application of carbon nanotube-reinforced polymer composite: An overview. *Polymers*. *2021; 13*(7):1047. https://doi.org/10.3390/polym13071047

Obitayo, W., & Liu, T. (2012). A review: Carbon nanotube-based piezoresistive strain sensors. *Journal of Sensors*. *2012,* 1–15. https://doi.org/10.1155/2012/652438

Oliva-Avilés, A. I., Avilés, F., & Sosa, V. (2011). Electrical and piezoresistive properties of multi-walled carbon nanotube/polymer composite films aligned by an electric field. *Carbon*, *49*(9), 2989–2997. https://doi.org/10.1016/j.carbon.2011.03.017

Pahl, G., Beitz, W., Feldhusen, J., & Grote, K. H. (2007). Engineering design: A systematic approach. Springer London. https://doi.org/10.1007/978-1-84628-319-2

Patel, D. K., Sakhaei, A. H., Layani, M., Zhang, B., Ge, Q., & Magdassi, S. (2017). Highly stretchable and UV curable elastomers for digital light processing based 3D printing. *Advanced Materials*, *29*(15), 1–7. https://doi.org/10.1002/adma.201606000

Peshkin, M., & Colgate, J. E. (1996). "Cobots" Work with People. *IEEE Robotics and Automation Magazine*, *3*(4), 8–9.

Pike, G. E., & Seager, C. H. (1974). Percolation and conductivity: A computer study. I. *Physical Review B*, *10*(4), 1421–1434. https://doi.org/10.1103/PhysRevB.10.1421

Pötschke, P., Dudkin, S. M., & Alig, I. (2003). Dielectric spectroscopy on melt processed

polycarbonate - Multiwalled carbon nanotube composites. *Polymer*, *44*(17), 5023–5030. https://doi.org/10.1016/S0032-3861(03)00451-8

Pradhan, B., & Srivastava, S. K. (2014). Synergistic effect of three-dimensional multi-walled carbon nanotube-graphene nanofiller in enhancing the mechanical and thermal properties of high-performance silicone rubber. *Polymer International*, *63*(7), 1219–1228. https://doi.org/10.1002/pi.4627

Qin, B., Li, B., Zhang, J., Xie, X., & Li, W. (2020). Highly sensitive strain sensor based on stretchable sandwich-type composite of carbon nanotube and poly(styrene–butadiene–styrene). *Sensors and Actuators, A: Physical*, *315*, 112357. https://doi.org/10.1016/j.sna.2020.112357

Regev, O., ElKati, P. N. B., Loos, J., & Koning, C. E. (2004). Preparation of conductive nanotube-polymer composites using latex technology. *Advanced Materials*, *16*(3), 248–251. https://doi.org/10.1002/adma.200305728

Robotiq. (2020). *Collaborative Robot Buyer's Guide*. Retrieved from https://blog.robotiq.com/collaborative-robot-ebook

Roh, C., Lee, J., & Kang, C. (2016). The deformation of polydimethylsiloxane (PDMS) microfluidic channels filled with embedded circular obstacles under certain circumstances. *Molecules*, *21*(6), 798. https://doi.org/10.3390/molecules21060798

Roh, E., Hwang, B. U., Kim, D., Kim, B. Y., & Lee, N. E. (2015). Stretchable, Transparent, Ultrasensitive, and Patchable Strain Sensor for Human-Machine Interfaces Comprising a Nanohybrid of Carbon Nanotubes and Conductive Elastomers. *ACS Nano*, *9*(6), 6252–6261. https://doi.org/10.1021/acsnano.5b01613

Roy, S., Petrova, R. S., & Mitra, S. (2018). Effect of carbon nanotube (CNT) functionalization in epoxy-CNT composites. *Nanotechnol Rev*, *7*(6), 475–485. https://doi.org/10.1515/ntrev-2018-0068

Sahoo, N. G., Cheng, H. K. F., Bao, H., Li, L., Chan, S. H., & Zhao, J. (2011). Nitrophenyl functionalization of carbon nanotubes and its effect on properties of MWCNT/LCP composites. *Macromolecular Research*, *19*(7), 660–667. https://doi.org/10.1007/s13233-011-0710-6

Sandler, J. K. W., Kirk, J. E., Kinloch, I. A., Shaffer, M. S. P., & Windle, A. H. (2003). Ultra-low electrical percolation threshold in carbon-nanotube-epoxy composites.

Polymer, *44*(19), 5893–5899. https://doi.org/10.1016/S0032-3861(03)00539-1

Schneider, F., Draheim, J., Kamberger, R., & Wallrabe, U. (2009). Process and material properties of polydimethylsiloxane (PDMS) for optical MEMS. *Sensors and Actuators, A: Physical*, *151*(2), 95–99. https://doi.org/10.1016/j.sna.2009.01.026

Stauffer, D., Adler, J., & Aharony, A. (1994). Universality at the three-dimensional percolation threshold. *Journal of Physics A: Mathematical and General*, *27*(13), L475. https://doi.org/10.1088/0305-4470/27/13/003

Suh, N. P. (1998). Axiomatic Design Theory for Systems. *Research in Engineering Design - Theory, Applications, and Concurrent Engineering*, *10*(4), 189–209. https://doi.org/10.1007/s001639870001

Sun, X., Wang, C., Chi, C., Xue, N., & Liu, C. (2018). A highly-sensitive flexible tactile sensor array utilizing piezoresistive carbon nanotube–polydimethylsiloxane composite. *Journal of Micromechanics and Microengineering*, *28*(10), 105011. https://doi.org/10.1088/1361-6439/aaceb9

Swain, C. G., Schaad, L. J., & Kresge, A. J. (1958). The mechanism of decomposition of benzoyl peroxide in cyclohexane solution. *Journal of the American Chemical Society*, *80*(19), 5313–5319. https://doi.org/10.1021/ja01552a077

Tee, B. C. K., Wang, C., Allen, R., & Bao, Z. (2012). An electrically and mechanically self-healing composite with pressure- and flexion-sensitive properties for electronic skin applications. *Nature Nanotechnology*, *7*(12), 825–832. https://doi.org/10.1038/nnano.2012.192

Thakur, V. K., & Kessler, M. R. (2015). Self-healing polymer nanocomposite materials: A review. *Polymer (United Kingdom)*, *69*, 369–383. https://doi.org/10.1016/j.polymer.2015.04.086

The Dow Chemical Company. (2017). SYLGARD™ 184 silicone elastomer applications. *Silicone Elastomer Technical Data Sheet*. https://www.dow.com/content/dam/dcc/documents/en-us/productdatasheet/11/11-31/11-3184-sylgard-184-elastomer.pdf?iframe=true

Vadukumpully, S., Paul, J., Mahanta, N., & Valiyaveettil, S. (2011). Flexible conductive graphene/poly(vinyl chloride) composite thin films with high mechanical strength and thermal stability. *Carbon*, *49*(1), 198–205.

https://doi.org/10.1016/j.carbon.2010.09.004

Vatani, M., Engeberg, E. D., & Choi, J. W. (2013). Force and slip detection with direct-write compliant tactile sensors using multi-walled carbon nanotube/polymer composites. *Sensors and Actuators, A: Physical*, *195*, 90–97. https://doi.org/10.1016/j.sna.2013.03.019

Wang J. W., Wang H. F., Zhou Y.M., Wang Y. and Zhang W.J. (2019). On an integrated approach to resilient transportation systems in emergency situations. *Natural computing*. *18*(4), 815–823. https://doi:10.1007/s11047-016-9605-y.

Wang, X., Tang, F., Cao, Q., Qi, X., Pearson, M., Li, M., … Lin, Z. (2020). Comparative study of three carbon additives: Carbon nanotubes, graphene, and fullerene-c60, for synthesizing enhanced polymer nanocomposites. *Nanomaterials*, *10*(5), 838. https://doi.org/10.3390/nano10050838

Wu, D. Y., Meure, S., & Solomon, D. (2008). Self-healing polymeric materials: A review of recent developments. *Progress in Polymer Science (Oxford)*, *33*(5), 479–522. https://doi.org/10.1016/j.progpolymsci.2008.02.001

Wu, N., She, X., Yang, D., Wu, X., Su, F., & Chen, Y. (2012). Synthesis of network reduced graphene oxide in polystyrene matrix by a two-step reduction method for superior conductivity of the composite. *Journal of Materials Chemistry*, *22*(33), 17254–17261. https://doi.org/10.1039/c2jm33114d

Wu, X. C., Sammynaiken, R., Zhang, W. J., Wu, D. Q., Yang, Q., Yang, W., & Wang, R. (2007). Measurement of low concentration and nano-quantity hydrogen sulfide in aqueous solution: Measurement mechanisms and limitations. *Measurement Science and Technology*, *18*(5), 1315–1320. https://doi.org/10.1088/0957-0233/18/5/017

Wu, X. C., Zhang, W. J., Wu, D. Q., Sammynaiken, R., Wang, R., & Yang, Q. (2006). Using carbon nanotubes to absorb low-concentration hydrogen sulfide in fluid. *IEEE Transactions on Nanobioscience*, *5*(3), 204–209. https://doi.org/10.1109/TNB.2006.880843

Wu, X C, Zhang, W. J., Sammynaiken, R., Meng, Q. H., Yang, Q., Zhan, E., … Wang, R. (2008). Non-functionalized carbon nanotube binding with hemoglobin. *Journal of Physics: Conference Series*, *127*(1), 012009. https://doi.org/10.1088/1742-6596/127/1/012009

Wu, Xiao Chu, Wu, D. Q., Sammynaiken, R., Yang, W., Wang, R., & Zhang, W. J. (2008). Toward new instruments for measurement of low concentration hydrogen sulfide in small-quantity aqueous solutions. *Measurement Science and Technology*, *19*(11), 115602. https://doi.org/10.1088/0957-0233/19/11/115602

Yang, S. Y., Lin, W. N., Huang, Y. L., Tien, H. W., Wang, J. Y., Ma, C. C. M., … Wang, Y. S. (2011). Synergetic effects of graphene platelets and carbon nanotubes on the mechanical and thermal properties of epoxy composites. *Carbon, 49*(3), 793–803. https://doi.org/10.1016/j.carbon.2010.10.014

Yuan, C., Tony, A., Yin, R., Wang, K., & Zhang, W. (2021). Tactile and thermal sensors built from carbon–polymer nanocomposites—a critical review. *Sensors. 21*(4), 1–26. https://doi.org/10.3390/s21041234

Zhang, T., Zhang, W., & Gupta, M. M. (2017). Resilient robots: Concept, review, and future directions. *Robotics. 2017, 6*(4):22. https://doi.org/10.3390/robotics6040022

Zhang, W. J., & Lin, Y. (2010). On the principle of design of resilient systems - application to enterprise information systems. *Enterprise Information Systems, 4*(2), 99–110. https://doi.org/10.1080/17517571003763380

Zhang, W. J., Lin, Y., & Sinha, N. (2011). On the function-behavior-structure model for design. *Proceedings of the Canadian Engineering Education Association (CEEA)*. https://doi.org/10.24908/pceea.v0i0.3884

Zhang, W. J., & Van Luttervelt, C. A. (2011). Toward a resilient manufacturing system. *CIRP Annals - Manufacturing Technology, 60*(1), 469–472. https://doi.org/10.1016/j.cirp.2011.03.041

Zhang, W. J., & Wang, J. W. (2016). Design theory and methodology for enterprise systems. *Enterprise Information Systems*. *10*(3), 245–248. https://doi.org/10.1080/17517575.2015.1080860

Zhu, J., Peng, H., Rodriguez-Macias, F., Margrave, J. L., Khabashesku, V. N., Imam, A. M., … Barrera, E. V. (2004). Reinforcing epoxy polymer composites through covalent integration of functionalized nanotubes. *Advanced Functional Materials*, *14*(7), 643–648. https://doi.org/10.1002/adfm.200305162

APPENDIX A

Compressive modulus test by Instron 3363

Tool: Instron 3363 (Figure A.1).

Sample size: diameter: 31mm, thickness: 6.5mm.

Applying area: 0.7854 cm^2

Starting load: 0 N.

Ending load: 7.5 N.

Compressive extension: 4.45mm at 7.5 N.

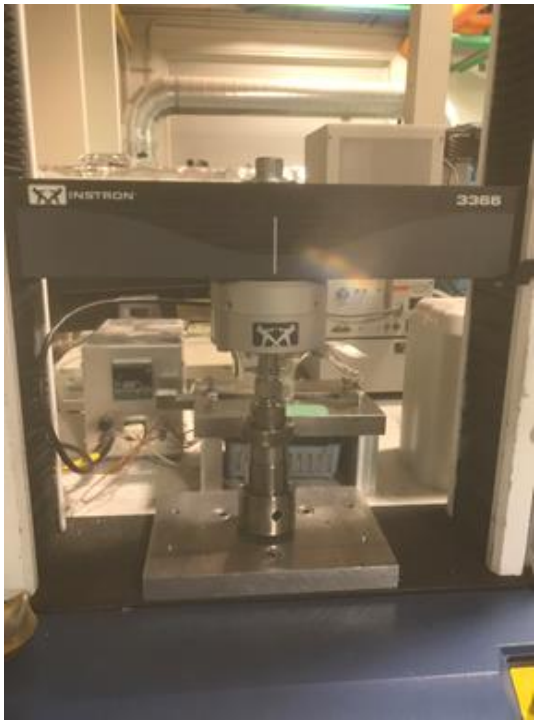

Figure A1. The Instron 3363.

APPENDIX B

Axiomatic Design Theory (adapted from Suh, 1990)

B1. Introduction

Axiomatic design theory (**ADT**) is a systematic design theory and methodology to analyze the customer needs and the design solutions (Suh, 1990; Fan et al., 2015). In ADT, the design process has four domains: the customer domain, the functional domain, the physical domain, and the process domain. In the customer domain, the customer needs are represented as Customer Attributes (**CAs**). Functional requirements (**FRs**) along with Constraint Requirements (**CRs**) and Performance Requirements (**PRs**)[2] in the functional domain are determined to capture the customer needs. The design solutions in the physical domain are represented as design parameters (DPs). DPs are determined to satisfy the FRs. In the process domain, Process Variables (PVs) are defined to produce the product specified in terms of DPs. The relationship between the four domains is illustrated in Figure B1.

[2] In the original description of ADT, Suh (1990) did not explicitly express CR and PR. The first explicit expression of CR and PR refers to a Master thesis (Dai, 2019).

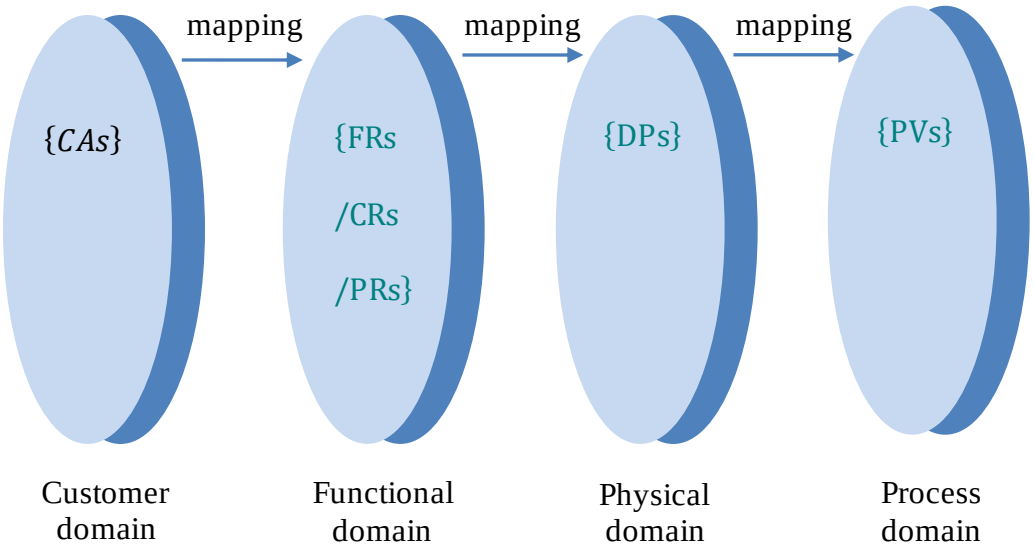

Figure B1. Four domains of the design process. Adapted from (Suh, 1998).

B2. Definitions

- Axiom: According to Suh (1998), "a self-evident truth or fundamental truth for which there are no counter examples or exceptions. axioms may not be derived from other laws of nature or principles."
- Functional Requirement: According to Suh (1998), "a minimum set of independent requirements that completely characterizes the functional needs of the product (or software, organizations, systems, etc.) in the functional domain. By definition, each FR is independent of every other one at the time the FRs are established."
- Constraint: According to Suh (1998), "constraints are bounds on acceptable solutions. There are two kinds of constraints: input constraints and system constraints. Input constraints are imposed as part of design specifications. System constraints are constraints imposed by the system in which the design solution must function."

- Design Parameter: According to Suh (1998), "design parameters are the key physical (or other equivalent terms in the case of software design, etc.) variables in the physical domain that characterize the design satisfying the specified FRs."
- Process Variable: According to Suh (1998), "process variables are the key variables (or other equivalent term in the case of software design, etc.) in the process domain that characterize the process which can generate the specified DPs."

B3. The First Axiom: The Independence Axiom

The Independence Axiom is stated as maintaining the independence of the Functional Requirements (FRs). The Independence Axiom is used when processing from the functional domain to the physical domain. A set of FRs is the description of design goals (Suh, 1998). The Independence Axiom states that 'when there are two or more functional requirements, the design solution must be such that each one of the functional requirements can be satisfied without affecting the other functional requirement'. The mapping process between the domains can be expressed by characteristic vectors. The relationship between a set of FRs and DPs can be written as

$$\{FRs\} = [A]\{DPs\} \quad \text{(B-1)}$$

For the design process from physical domain to the process domain, the design equation can be written as

$$\{DPs\} = [B]\{PVs\} \quad \text{(B-2)}$$

$[A]$ and $[B]$ are the matrices that define the product design and process design. It is noted that there are two special cases of the design matrix: the diagonal matrix and the triangular matrix. The diagonal matrix is that all A_{ij}s except those i=j are equal to zero. The triangular matrix is that either upper or lower triangular elements are equal to zero (Suh, 1998). To meet the Independence Axiom, the design matrix should be either diagonal or triangular. If the design matrix $[A]$ is diagonal, each of the FRs can be satisfied by one DP. Then this design is called *uncoupled design*. If the design matrix is triangular, the independence of FRs can be achieved by changing the DPs in a proper sequence. This design is called *decoupled design*. For those design matrixes that cannot achieve independence of FRs are called *coupled design*. According to the Independence Axiom, a best design is an

uncoupled design, and a better design is a decoupled design, while a coupled design should be avoided.

B4. The Second Axiom: The information Axiom

When more than one design solution satisfies the Independence Axiom, the Information Axiom is used to select the best one. The Information Axiom states that "the one with the highest probability of success is the best design", according to (Suh, 1998). The highest probability of success is further represented by the least information content (**I**). As such, the Information Axiom can also be stated as to minimize the information content (Suh, 1998).

The information content I can be expressed as (Suh, 1998)

$$I = -\log_2 P \tag{B3}$$

P is the probability of success of satisfying a given FR. For an uncoupled design that has n FRs, the information content I is expressed by

$$I = \sum_{i=1}^{n} \left[\log {}^{1}/_{p_i}\right] \tag{B4}$$

where the log is either the logarithm based on 2 or the natural logarithm. The p_i is the probability of DP_i satisfying FR_i, where i=1, 2, …, n. The Information Axiom states that the design with the smallest I is the best design (Suh, 1998).

APPENDIX C

Permissions to Use Figures

Figure 1.2

Piezoresistive Polymer Diaphragm Sensor Array Using Conductive Elastomeric Nanocomposite Films for Skin-Mountable Keypad Applications
Author: Jeong-Ho Kong
Publication: Journal of Microelectromechanical Systems
Publisher: IEEE
Date: June 2015
Thesis / Dissertation Reuse

The IEEE does not require individuals working on a thesis to obtain a formal reuse license; however, you may print out this statement to be used as a permission grant:

Requirements to be followed when using any portion (e.g., figure, graph, table, or textual material) of an IEEE copyrighted paper in a thesis:

1) In the case of textual material (e.g., using short quotes or referring to the work within these papers) users must give full credit to the original source (author, paper, publication) followed by the IEEE copyright line © 2011 IEEE.
2) In the case of illustrations or tabular material, we require that the copyright line © [Year of original publication] IEEE appear prominently with each reprinted figure and/or table.
3) If a substantial portion of the original paper is to be used, and if you are not the senior author, also obtain the senior author's approval.

Requirements to be followed when using an entire IEEE copyrighted paper in a thesis:

1) The following IEEE copyright/ credit notice should be placed prominently in the references: © [year of original publication] IEEE. Reprinted, with permission, from [author names, paper title, IEEE publication title, and month/year of publication]
2) Only the accepted version of an IEEE copyrighted paper can be used when posting the paper or your thesis on-line.
3) In placing the thesis on the author's university website, please display the following message in a prominent place on the website: In reference to IEEE copyrighted material, which is used with permission in this thesis, the IEEE does not endorse any of [university/educational entity's name goes here]'s products or services. Internal or personal use of this material is permitted. If interested in reprinting/republishing IEEE copyrighted material for advertising or promotional purposes or for creating new collective works for resale or redistribution, please go to http://www.ieee.org/publications_standards/publications/rights/rights_link.html to learn how to obtain a License from RightsLink.

If applicable, University Microfilms and/or ProQuest Library, or the Archives of Canada may supply single copies of the dissertation.

Figure 2.4

Permissions
No special permission is required to reuse all or part of article published by MDPI, including figures and tables. For articles published under an open access Creative Common CC BY license, any part of the article may be reused without permission provided that the original article is clearly cited. Reuse of an article does not imply endorsement by the authors or MDPI.

Figure 2.5

ELSEVIER LICENSETERMS AND CONDITIONS

Jul 18, 2021

This Agreement between Mr. Chenwang Yuan ("You") and Elsevier ("Elsevier") consists of your license details and the terms and conditions provided by Elsevier and Copyright Clearance Center.

License Number	5111801304347
License date	Jul 18, 2021
Licensed Content Publisher	Elsevier
Licensed Content Publication	Journal of Power Sources
Licensed Content Title	Preparation and properties of carbon nanotube/polypropylene nanocomposite bipolar plates for polymer electrolyte membrane fuel cells
Licensed Content Author	Shu-Hang Liao, Chuan-Yu Yen, Cheng-Chih Weng, Yu-FengLin, Chen-Chi M. Ma, Ching-Hung Yang, Ming-Chi Tsai, Ming-YuYen, Min-Chien Hsiao, Shuo-Jen Lee, Xiao-Feng Xie, Yi-Hsiu Hsiao
Licensed Content Date	Dec 1, 2008
Licensed Content Volume	185
Licensed Content Issue	2
Licensed Content Pages	8
Start Page	1225
End Page	1232
Type of Use	reuse in a thesis/dissertation
Portion	figures/tables/illustrations
Number of figures/tables/illustrations	1
Format	both print and electronic
Are you the author of this Elsevier article?	No

Will you be translating?	No
Title	INVESTIGATION OF A SOFT TACTILE SENSINGSYSTEM FOR HUMAN COLLABORATIVE ROBOTS
Institution name	University of Saskatchewan
Expected presentation date	Sep 2021
Portions	Figure 5
Requestor Location	Mr. Chenwang Yuan 35-135 Pawlychenko Lane Saskatoon, SK S7V 1K2, Canada. Attn: Chenwang Yuan
Publisher Tax ID	GB 494 6272 12
Total	0.00 CAD

Figure 2.7

WILEY AND SONS LICENSETERMS AND CONDITIONS

Jul 18, 2021

This Agreement between Mr. Chenwang Yuan ("You") and John Wiley and Sons ("John Wiley and Sons") consists of your license details and the terms and conditions provided by John Wiley and Sons and Copyright Clearance Center.

License Number	5111810779390
License date	Jul 18, 2021
Licensed Content Publisher	John Wiley and Sons
Licensed Content Publication	Advanced Materials
Licensed Content Title	Highly Stretchable and UV Curable Elastomers for Digital Light Processing Based 3D Printing
Licensed Content Author	Shlomo Magdassi, Qi Ge, Biao Zhang, et al

Licensed Content Date	Feb 7, 2017
Licensed Content Volume	29
Licensed Content Issue	15
Licensed Content Pages	1
Type of use	Dissertation/Thesis
Requestor type	University/Academic
Format	Print and electronic
Portion	Figure/table
Number of figures/tables	1
Will you be translating?	No
Title	INVESTIGATION OF A SOFT TACTILE SENSING SYSTEMFOR HUMAN COLLABORATIVE ROBOTS
Institution name	University of Saskatchewan
Expected presentation date	Sep 2021
Portions	Figure 4
Requestor Location	Mr. Chenwang Yuan 35-135 Pawlychenko Lane Saskatoon, SK S7V 1K2, Canada. Attn: Chenwang Yuan
Publisher Tax ID EU826007151	
Total	0.00 CAD

Figure 2.8

Using AAAS material in a thesis or dissertation

NOTE: If you are the original author of the AAAS article being reproduced, please refer to your License to Publish for rules on reproducing your paper in a dissertation or thesis. AAAS permits the use of content published in its journals Science, Science Immunology,

Science Robotics, Science Signaling, and Science Translational Medicine, but only provided the following criteria are met:

If you are using figure(s)/table(s), permission is granted for use in print and electronic versions of your dissertation or thesis.

A full-text article may be used only in print versions of a dissertation or thesis. AAAS does not permit the reproduction of full-text articles in electronic versions of theses or dissertations.

The following credit line must be printed along with the AAAS material: "From [Full Reference Citation]. Reprinted with permission from AAAS."

All required credit lines and notices must be visible any time a user accesses any part of the AAAS material and must appear on any printed copies that an authorized user might make.

The AAAS material may not be modified or altered except that figures and tables may be modified with permission from the author. Author permission for any such changes must be secured prior to your use.

AAAS must publish the full paper prior to your use of any of its text or figures.

If the AAAS material covered by this permission was published in Science during the years 1974–1994, you must also obtain permission from the author, who may grant or withhold permission, and who may or may not charge a fee if permission is granted. See original article for author's address. This condition does not apply to news articles.

If you are an original author of the AAAS article being reproduced, please refer to your License to Publish for rules on reproducing your paper in a dissertation or thesis.

Permission covers the distribution of your dissertation or thesis on demand by a third-party distributor (e.g., ProQuest / UMI), provided the AAAS material covered by this permission remains in situ and is not distributed by that third party outside of the context of your thesis/dissertation.

Permission does not apply to figures/photos/artwork, or any other content or materials included in your work that are credited to non-AAAS sources. If the requested material is sourced to or references non-AAAS sources, you must obtain authorization from that source as well before using that material. You agree to hold harmless and indemnify AAAS

against any claims arising from your use of any content in your work that is credited to non-AAAS sources.

By using the AAAS material identified in your request, you agree to abide by all the terms and conditions herein.

AAAS makes no representations or warranties as to the accuracy of any information contained in the AAAS material covered by this permission, including any warranties of merchantability or fitness for a particular purpose.

Questions about these terms can be directed to the AAAS Permissions Department at permissions@aaas.org.

Figure 2.9

ELSEVIER LICENSETERMS AND CONDITIONS

Jul 18, 2021

This Agreement between Mr. Chenwang Yuan ("You") and Elsevier ("Elsevier") consists of your license details and the terms and conditions provided by Elsevier and Copyright Clearance Center.

License Number	5111821063575
License date	Jul 18, 2021
Licensed Content Publisher	Elsevier
Licensed Content Publication	Sensors and Actuators A: Physical
Licensed Content Title	The development of a highly twistable tactile sensing array with stretchable helical electrodes
Licensed Content Author	M.-Y. Cheng, C.-M. Tsao, Y.-Z. Lai, Y.-J. Yang
Licensed Content Date	Apr 1, 2011
Licensed Content Volume	166
Licensed Content Issue	2

Licensed Content Pages	8
Start Page	226
End Page	233
Type of Use	reuse in a thesis/dissertation
Portion	figures/tables/illustrations
Number of figures/tables/illustrations	1
Format	both print and electronic

Are you the author of this Elsevier article?	No
Will you be translating?	No
Title	INVESTIGATION OF A SOFT TACTILE SENSINGSYSTEM FOR HUMAN COLLABORATIVE ROBOTS
Institution name	University of Saskatchewan
Expected presentation date	Sep 2021
Portions	Figure 1
Requestor Location	Mr. Chenwang Yuan 35-135 Pawlychenko Lane, Saskatoon, SK S7V 1K2, Canada Attn: Chenwang Yuan
Publisher Tax ID	GB 494 6272 12
Total	0.00 CAD